Model Configuration and Performance with Wind Profiler Nudging

Grant Activity No. 582-5-64593-FY07-20
Analysis of TexAQS II Meteorological Data

A report to the Texas Commission on Environmental Quality

John W. Nielsen-Gammon
Department of Atmospheric Sciences
Texas A&M University
College Station, Texas

March 21, 2008

1. Purpose and Overview

This report addresses Tasks 3.4 and 3.5 of Grant Activity No. 582-5-64593-FY07-20, Amendment 3. These tasks are summarized as follows:

Task 3.4: Evaluate the observational nudging files created in Task 3.1 with the meteorological model MM5 for photochemical model input. These evaluations shall include, but not be limited to: (a) Wind, temperature, and humidity statistics; (b) Vertical profiles of winds and temperature; (c) Location and intensity of clouds and precipitation; (d) Land/sea breeze timing and penetration; and (e) Planetary boundary layer height. Observational nudging shall be conducted on the 4 km domain.

Task 3.5: Determine the representative MM5 INTERPF base state constants for certain air quality episodes for the 108 km, 36 km, 12 km, and 4 km MM5 modeling domains. Use observational data to determine appropriate base state constants. MM5 modeling may be used to verify the choice(s) in base state constants.

In support of these tasks, five model runs were conducted and various graphical and diagnostic output files were produced. Section 2 of this report describes the model runs and preliminary data analysis. Section 3 describes the model output with respect to location and intensity of clouds and precipitation. Section 4 describes the model output with respect to planetary boundary layer height and land/sea breeze timing and penetration. Section 5 describes the model performance with respect to wind and temperature statistics. Section 6 describes the model performance and base state constants with respect to vertical profiles of wind and temperature. Section 7 summarizes the results of this study and provides recommendations for future work.

2. Model Runs and Preliminary Data Analysis

The period July 30 through August 2, 2005, was chosen for the numerical experiments by TCEQ. This period had a mix of clear days and days with scattered convective activity, allowing evaluation of nudging performance both on days with benign weather and days on which nudging of wind fields may affect the onset and distribution of convection. The period was also of interest because of the high ozone levels observed in the Houston and Dallas areas.

The first step in the nudging test procedure was the direct examination of profiler winds for outliers and other suspicious characteristics. This examination was entirely subjective and independent of the original wind profiler quality control. Suspicious winds were rated on the following scale: one question mark for winds that seem odd, two question marks for winds that may or may not be real, and three question marks for winds that seem clearly erroneous. The daily profiler wind plots on http://www.met.tamu.edu/texaqs2 were used for this task. The results of the survey are shown in Table 1.

Table 1: Subjective assessment notes of quality of winds used for nudging of MM5, July 30-August 2, 2005. All times are in CST.

Profiler	July 30	July 31	August 1	August 2
JFC	?01-05 strong nely llj 200-600m good continuity ?07-12 strong nly winds 700-1500m good continuity ??03-16 winds a bit noisy near upper limit about 2000 m	?07-13 strong nly winds 700-1200m good continuity	fine	fine
LPT	?04-17 strong nly winds 1200-2500m good continuity	fine	fine	fine
LVW	?03-06 strong nely 900-1700m earlier winds screened ?07-12 strong nly winds 1100-2500m good continuity	fine	fine	fine
HVE	?06-13 strong nly 1200-2500m good continuity ??13-16 erratic nly-nely winds 0-1000m	??01 strong nely 2300-2600m	fine (but strange mixing heights)	fine (but strange mixing heights)
PAT	fine	fine	fine	fine
BVL	???16 strong ely 0-500m	?05-13 strong nly 1200-2800m	fine	fine
LDB	fine	fine	fine	fine
CLE	?00-24 variable nly winds above 2000m	?00-24 variable	fine	fine

		winds above 2300m		
NBF	fine	?00-12 strong nly 2000-3000m	fine	fine (but strange mixing heights
SNR	fine	fine	fine	fine
JTN	fine	fine	?10-18 erratic winds 1200-1500m	?10-16 erratic winds 1200-1800m

The sole case in which winds were identified as clearly erroneous was at 1600 CST July 30 at Beeville (BVL). Further inspection of the meteorological situation revealed that there were thunderstorms in the area, meaning that the BVL winds were probably real but unrepresentative. Since these were low-level winds far from the area of interest, no attempt was made to remove the unrepresentative winds from the nudging file.

The model runs were performed on the TCEQ computer storm2met. TCEQ supplied the INTERPF output, the initial and boundary condition files, and a nudging file (which in turn had been provided by TAMU). TCEQ established an account for performing the model runs.

All model run configurations and output are available on the TCEQ computer storm2met at /met1/tamu/mm5v373/MM5. Specific Run directories for each model run were created using the naming convention Run.*name*, where "name" is the name of the specific model run. In the /met1/tamu/mm5v373/MM5 are also the job decks, with the naming convention mm5.deck.*name*.

The model runs are listed in Table 2. The grids for the model runs were determined by TCEQ. The model runs were one-way nests with a 4 km grid spacing.

Table 2: MM5 model runs discussed in this report.

Model run	**Nudging**	**Parameters**	**Convection Scheme**
orignudg4day3	all profilers	RINXY=240. TWINDO=40.	none (explicit)
nonudg4day3	none	same as orig	same as orig
testnudg4day3	all profilers	RINXY=150. TWINDO=90.	same as orig
nohve4day3	all but HVE (Huntsville)	same as orig	same as orig
grell4day3	all profilers	same as orig	Grell

Other aspects of model physics include Simple Ice microphysics, Eta Mellor-Yamada planetary boundary layer, Rapid Radiative Transfer Model radiation scheme, and Noah land surface scheme.

The **orignudg4day3** model run was a replication of the full profiler nudging model run as presently configured by TCEQ. The remaining runs involve slight differences from this original run, designed to test various aspects of nudging performance. The **nonudg4day3** run was a model run without observational nudging on the 4 km grid, though the effect of analysis nudging on the coarser grids is still felt through the initial and lateral boundary conditions. The **testnudg4day3** involved an adjustment of the nudging parameters to agree with the optimal configuration established by Nielsen-Gammon et al. (2007; hereafter NG07) for the TexAQS-2000 profiler network. The **nohve4day3** run involved withholding of the HVE (Huntsville) wind profiler data, to determine the influence of a single profiler and to allow estimation of nudging performance using independent profiler data. Finally, the **grell4day3** run included activation of the Grell cumulus parameterization scheme on the 4 km grid.

3. Clouds and Precipitation

a) July 30, 2005

July 30, 2005 featured scattered showers offshore and in south-central Texas, with scattered boundary-layer cumulus through most of East Texas. Figure 1 shows the distribution of radar echoes at 12Z (0600 CST), 18Z, 21Z, and 00Z, and Figure 2 shows the cloud pattern at 21Z.

Figure 1 (following two pages): Nowrad radar mosaics for 12Z, 18Z, and 21Z July 30, 2005 and 00Z July 31, 2005. Date and time (in UTC) are at the bottom of each image, and the reflectivity scale is at left.

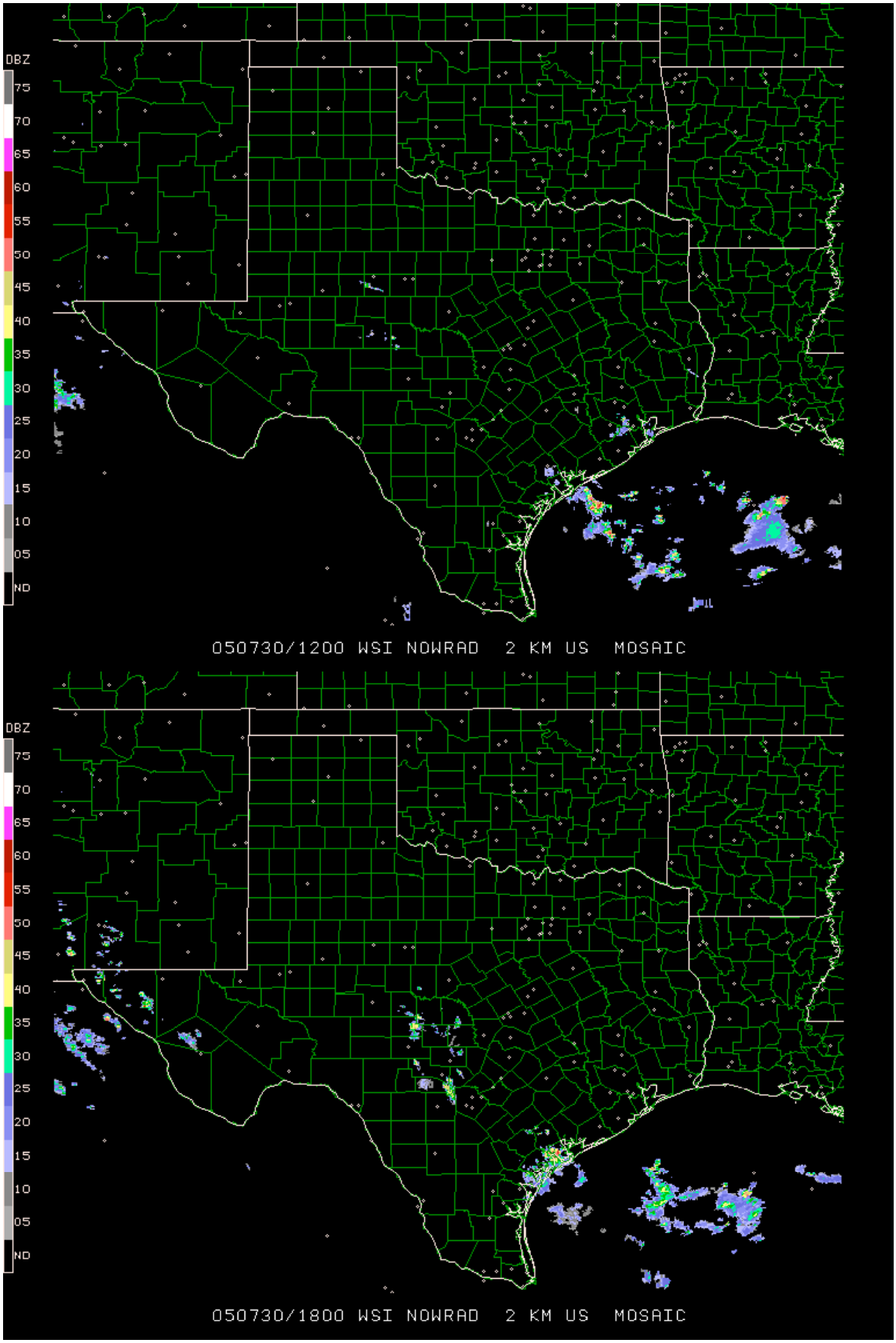
DBZ
75
70
65
60
55
50
45
40
35
30
25
20
15
10
05
ND
050730/1200 WSI NOWRAD 2 KM US MOSAIC
DBZ
75
70
65
60
55
50
45
40
35
30
25
20
15
10
05
ND
050730/1800 WSI NOWRAD 2 KM US MOSAIC

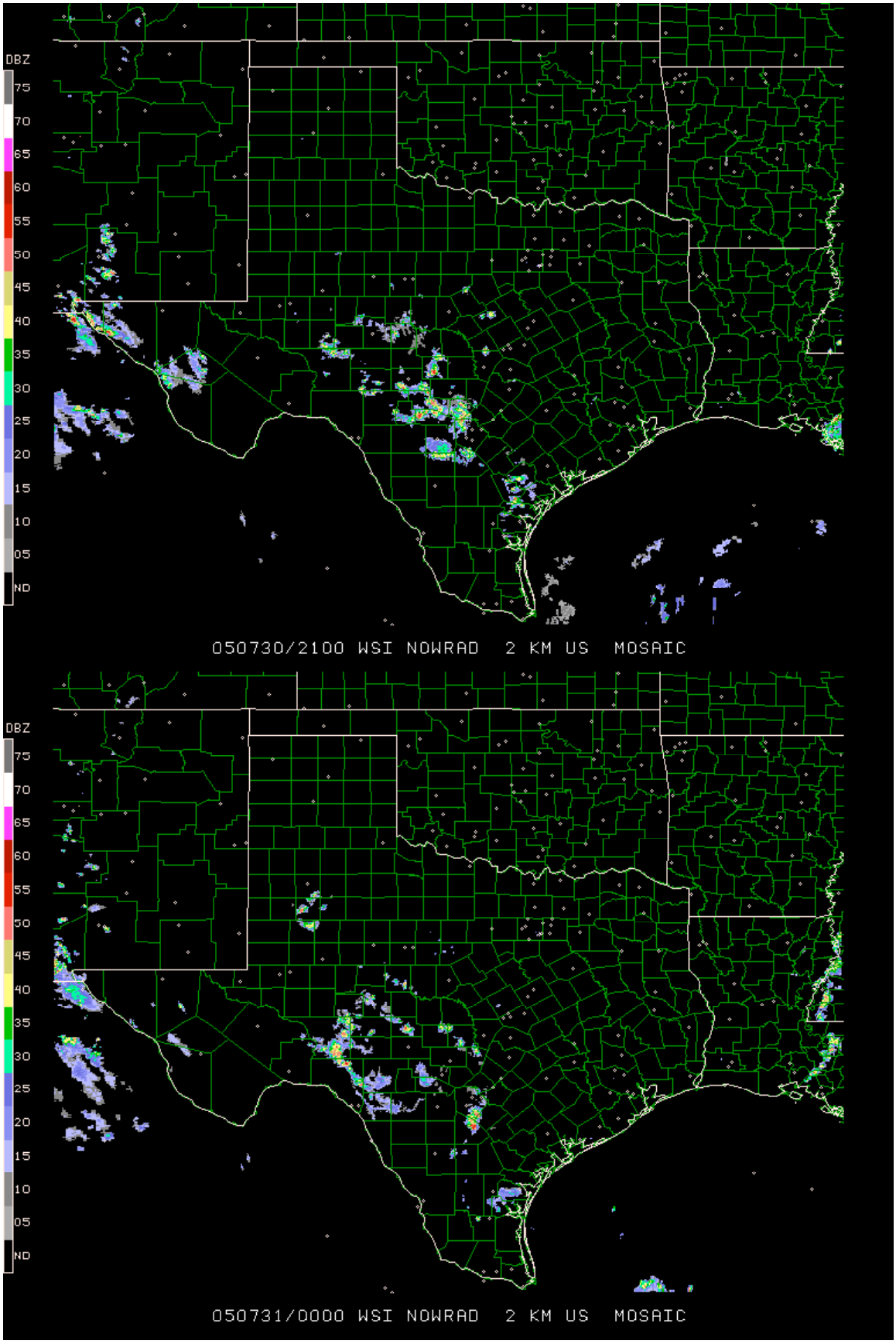
DBZ
75
70
65
60
55
50
45
40
35
30
25
20
15
10
05
ND
050730/2100 WSI NOWRAD 2 KM US MOSAIC
DBZ
75
70
65
60
55
50
45
40
35
30
25
20
15
10
05
ND
050731/0000 WSI NOWRAD 2 KM US MOSAIC

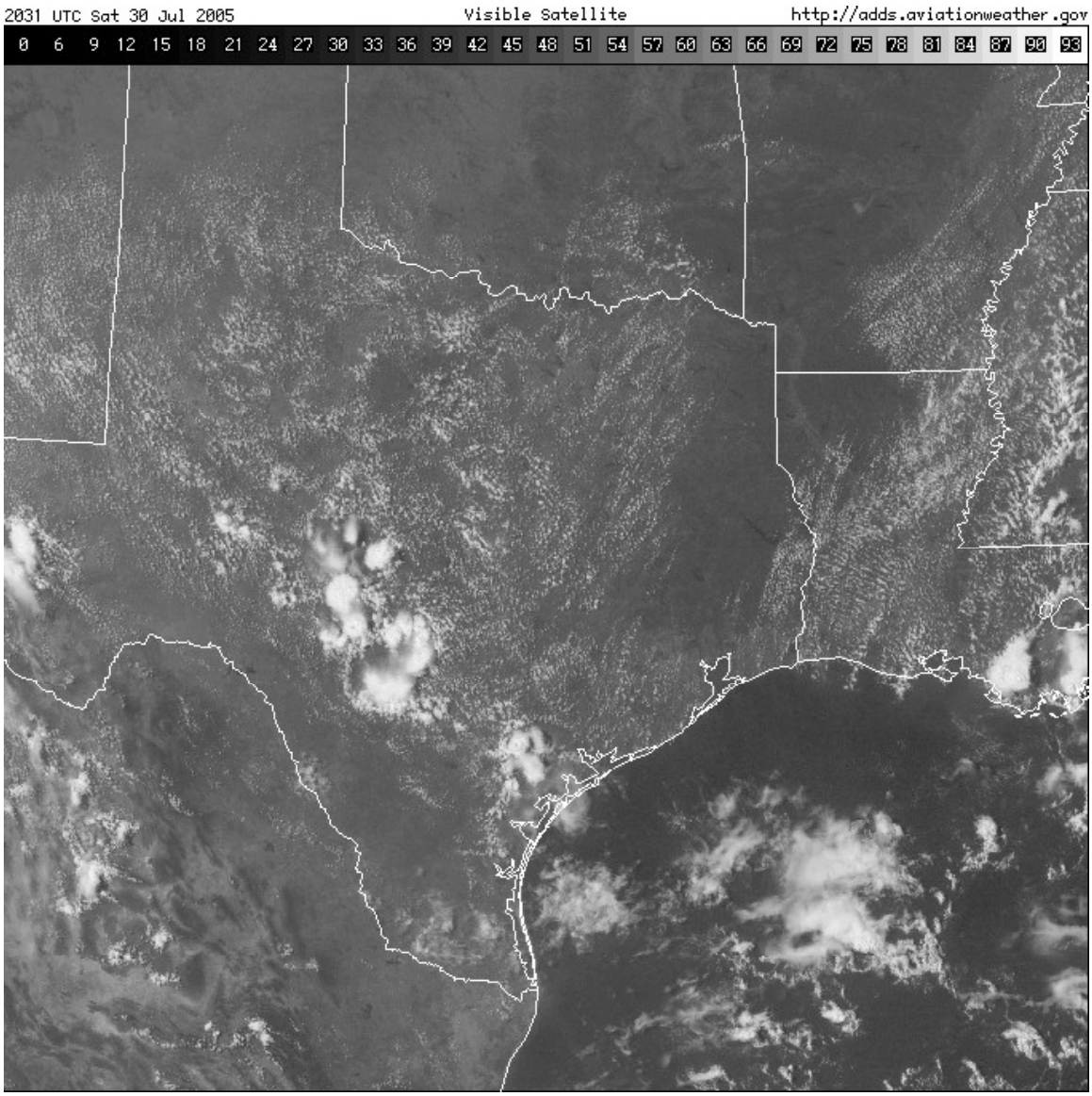

Figure 2: Visible satellite image, 2031Z (1531 CST) July 30, 2005. This satellite image is from approximately the same time as the radar image on the top of the previous page.

The model runs for this day have cloud and precipitation distributions that are broadly similar to the observations. Figure 3 shows the distribution of shortwave radiation reaching the ground (a good proxy for cloud cover, or lack thereof) and hourly precipitation (red contours, variable contour interval) in the orignud4day3 model run.

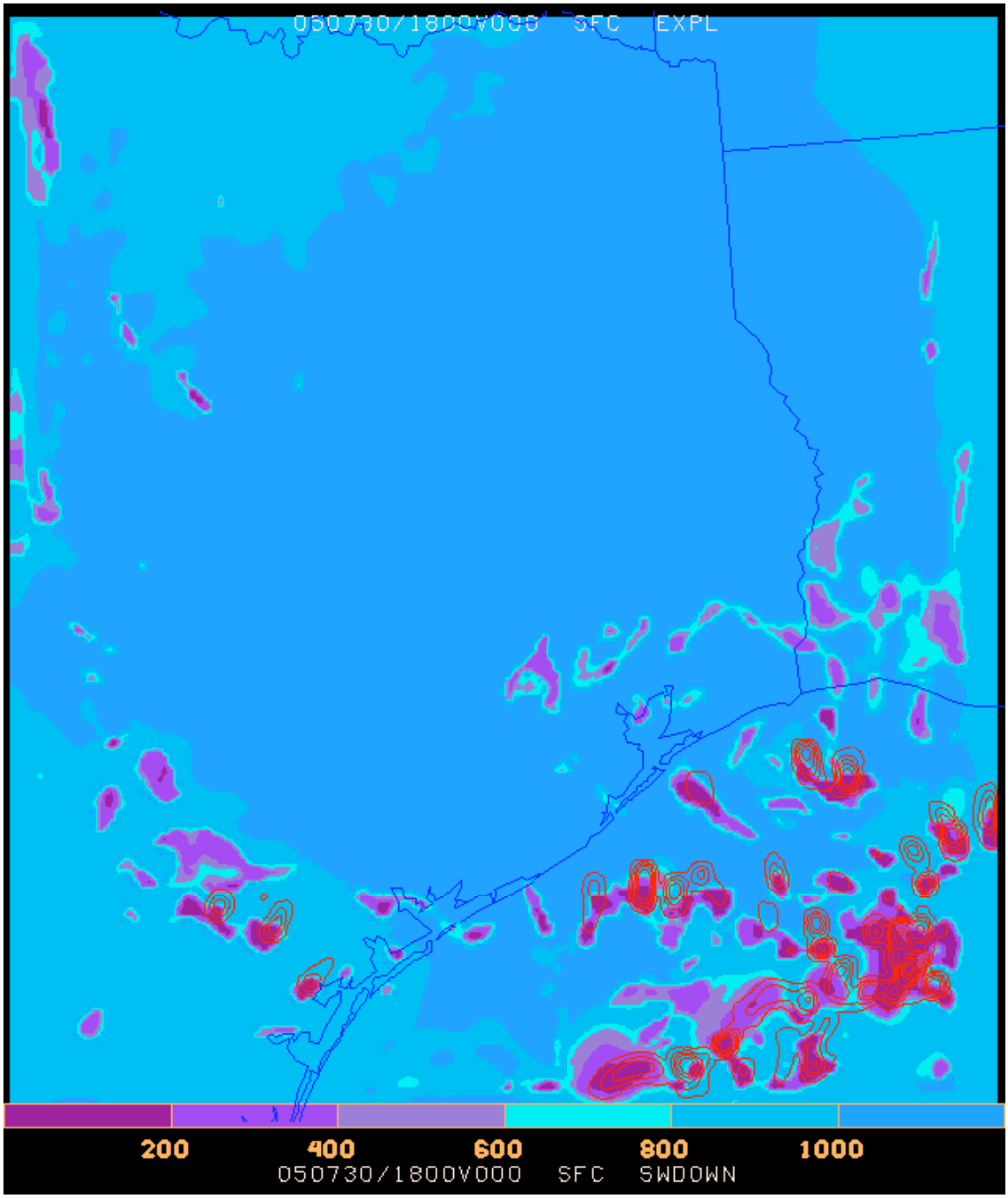

Figure 3: Shortwave solar radiation reaching the ground (shading) and 1-h precipitation (red contours), 18Z July 30, 2005, orignudg4day3 model run.

In this and other model figures, the entire 4 km model domain is shown. This model run has convection offshore and in southcentral Texas, in agreement with the observations, except that the precipitation is perhaps too close to the coast. The other three explicit runs are similar; the nonudg4day3 run is shown in Fig. 4.

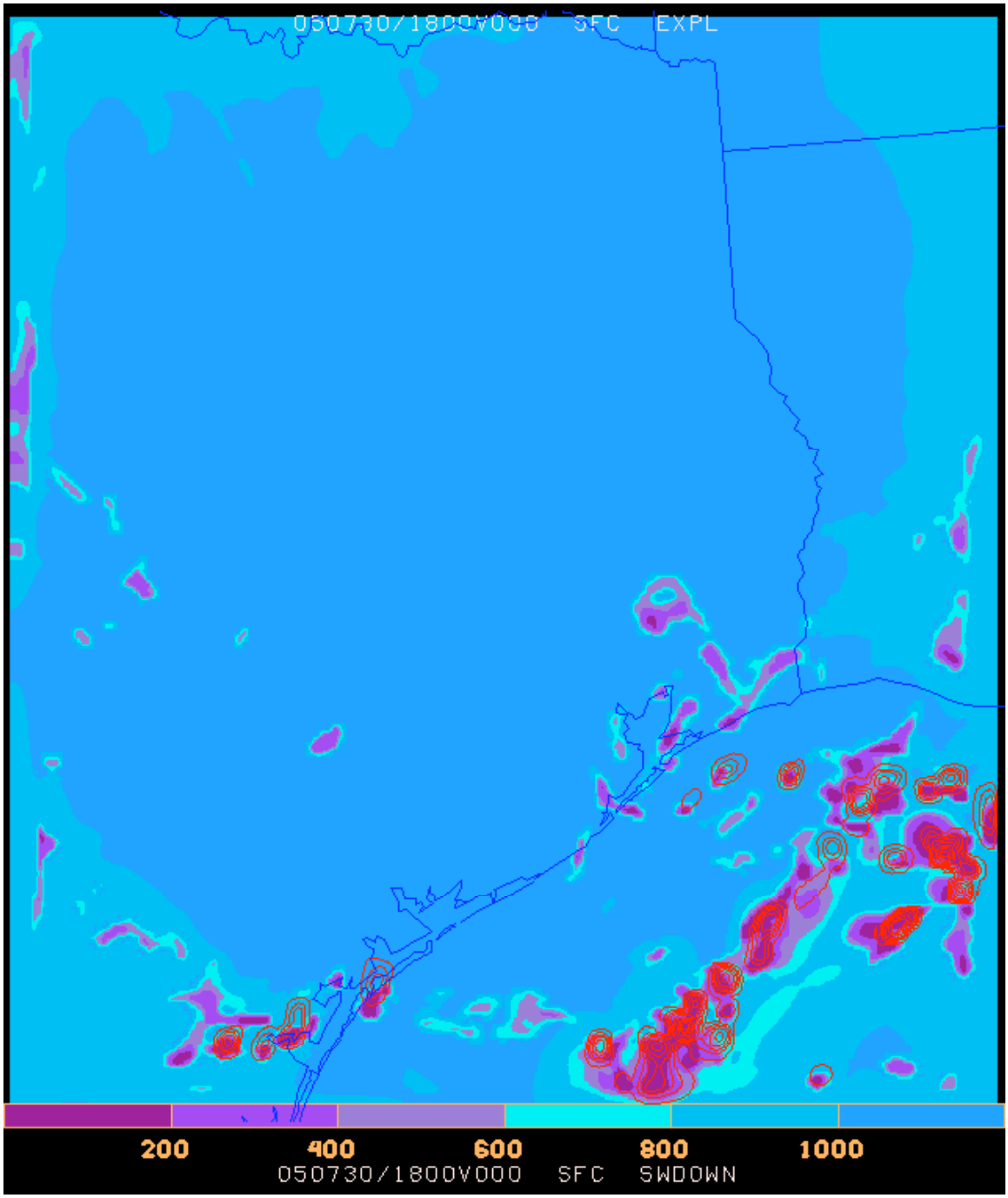

Figure 4: Shortwave solar radiation reaching the ground (shading) and 1-h precipitation (red contours), 18Z July 30, 2005, nonudg4day3 model run.

By 21Z, the simulated convection has moved farther offshore while becoming more widespread in central Texas, the explicit model runs have begun producing their own versions of boundary-layer cumulus. This is seen in the orignudg4day3 run (Fig. 5). The nonudg4day3run (Fig. 6) has the fewest scattered clouds, even though there was no nudging of temperature or moisture.

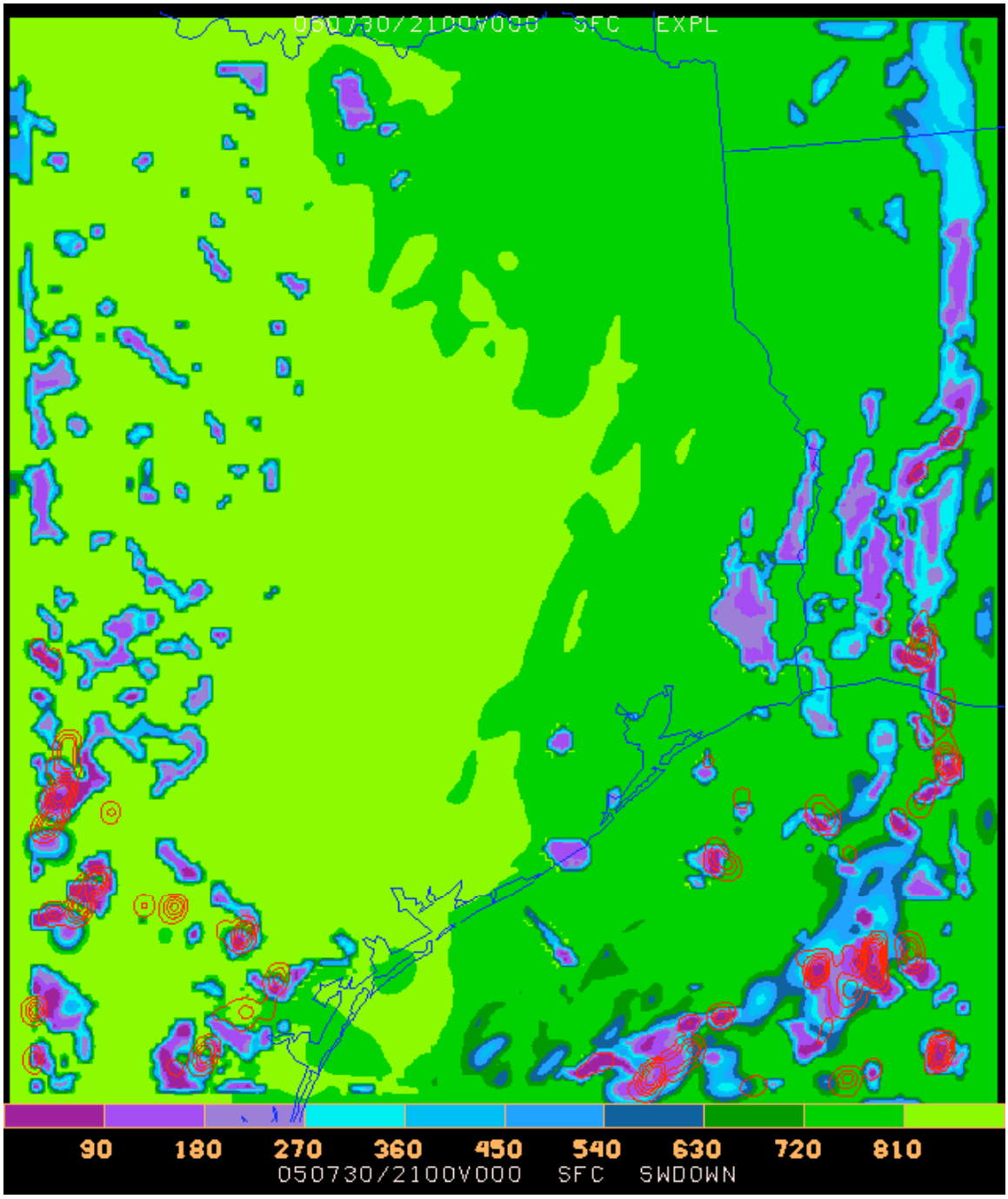

Figure 5: Shortwave solar radiation reaching the ground (shading) and 1-h precipitation (red contours), 21Z July 30, 2005, orignudg4day3 model run.

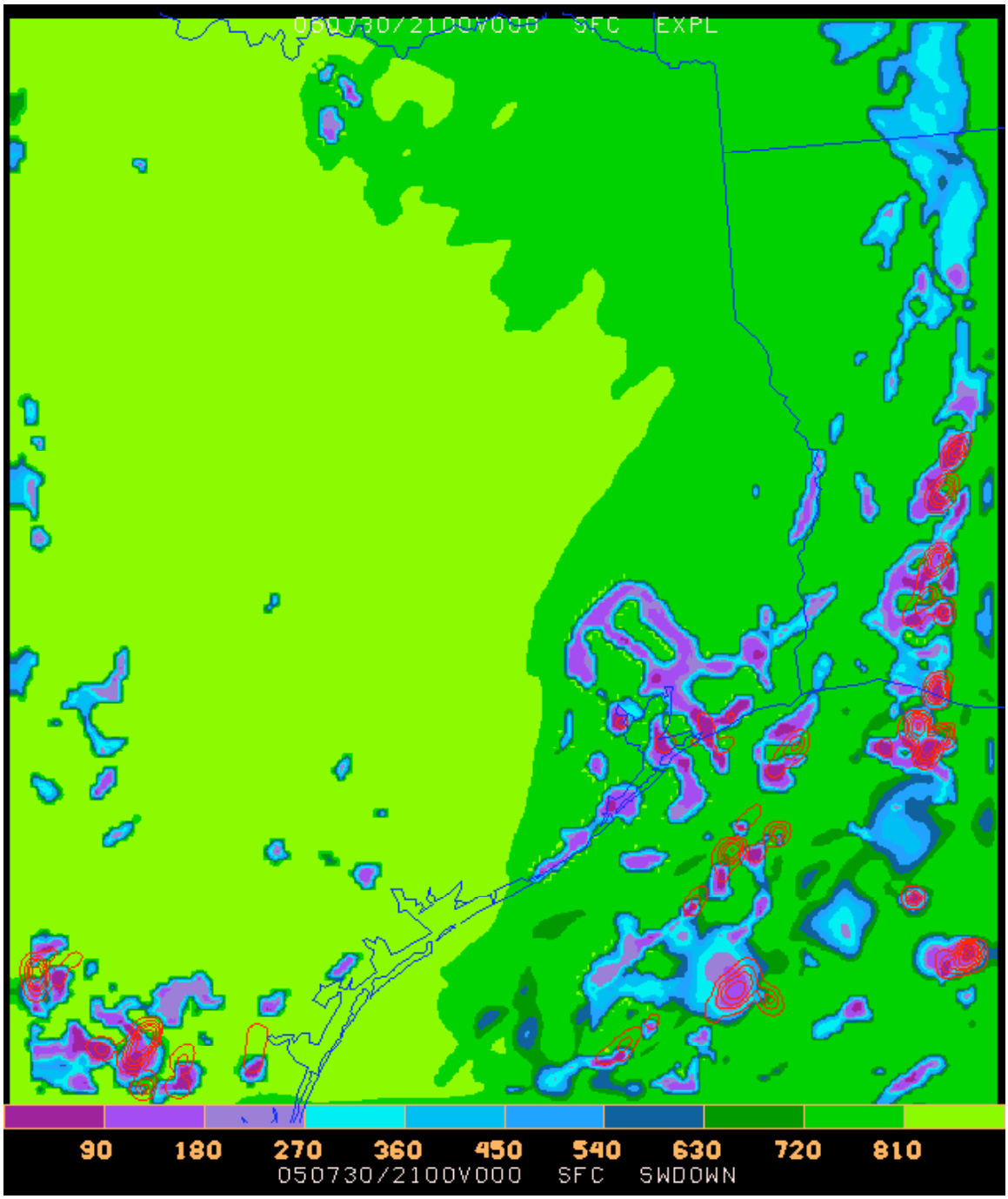

Figure 6: Shortwave solar radiation reaching the ground (shading) and 1-h precipitation (red contours), 21Z July 30, 2005, nonudg4day3 model run.

In summary, there is almost no systematic difference between the various explicit nudging runs with respect to clouds and precipitation on July 30, and the run without nudging seems to be slightly deficient in cloud cover.

Figs. 5 and 6 show considerable convection and precipitation offshore at 21Z. The observations (Figs. 1 and 2) indicate that the offshore convection had dissipated by that time. Shown in Fig. 7 is the grell4day3 run for 21Z. This run has much less convection along the coast and offshore, although there is still more than observed, and no precipitating convection in southcentral Texas. On balance, the grell4day3 run has the best precipitation distribution.

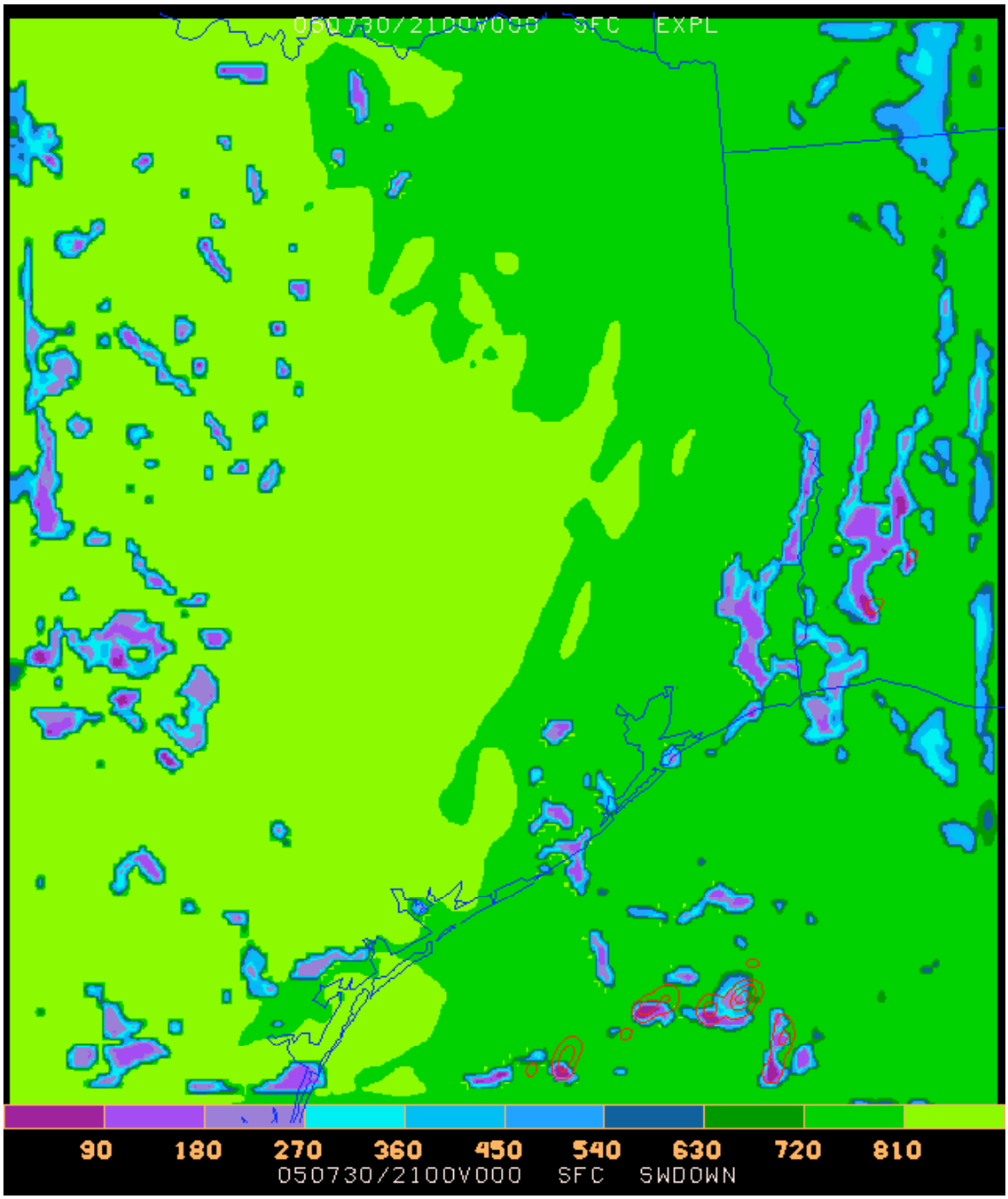

Figure 7: Shortwave solar radiation reaching the ground (shading) and 1-h precipitation (red contours), 18Z July 30, 2005, nonudg4day3 model run.

b) July 31, 2005

July 31, 2005 featured very scattered showers early offshore. Isolated showers also formed in East Texas and Louisiana by 21Z. Fig. 8 shows the distribution of radar echoes at 15Z, 18Z, 21Z, and 00Z, and Figs. 9 and 10 show the cloud patterns at 15Z and21Z.

Figure 8 (following two pages): Nowrad radar mosaics for 15Z, 18Z, and 21Z July 31, 2005 and 00Z August 1, 2005. Date and time (in UTC) are at the bottom of each image, and the reflectivity scale is at left.

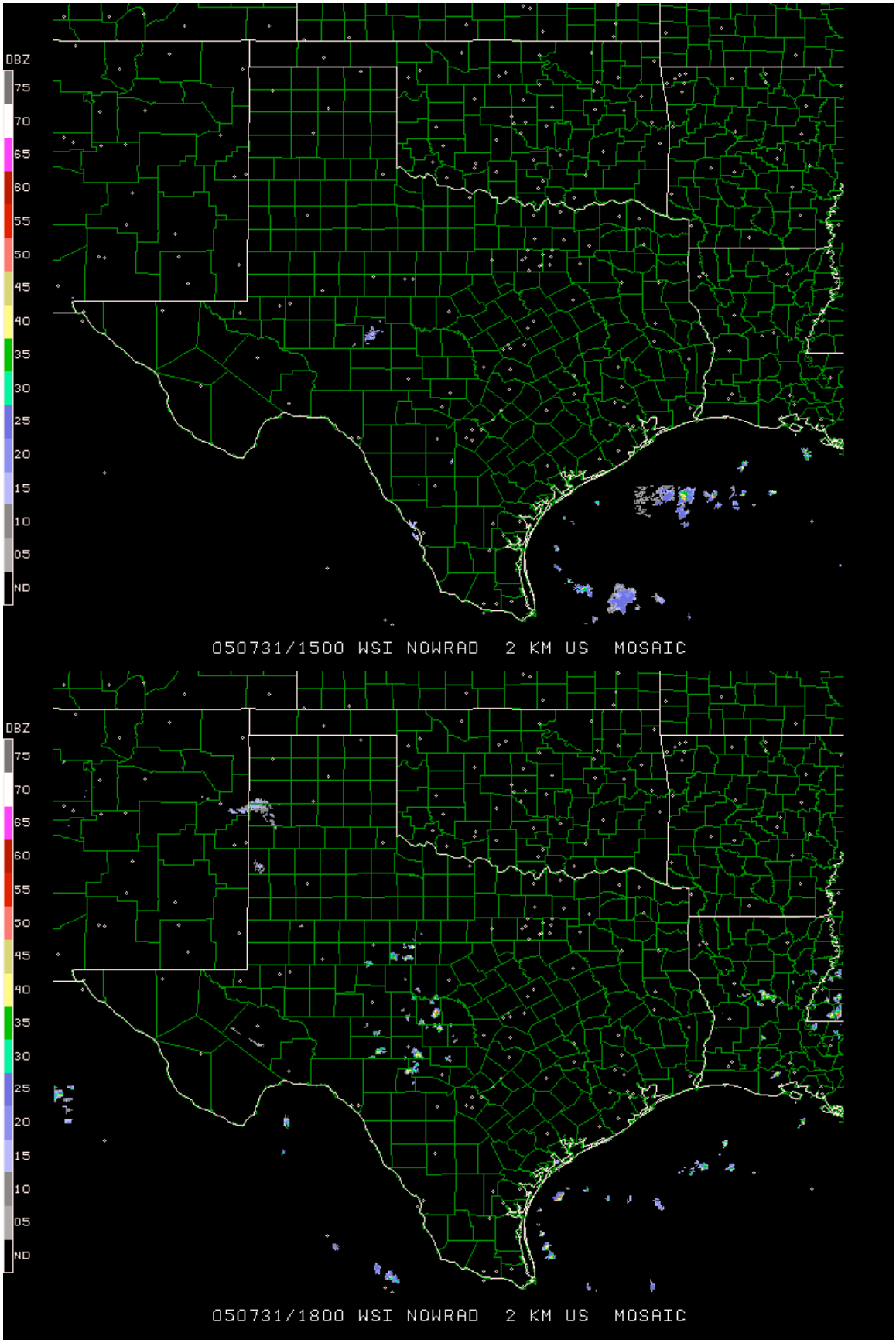
DBZ
75
70
65
60
55
50
45
40
35
30
25
20
15
10
05
ND
050731/1500 WSI NOWRAD 2 KM US MOSAIC
DBZ
75
70
65
60
55
50
45
40
35
30
25
20
15
10
05
ND
050731/1800 WSI NOWRAD 2 KM US MOSAIC

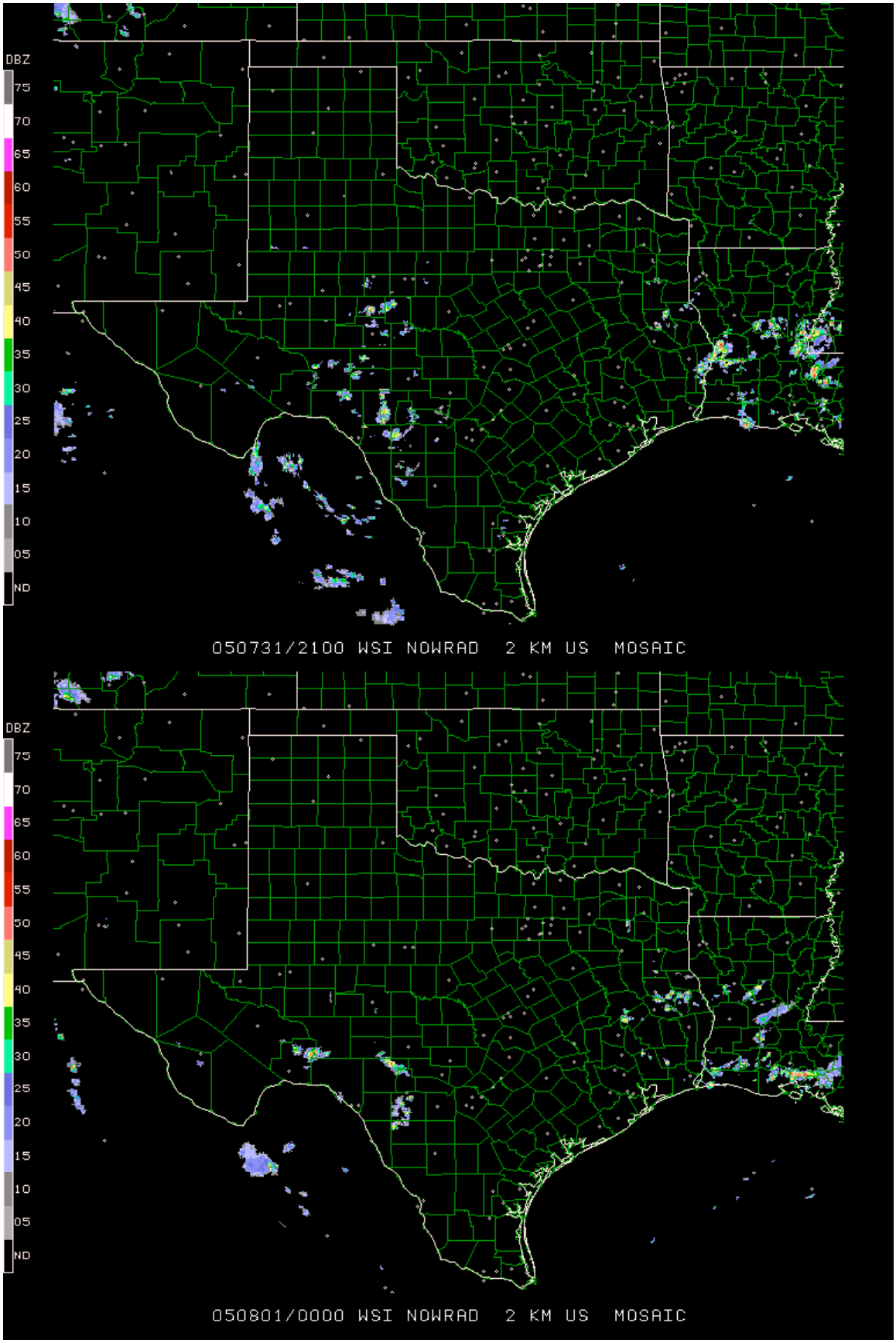
DBZ
75
70
65
60
55
50
45
40
35
30
25
20
15
10
05
ND
050731/2100 WSI NOWRAD 2 KM US MOSAIC
DBZ
75
70
65
60
55
50
45
40
35
30
25
20
15
10
05
ND
050801/0000 WSI NOWRAD 2 KM US MOSAIC

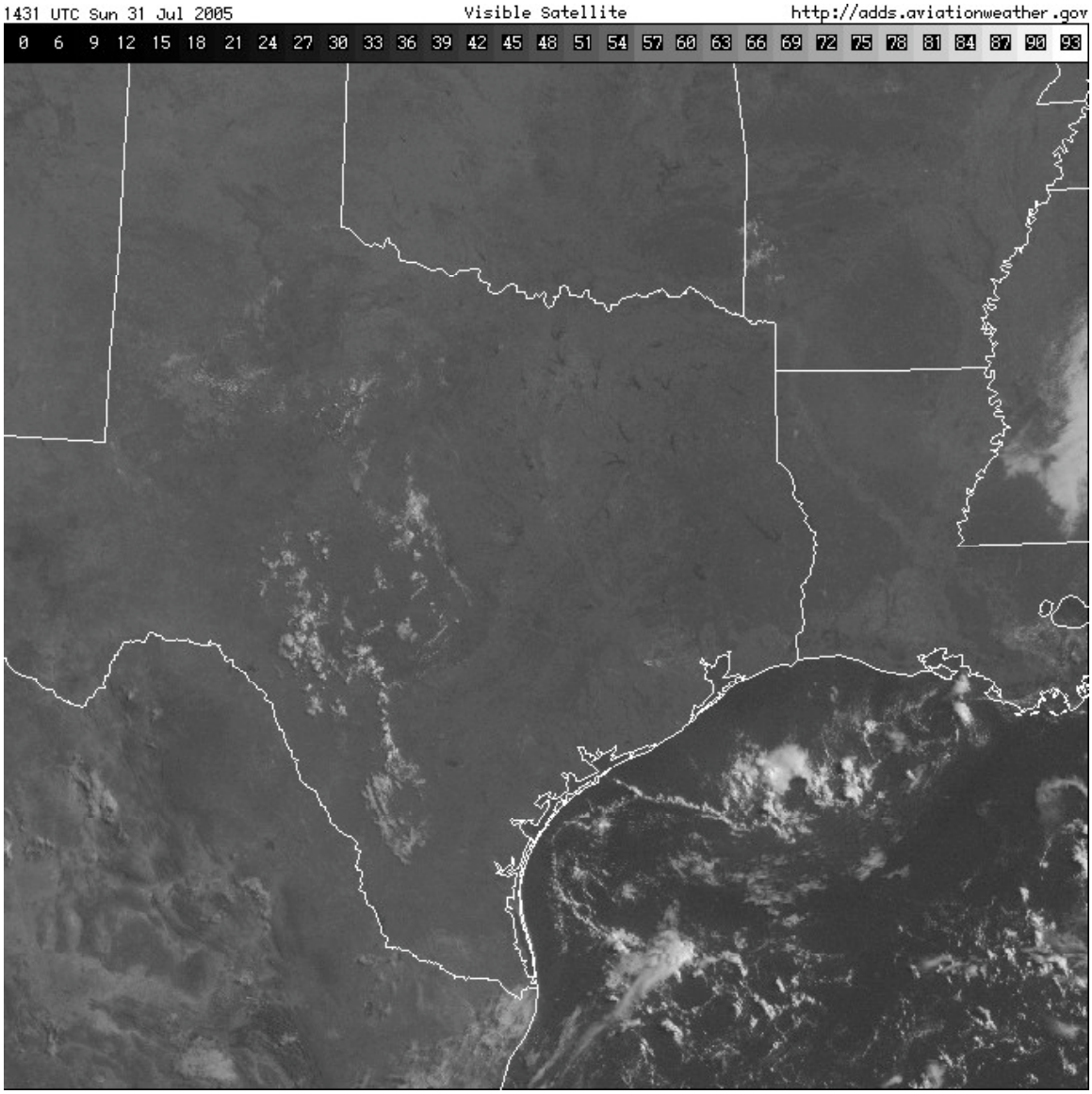

Figure 9: Visible satellite image, 1431Z (0831 CST) July 31, 2005.

The output from all five model runs is shown in Figs. 11-15. All model runs have too much convection offshore. The grell4day3 run, at least, only has somewhat excessive convection. The other four model runs have widespread clouds and precipitation throughout the offshore portion of the 4 km domain. These four extend the cloud cover over land so that the Houston area is simulated to be cloudy in the morning, in direct contrast to the satellite image (Fig. 9) that shows that almost all of East Texas, including coastal areas, was clear.

All five model runs also have a small area of clouds and precipitation in northeast Texas. As seen in the satellite image, no such area was actually present.

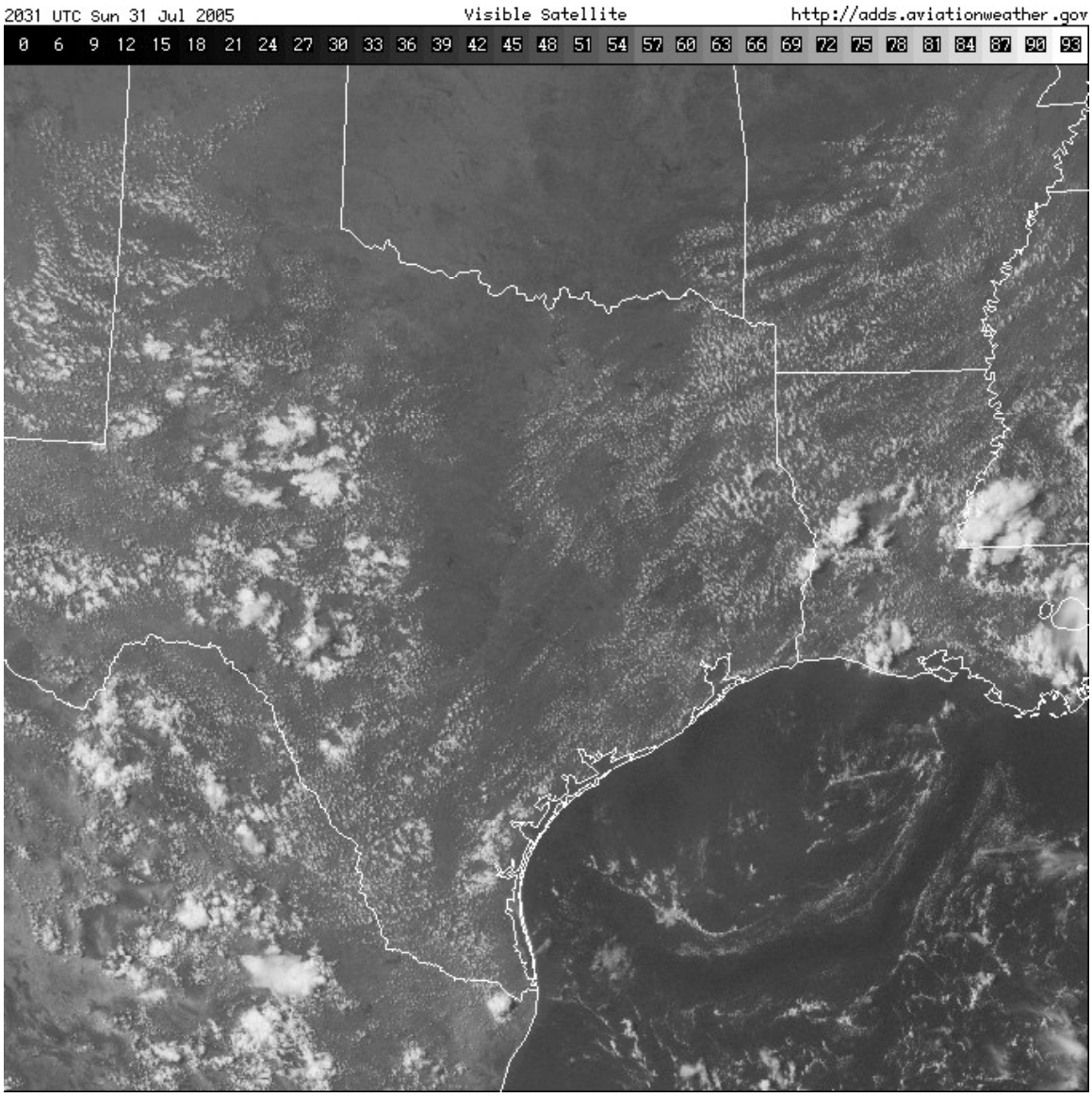

Figure 10: Visible satellite image, 2031Z July 31, 2005.

At 21Z, a correct model simulation would have scattered boundary layer cumulus throughout eastern Texas, mostly clear skies offshore, and some initial convection breaking out over land, particularly in east-central Texas and western Louisiana.

The orignudg4day3 run (Fig. 16), like the testnudg4day3 and nohve4day3, grossly overestimates the amount of cloud cover and convection. Coastal and offshore regions are mostly cloudy, with widespread precipitating convection. Farther north, scattered convection is present through most of East Texas.

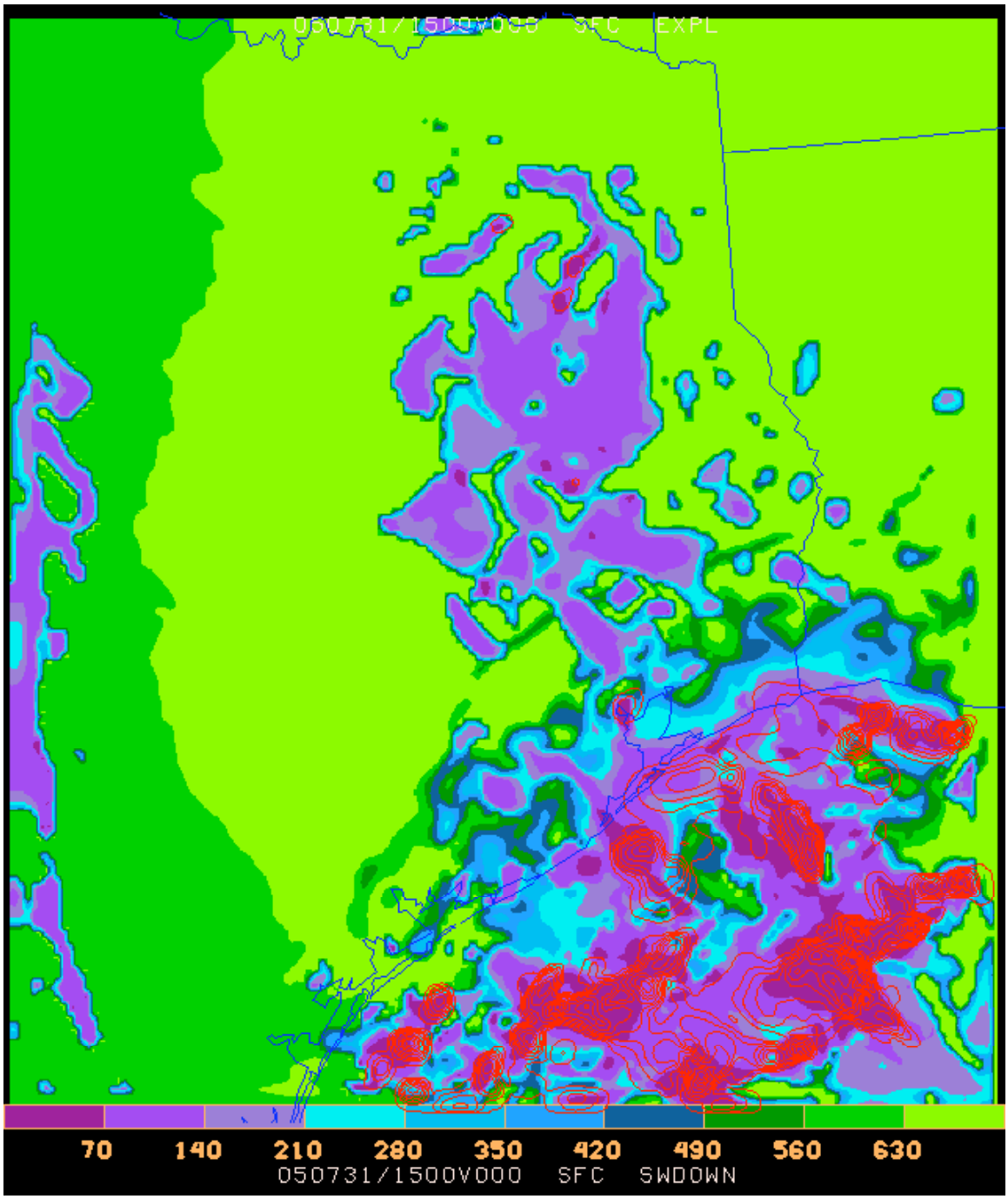

Figure 11: Shortwave solar radiation reaching the ground (shading) and 1-h precipitation (red contours), 15Z July 31, 2005, orignudg4day3 model run.

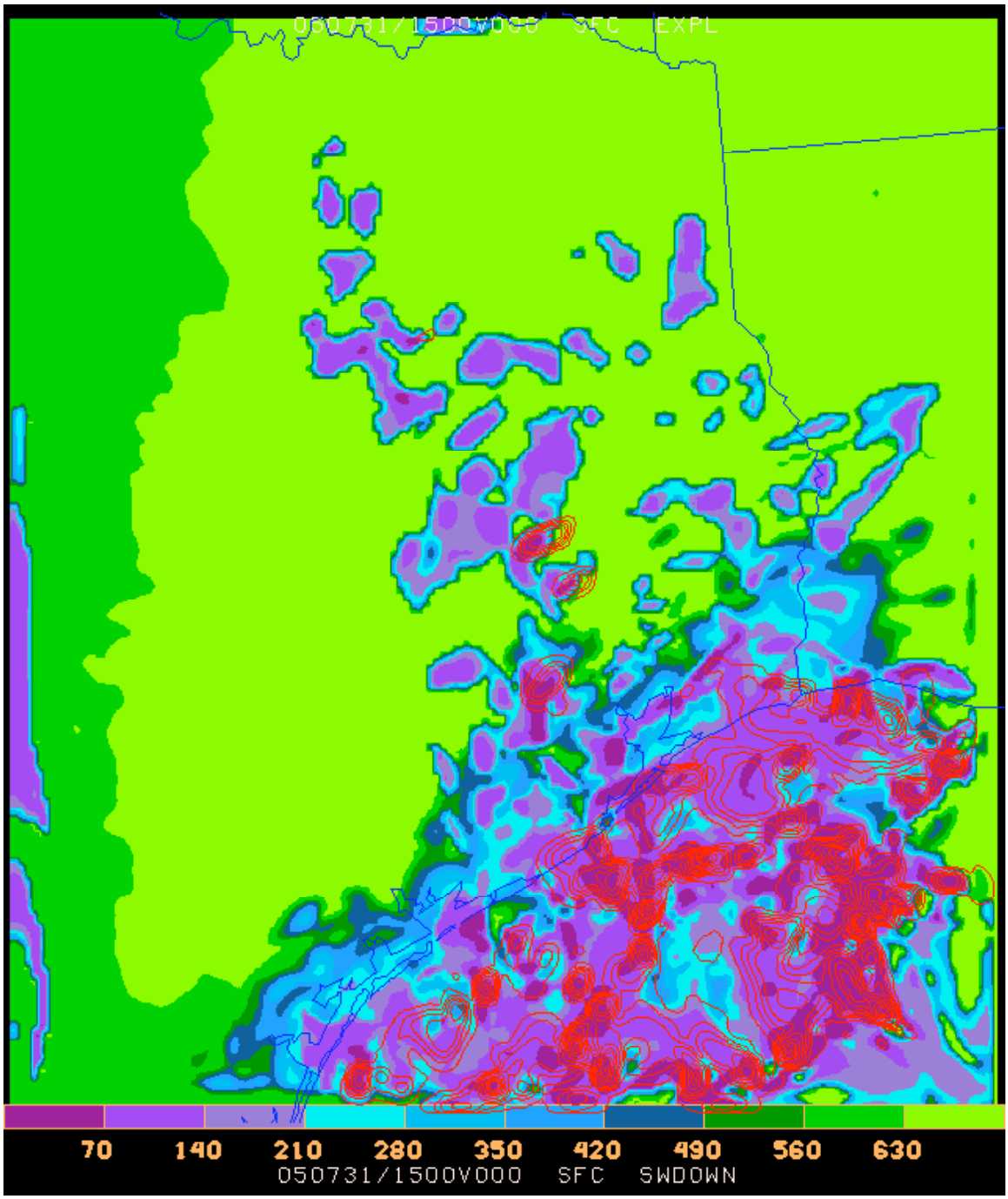

Figure 12: Shortwave solar radiation reaching the ground (shading) and 1-h precipitation (red contours), 15Z July 31, 2005, nonudg4day3 model run.

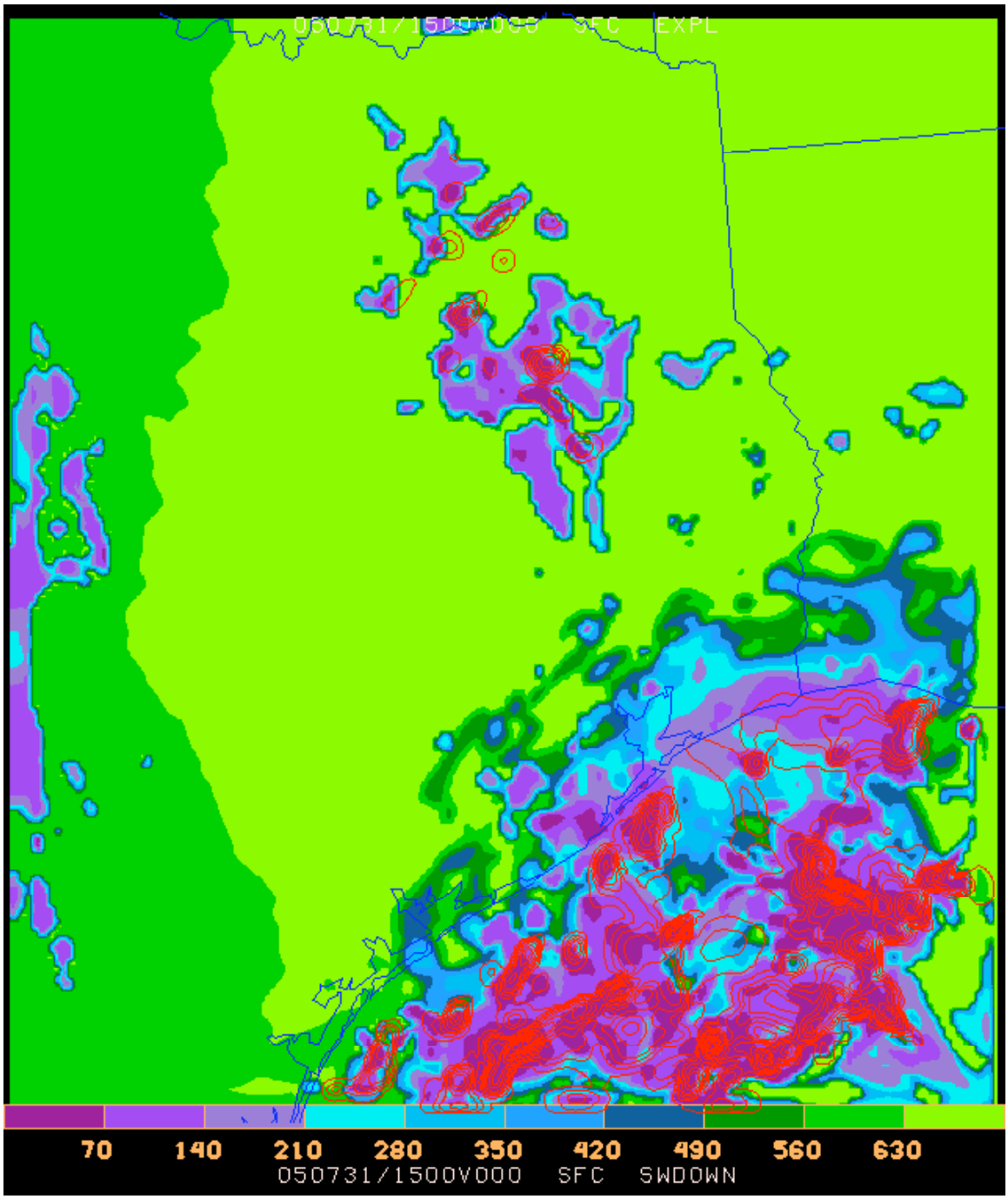

Figure 13: Shortwave solar radiation reaching the ground (shading) and 1-h precipitation (red contours), 15Z July 31, 2005, testnudg4day3 model run.

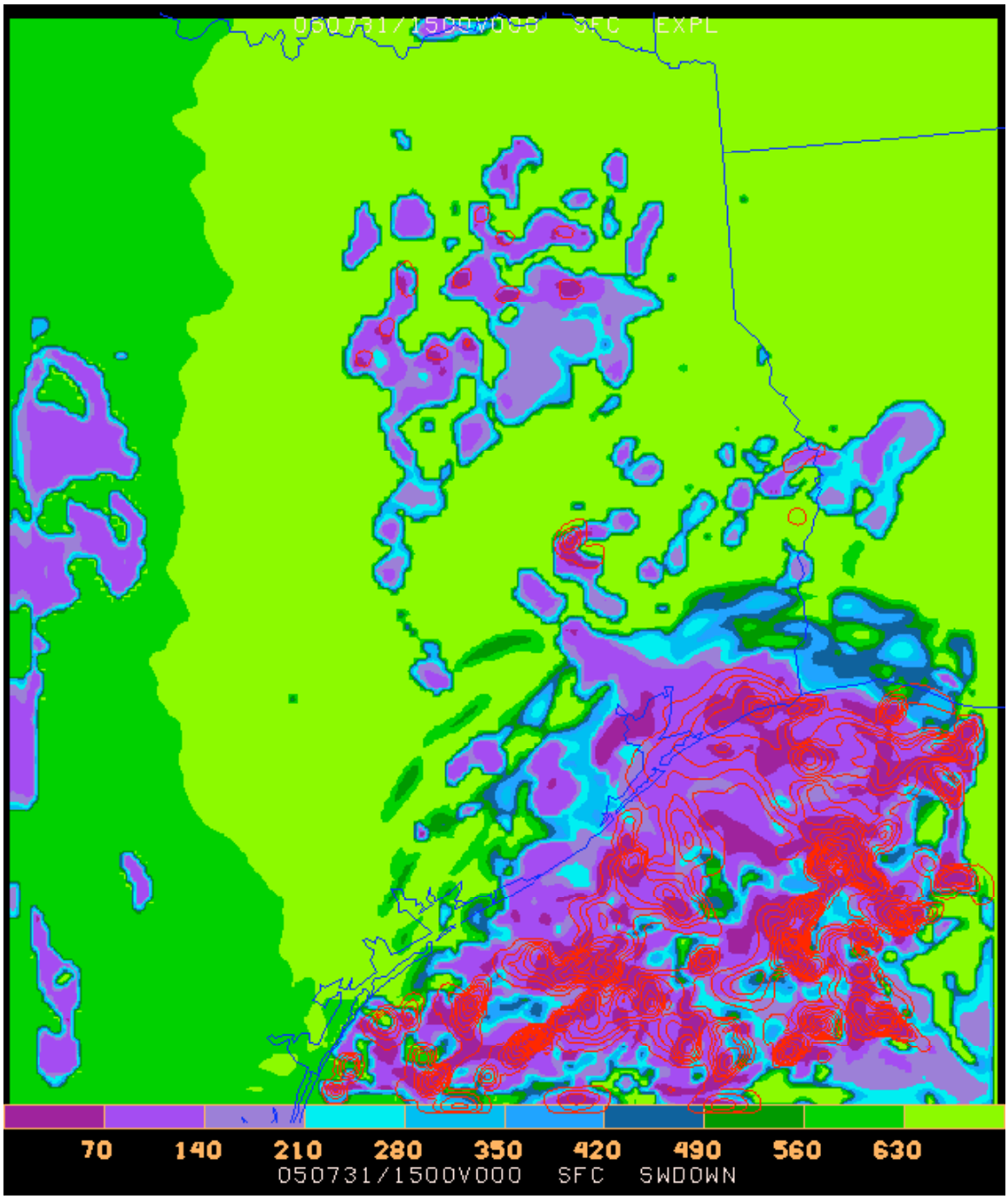

Figure 14: Shortwave solar radiation reaching the ground (shading) and 1-h precipitation (red contours), 15Z July 31, 2005, nohve4day3 model run.

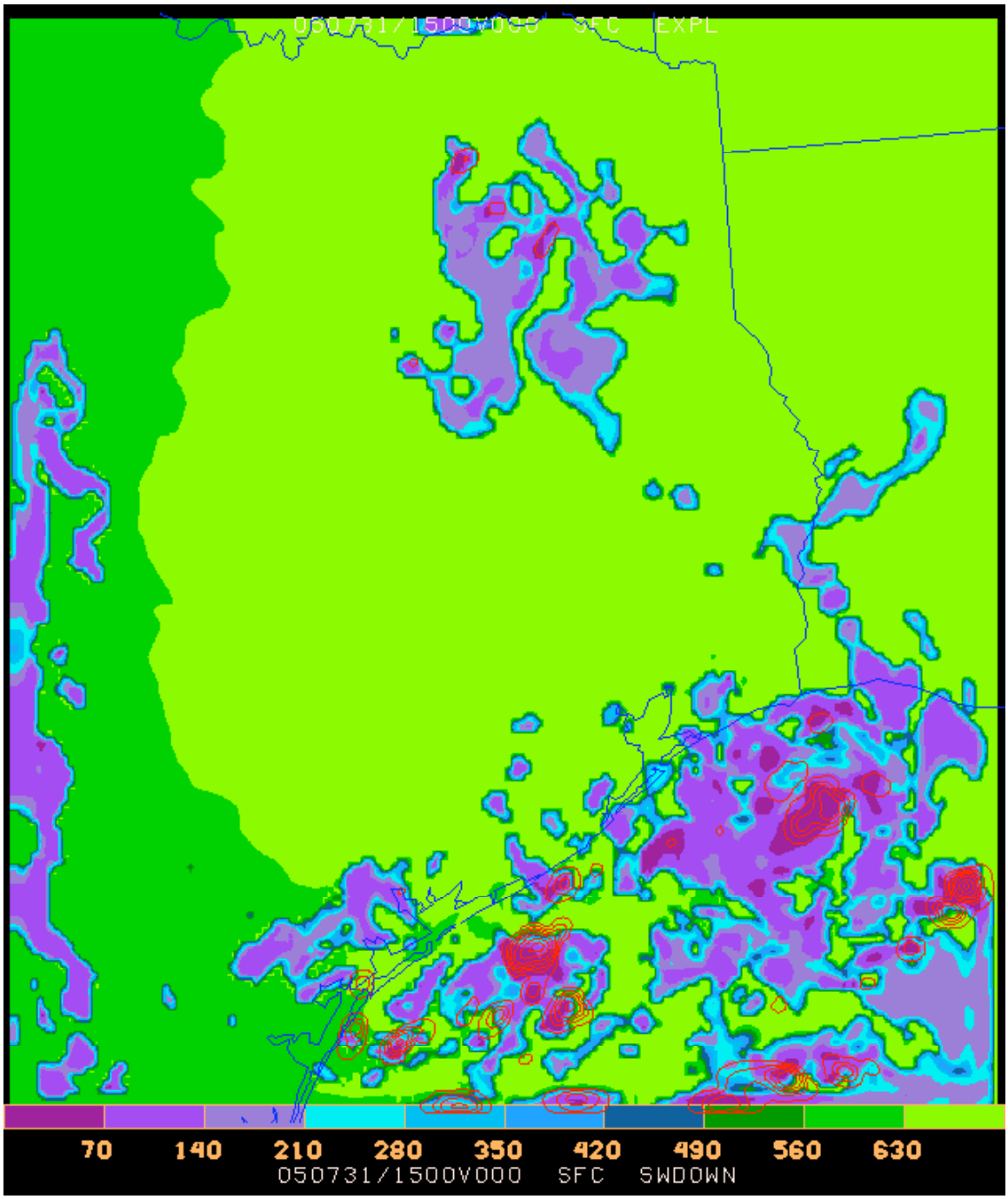

Figure 15: Shortwave solar radiation reaching the ground (shading) and 1-h precipitation (red contours), 15Z July 31, 2005, grell4day3 model run.

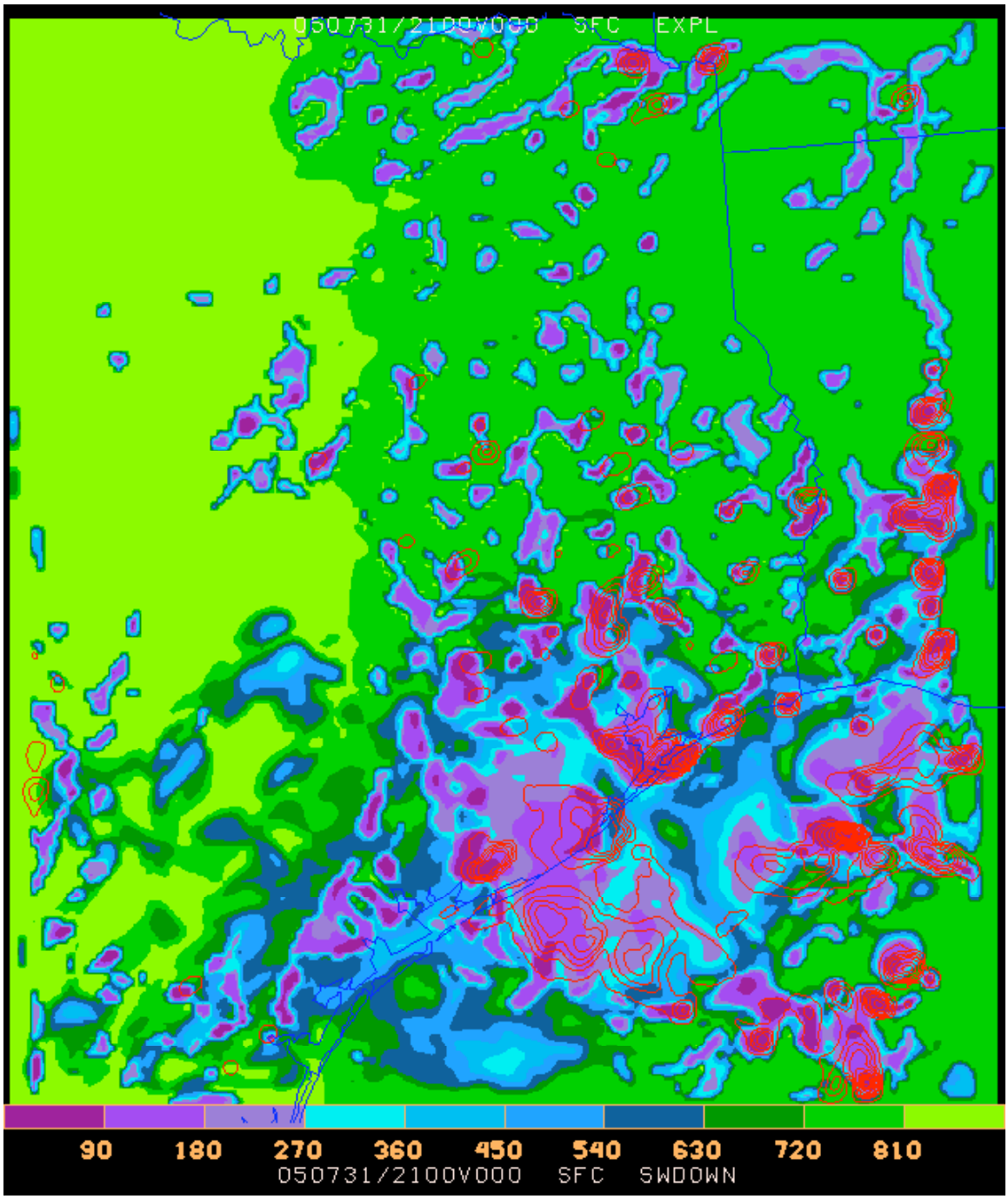

Figure 16: Shortwave solar radiation reaching the ground (shading) and 1-h precipitation (red contours), 21Z July 31, 2005, orignudg4day3 model run.

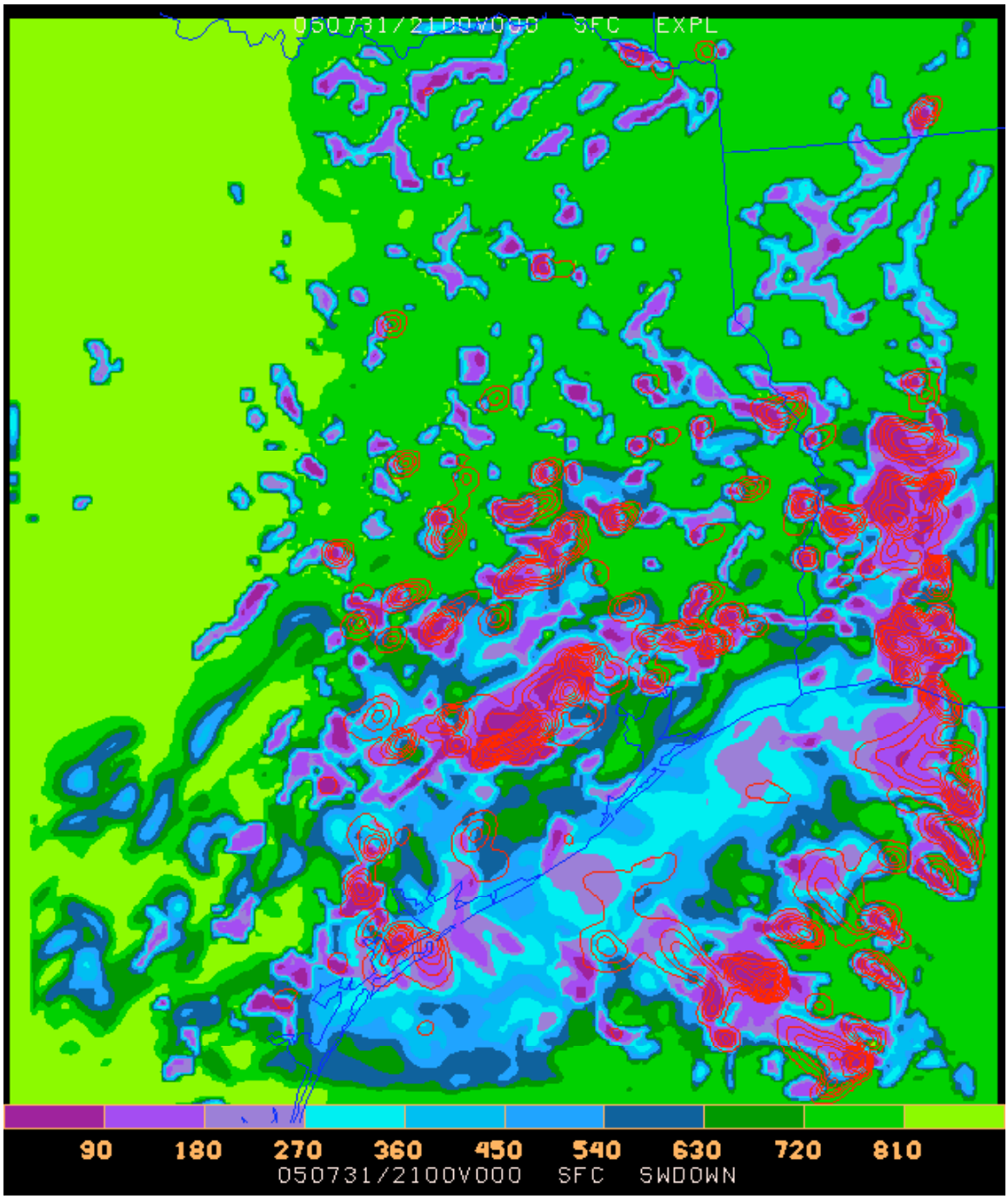

Figure 17: Shortwave solar radiation reaching the ground (shading) and 1-h precipitation (red contours), 21Z July 31, 2005, nonudg4day3 model run.

The model run without nudging is even worse (Fig. 17). Widespread convection dominates the whole of southeast Texas and southwest Louisiana. Coastal regions are mostly clear of precipitation, but are largely covered with clouds.

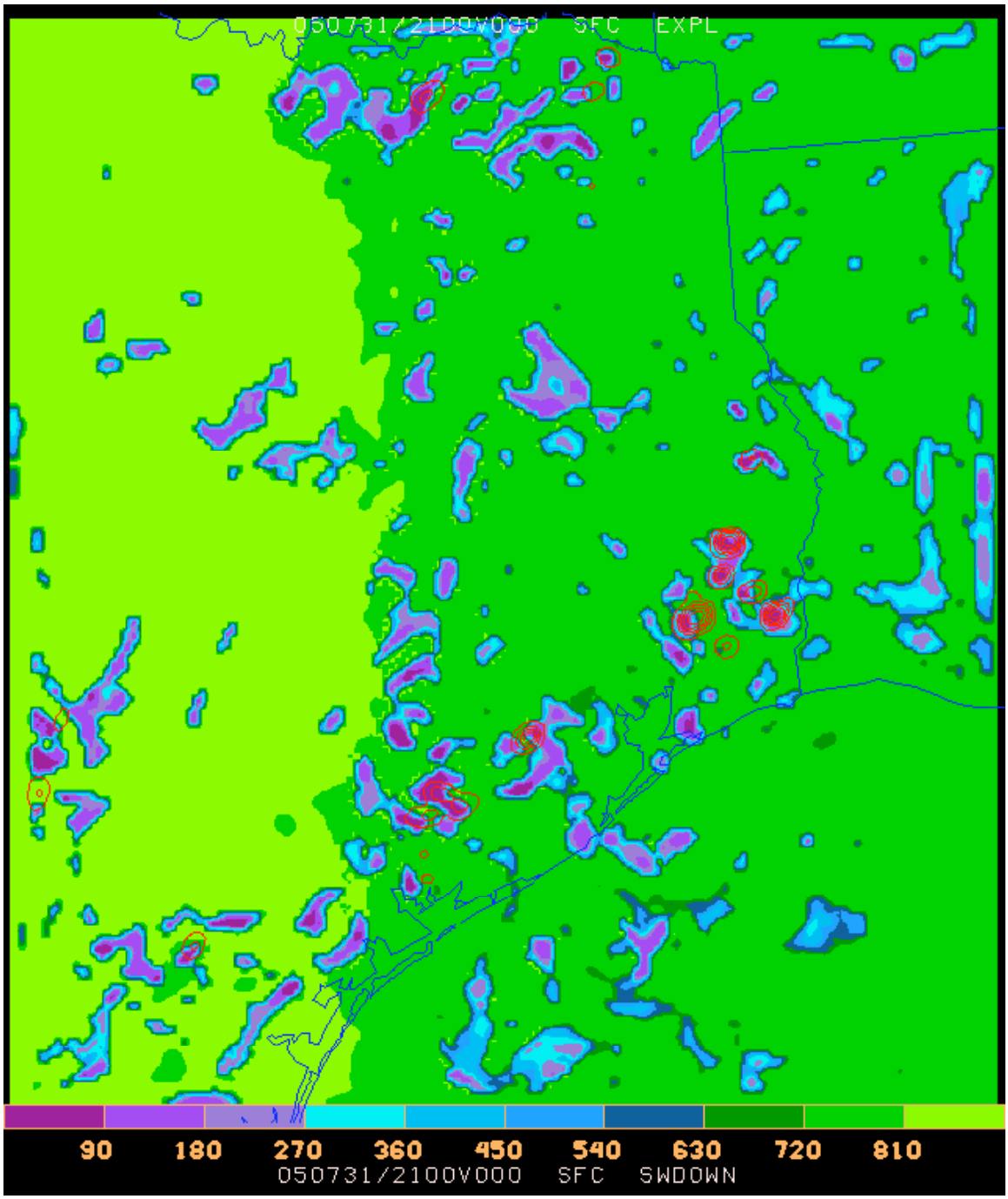

Figure 18: Shortwave solar radiation reaching the ground (shading) and 1-h precipitation (red contours), 21Z July 31, 2005, grell4day3 model run.

Only the grell4day3 has a reasonable distribution of convection. The convection north and northwest of Beaumont is not far from the actual area of convection, while the scattered precipitation west of Houston and north of Dallas is incorrect. On the whole, while convection is still too active in this model run, the simulation may be close enough

to the truth to permit a realistic photochemical simulation. The same cannot be said about the other four model runs.

c) August 1, 2005

The evolution of clouds and precipitation is clearly shown by the visible satellite imagery on this day. The day was wetter than the previous two days. Scattered convection was present offshore at 1431Z (Fig. 19), and an individual convective element had moved onshore east of Galveston Bay by 1731Z (Fig. 20). Also, boundary-layer cumulus had developed across most of East Texas. Convection was firing all along the coast by 2031Z (Fig. 21) as well as in widespread areas north and northwest of Houston. Finally, by 2331Z, most of the remaining deep convection was about 100 km inland from the Gulf Coast, with considerable anvil development.

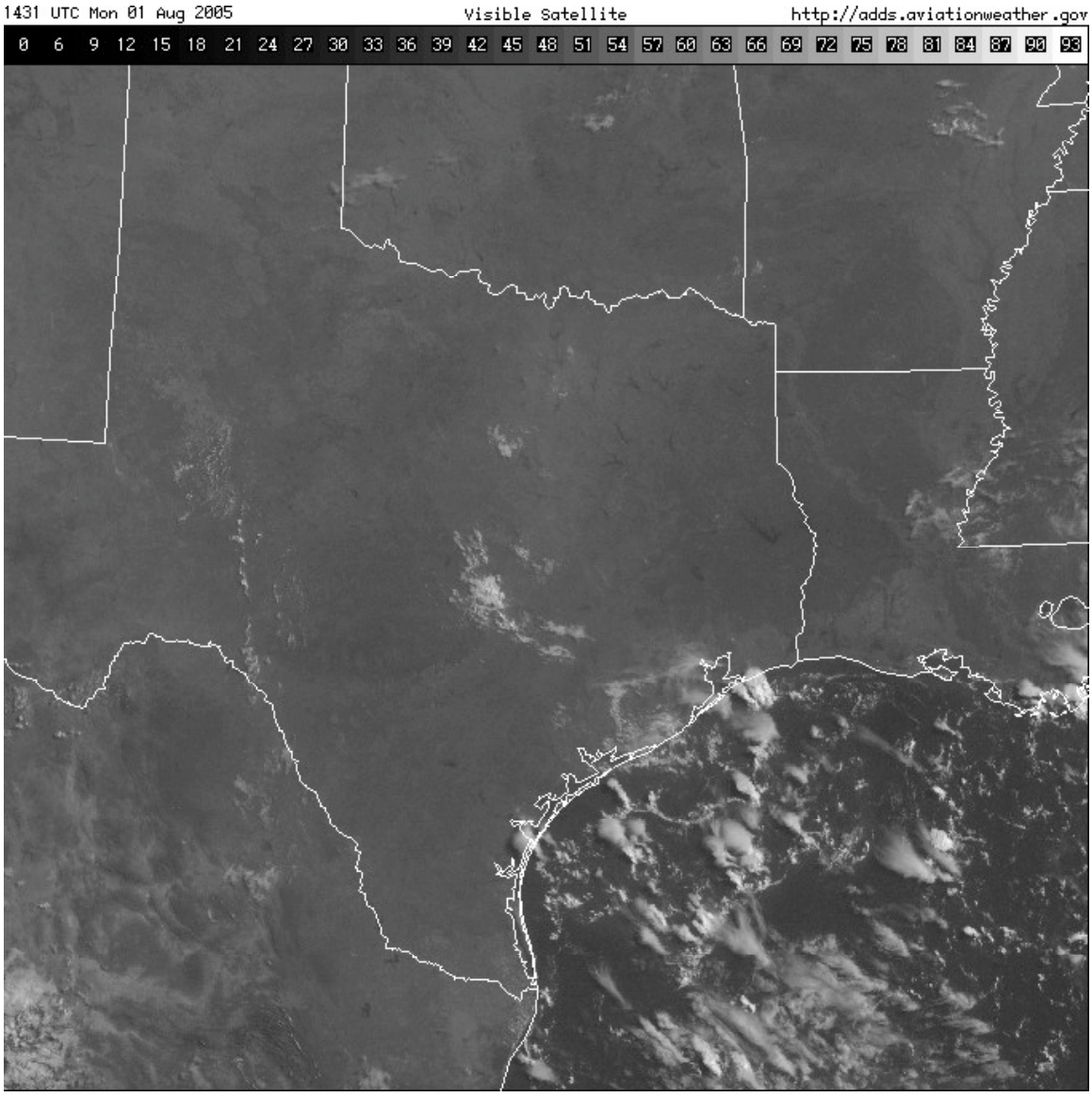

Figure 19: Visible satellite image, 1431Z August 1, 2005.

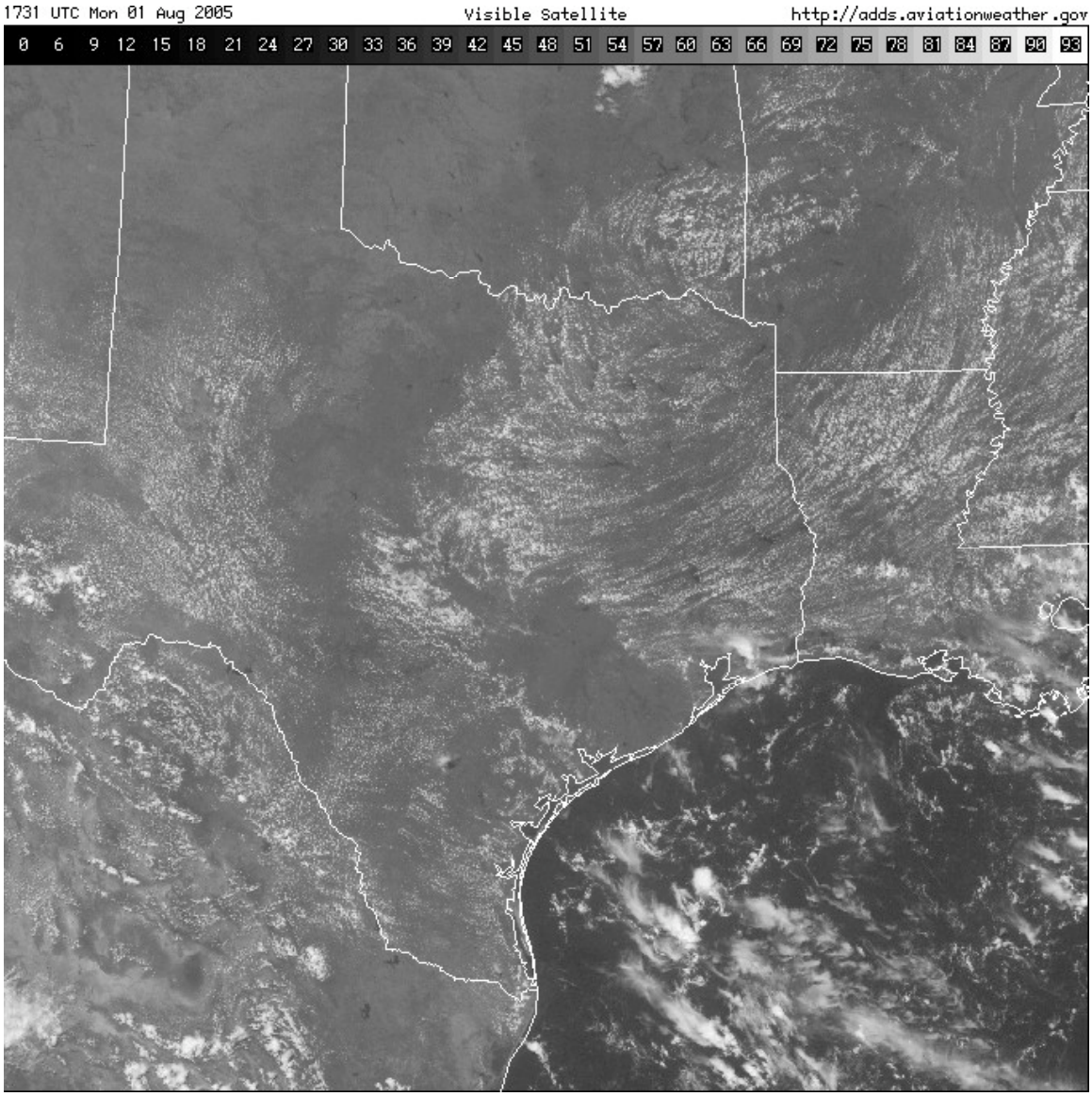

Figure 20: Visible satellite image, 1731Z August 1, 2005.

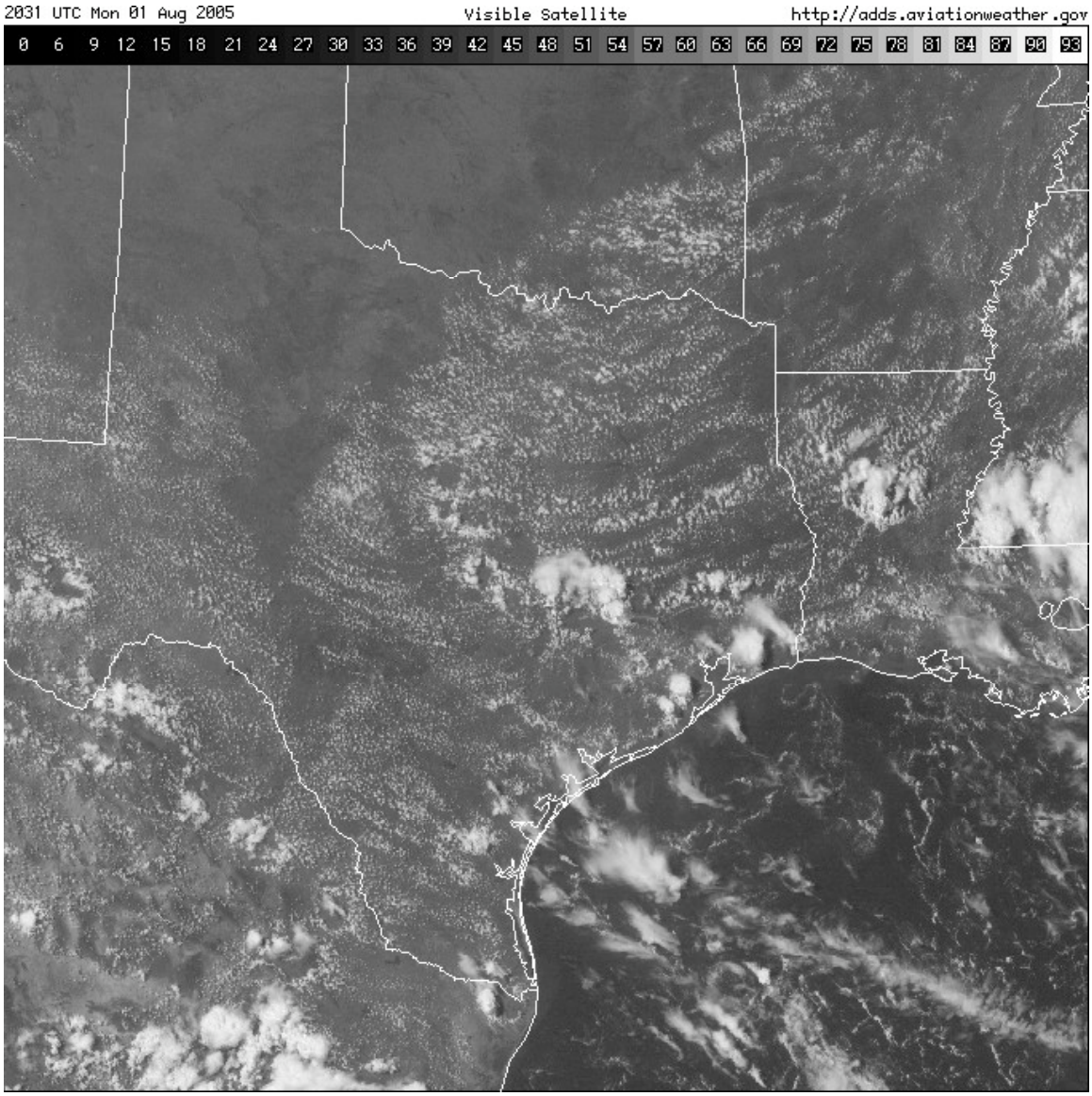

Figure 21: Visible satellite image, 2031Z August 1, 2005.

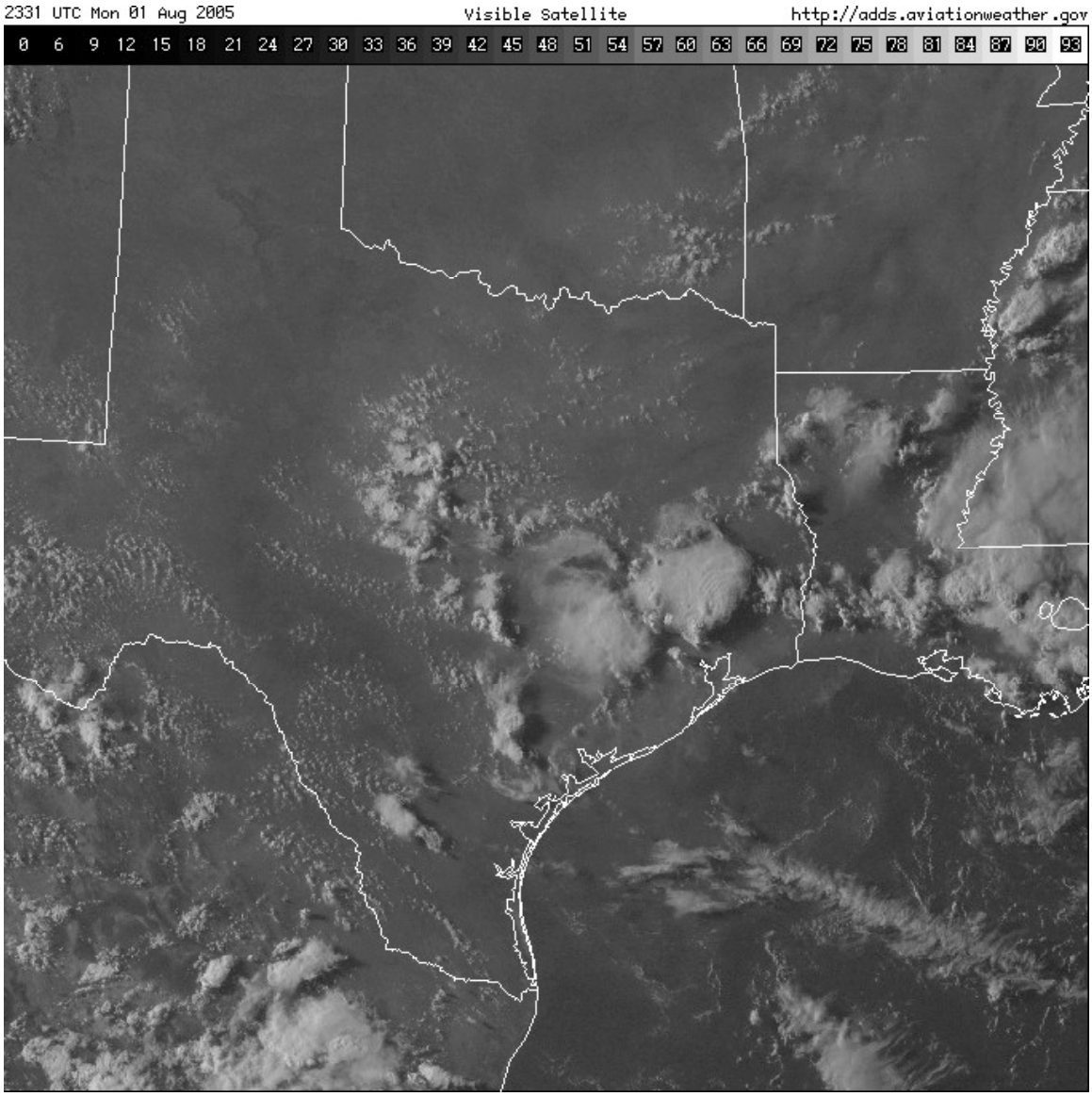

Figure 22: Visible satellite image, 2331Z August 1, 2005.

The orignudg4day3 model run continues the pattern of the previous two days, with too much convection. At 15Z (Fig. 23), convection is widespread offshore, affecting a much larger area than the observed convection. At 18Z (Fig. 24), rather than dying off, convection is still widespread offshore and has begun to occur inland in south-central Texas. While the satellite image (Fig. 21) indicates that skies remained generally scattered and open to solar radiation at 21Z, the orignudg4day3 run has produced widespread thick cloud cover across southeast Texas due to its overzealous convection (Fig. 25). Clouds continue to spread across southeast Texas through the rest of the afternoon (Fig. 26). The nonudg4day3 model run (not shown) has even more widespread convection, and the other explicit runs are similar to orignudg4day3.

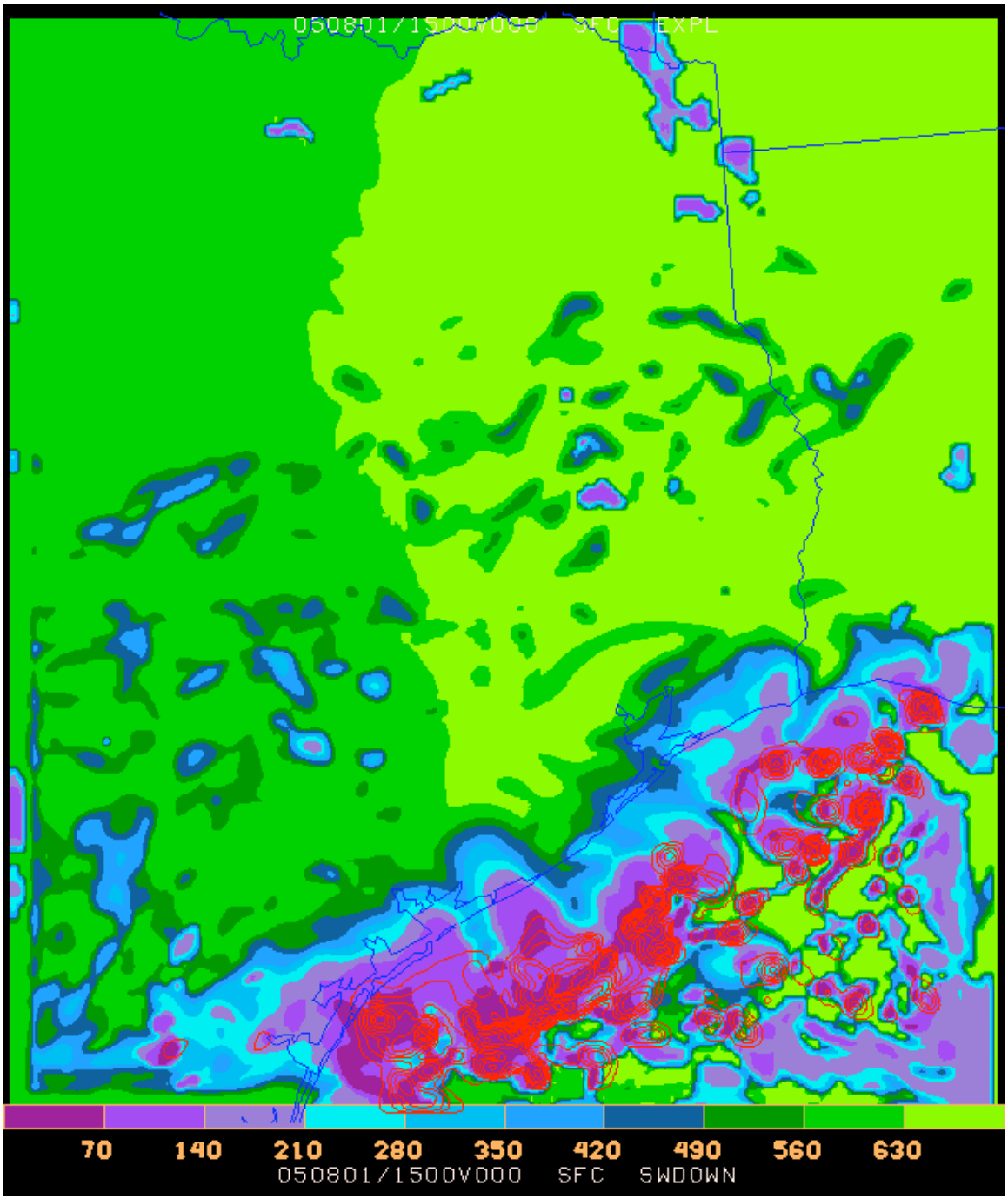

Figure 23: Shortwave solar radiation reaching the ground (shading) and 1-h precipitation (red contours), 15Z August 1, 2005, orignudg4day3 model run.

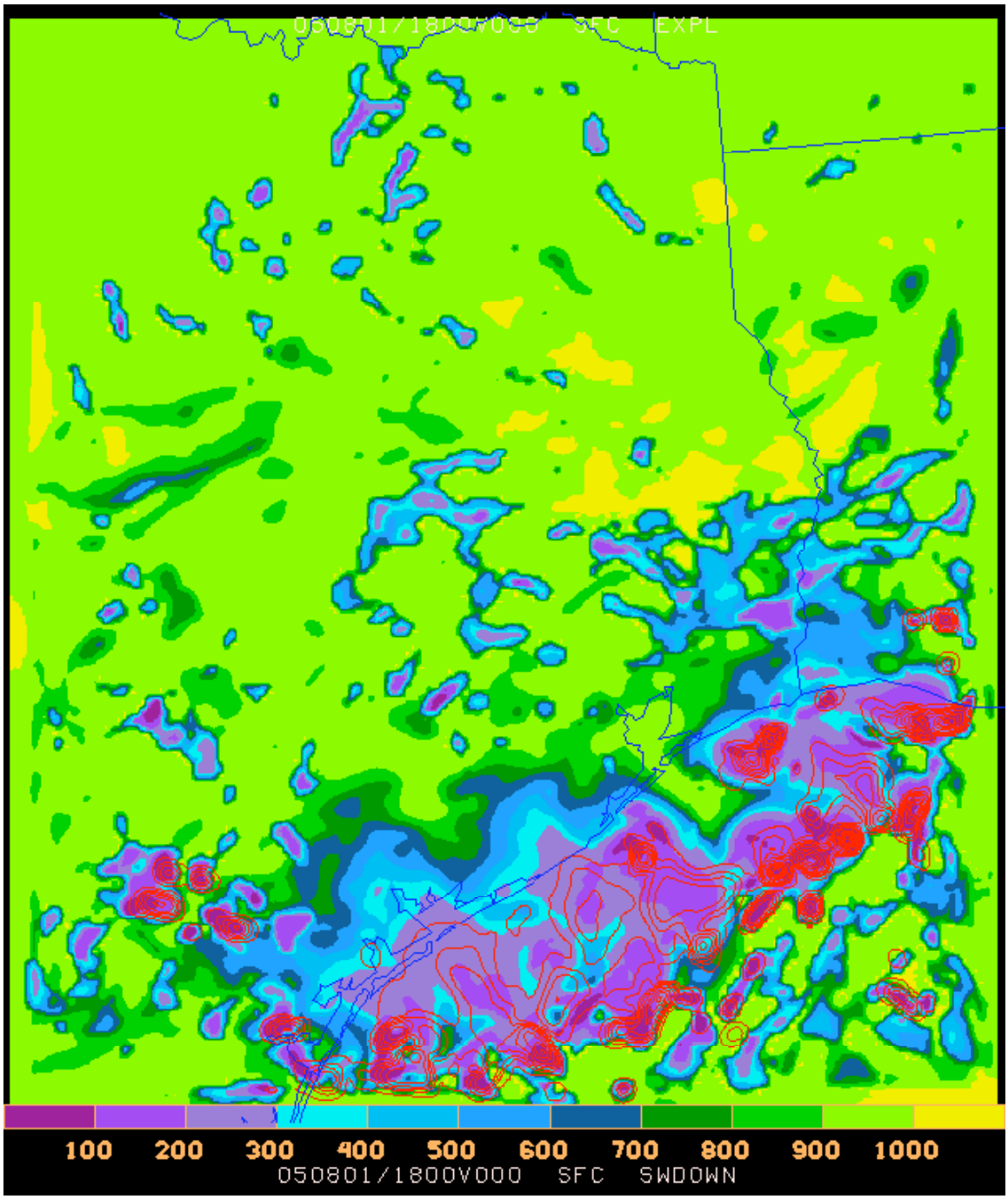

Figure 24: Shortwave solar radiation reaching the ground (shading) and 1-h precipitation (red contours), 18Z August 1, 2005, orignudg4day3 model run.

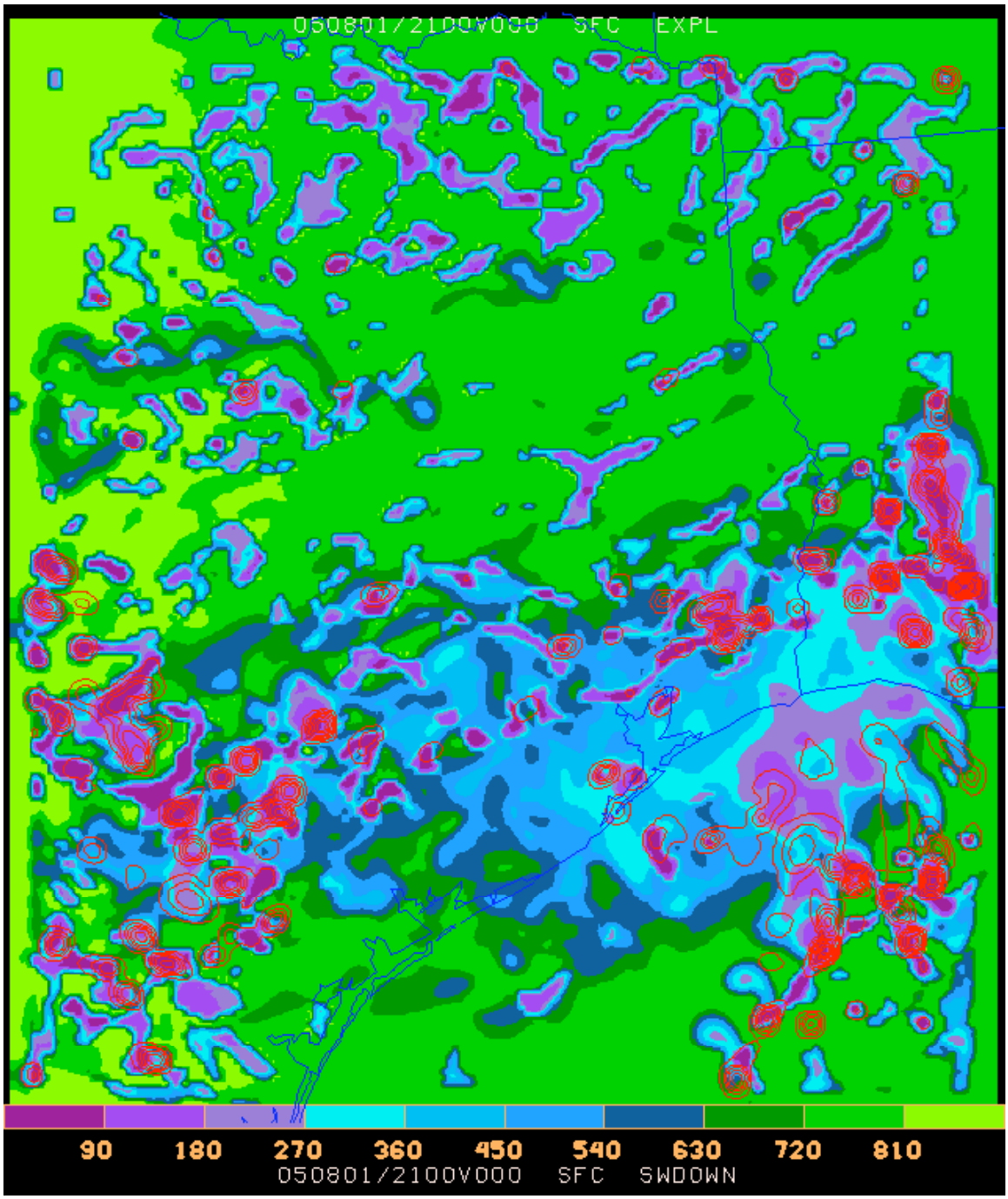

Figure 25: Shortwave solar radiation reaching the ground (shading) and 1-h precipitation (red contours), 21Z August 1, 2005, orignudg4day3 model run.

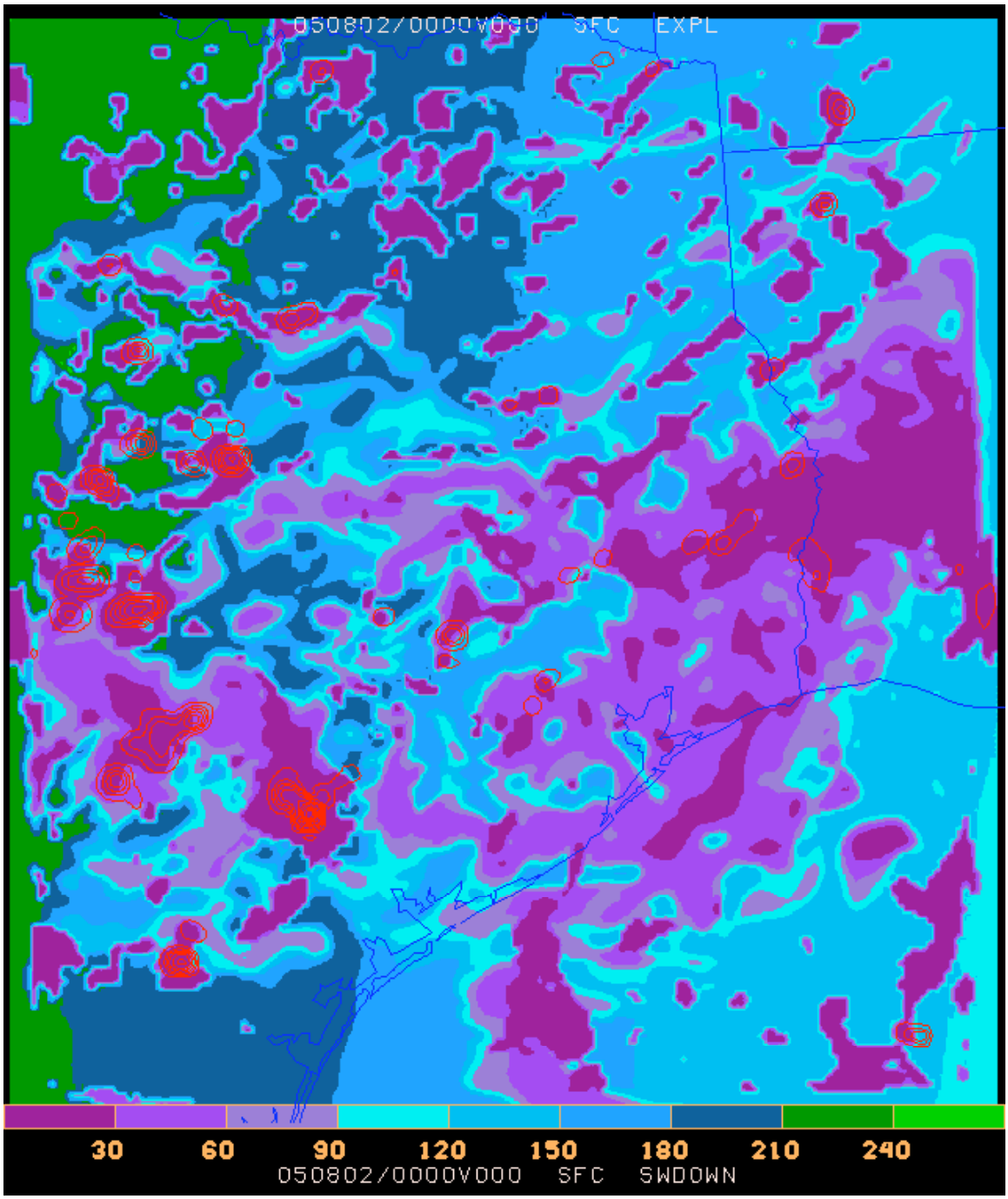

Figure 26: Shortwave solar radiation reaching the ground (shading) and 1-h precipitation (red contours), 00Z August 2, 2005, orignudg4day3 model run.

The grell4day3 run, by contrast, is remarkably accurate, if slightly dry. At 15Z August 1 (Fig. 27), the convection offshore has not only the appropriate spatial coverage, but almost manages to be accurate in terms of location. Three hours later (not shown), there are scattered clouds in the Houston area, but the only remnant precipitation is well

offshore. At 21Z (Fig. 28), scattered precipitating convection has begun over land at about the right time compared to observations, but the precipitation is too far south. Finally, at 00Z (not shown), scattered clouds remain, and the two most intense precipitating cells are about 100 km onshore, also in agreement with observations.

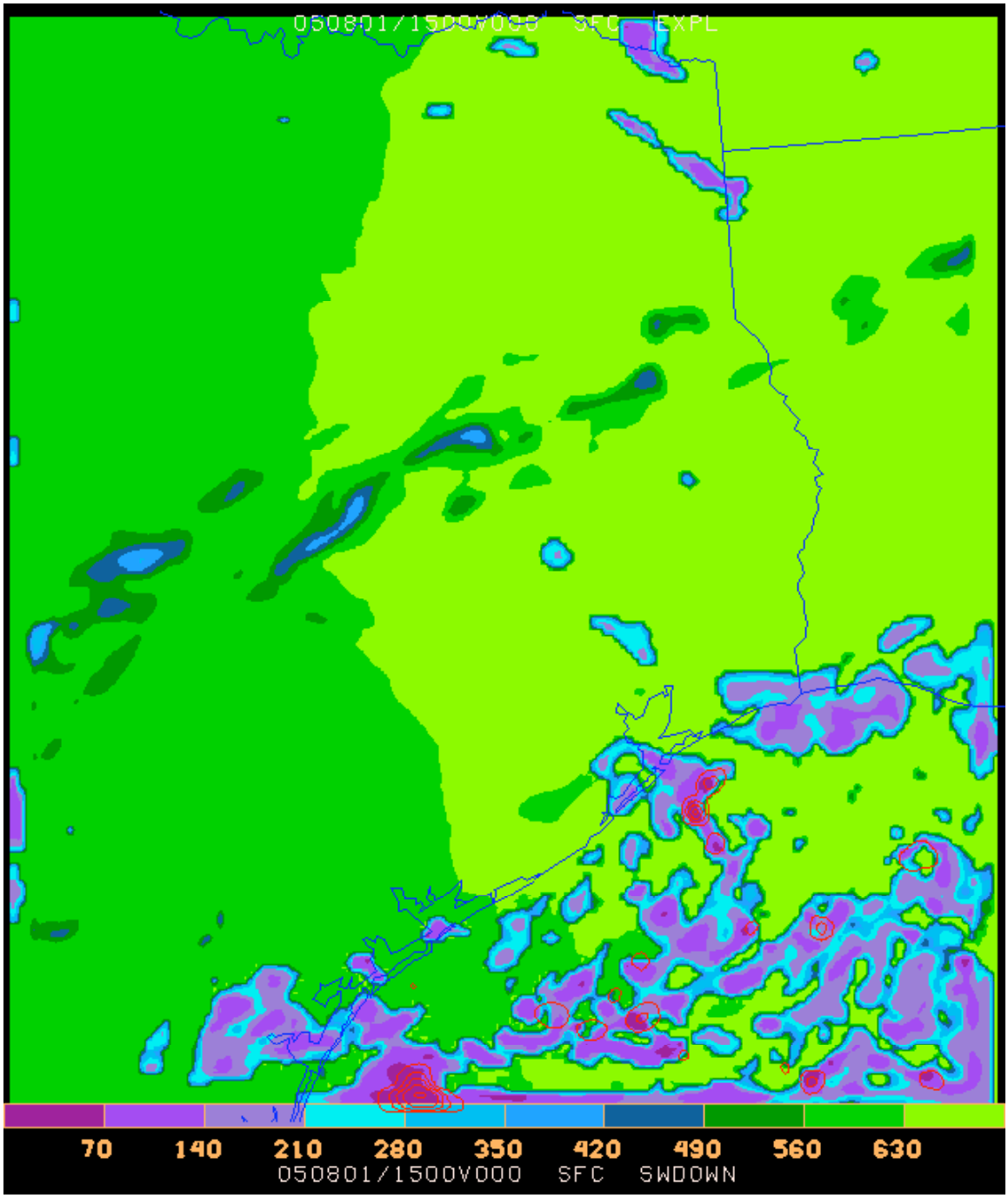

Figure 27: Shortwave solar radiation reaching the ground (shading) and 1-h precipitation (red contours), 15Z August 1, 2005, grell4day3 model run.

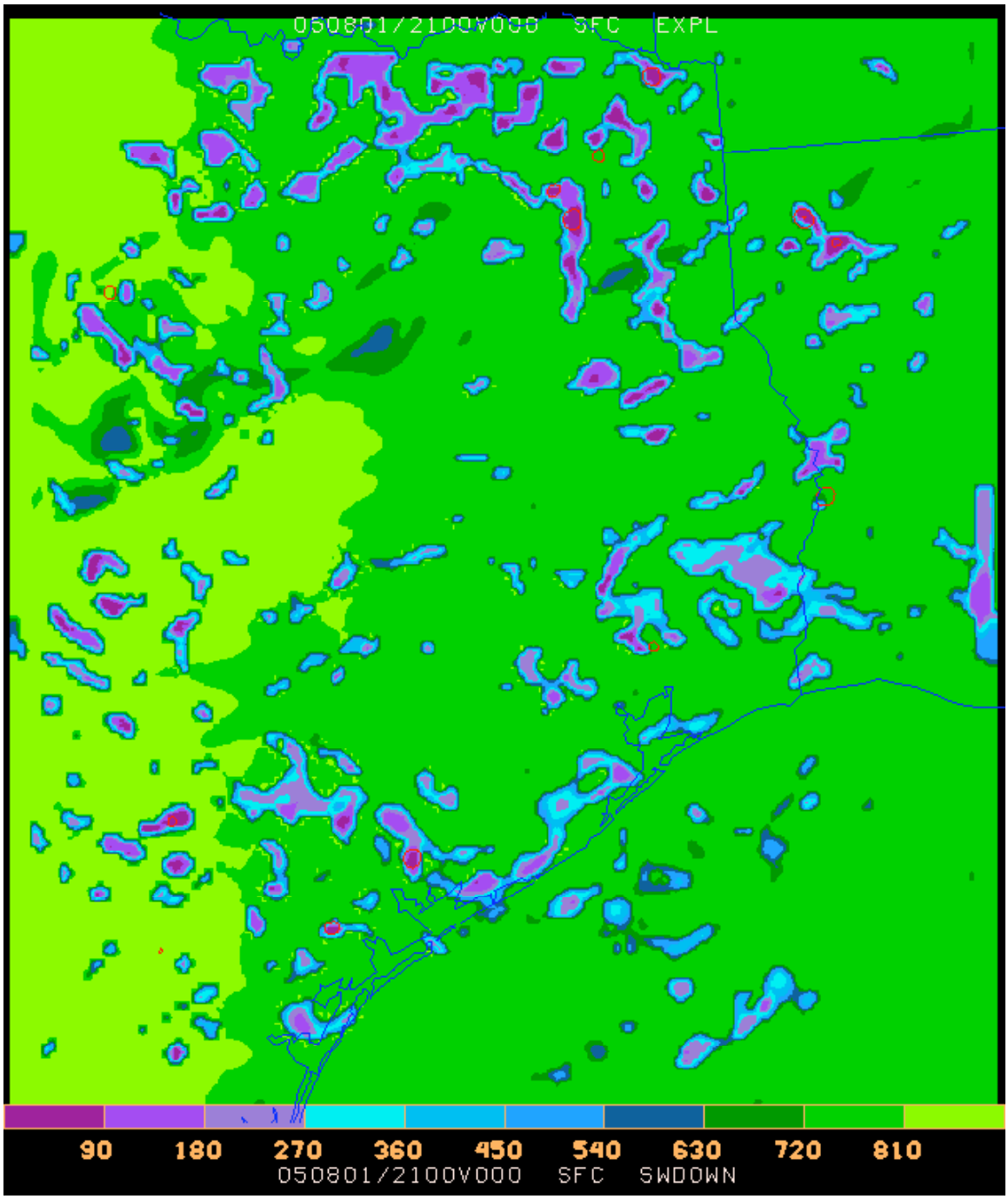

Figure 28: Shortwave solar radiation reaching the ground (shading) and 1-h precipitation (red contours), 21Z August 1, 2005, grell4day3 model run.

The streak of clouds running southwest to northeast across the center of Figs. 27 and 28 appear to be due to a band of higher clouds. These clouds were not present in the observations, but probably had little effect on the simulation.

d) August 2, 2005

Like the previous day, August 2, 2005 featured widespread afternoon convection. As usual, convection in the morning was confined to offshore locations (Fig. 29). In the afternoon, most of the convection occurred between Houston and Dallas, allowing plenty of photochemistry to take place in those two cities.

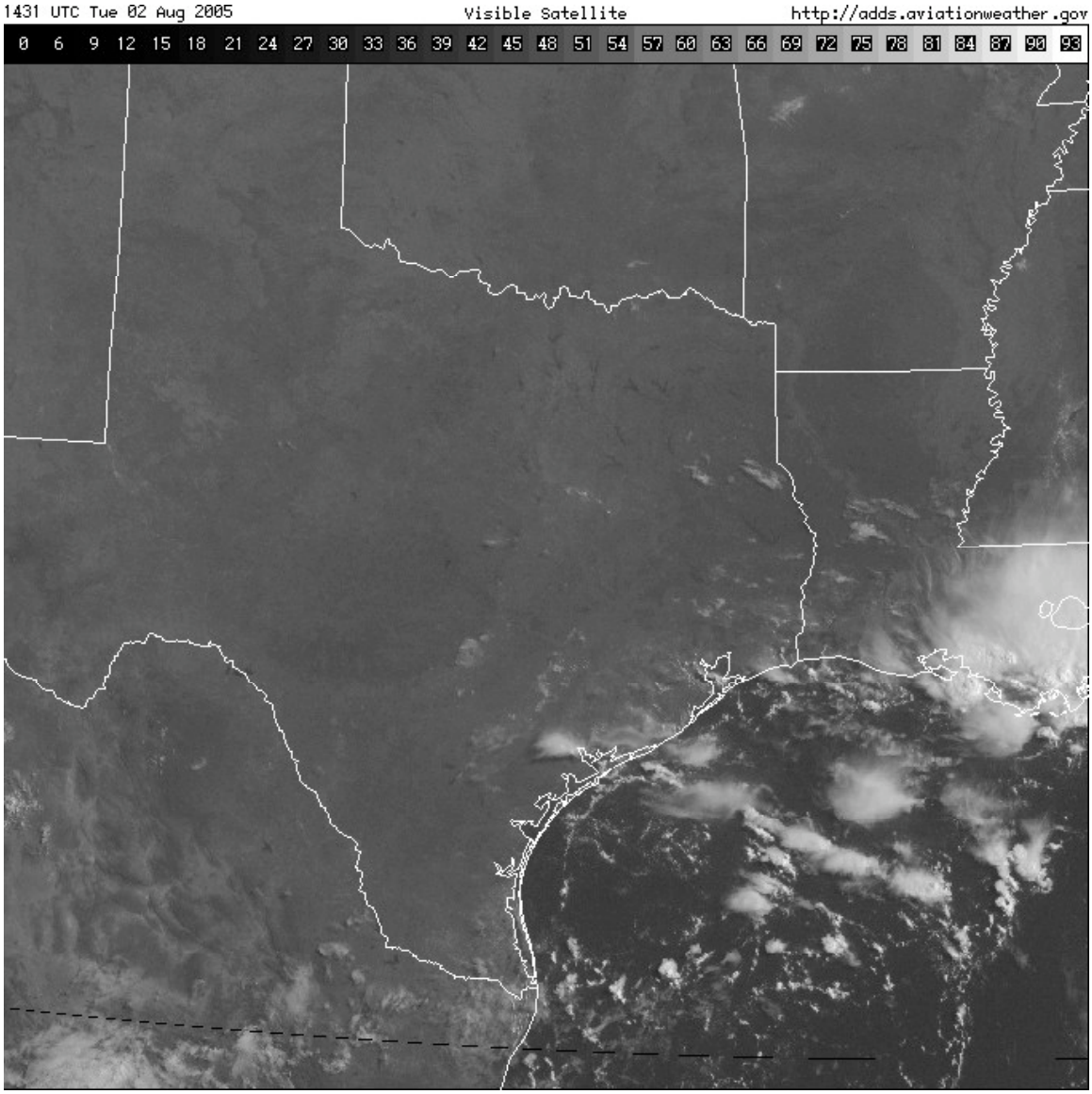

Figure 29: Visible satellite image, 1431Z August 2, 2005.

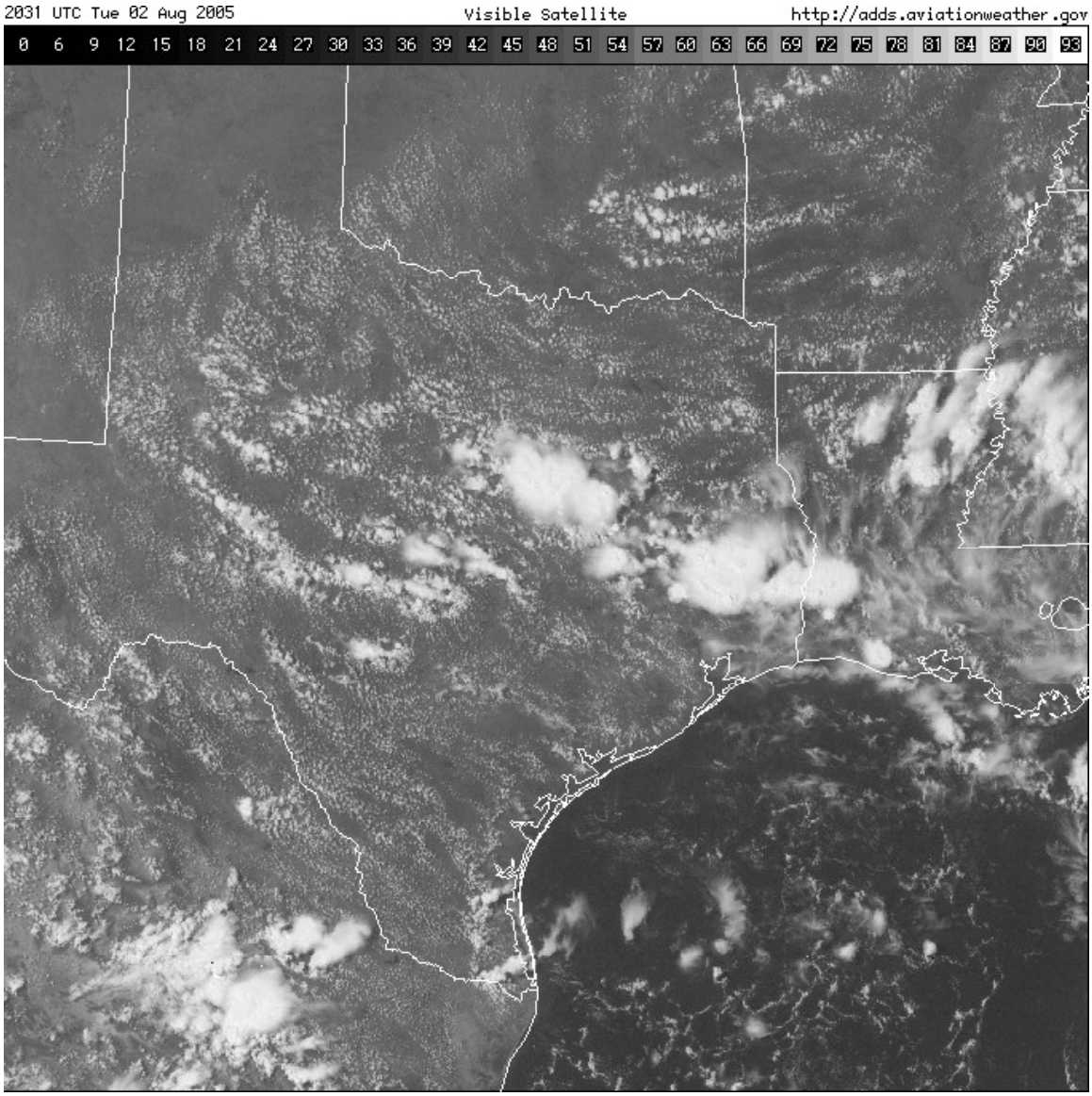

Figure 30: Visible satellite image, 2031Z August 2, 2005.

The orignudg4day3 model run, like the other three explicit runs, again produced too much convection. At 15Z (Fig. 31), the model erroneously had widespread convection and cloud cover along the coast, and considerable cloud cover left over from the previous day's convection inland. At 21Z (Fig. 32), Houston was completely socked in by clouds left over from the coastal convection. The model-simulated convection farther inland was better, with most of the active convection in east-central Texas.

The grell4day3 model run managed an excellent cloud and precipitation forecast for 15Z (Fig. 33), except that the only strong shower over land was directly over the Houston Ship Channel. At 21Z (Fig. 34), the model failed to produce the developing deep

convection across east-central Texas, and again had too many showers in the immediate Houston area.

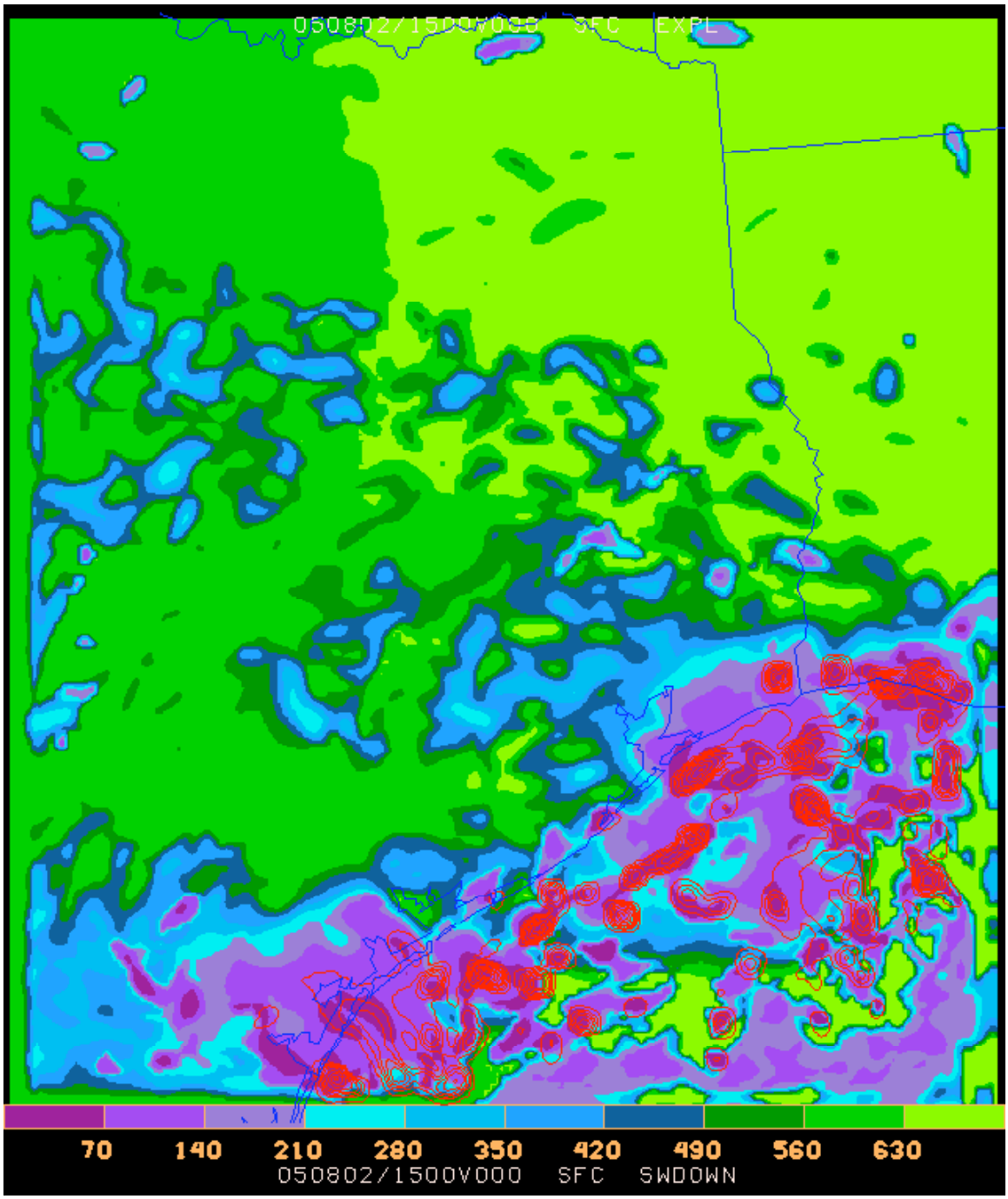

Figure 31: Shortwave solar radiation reaching the ground (shading) and 1-h precipitation (red contours), 15Z August 2, 2005, orignudg4day3 model run.

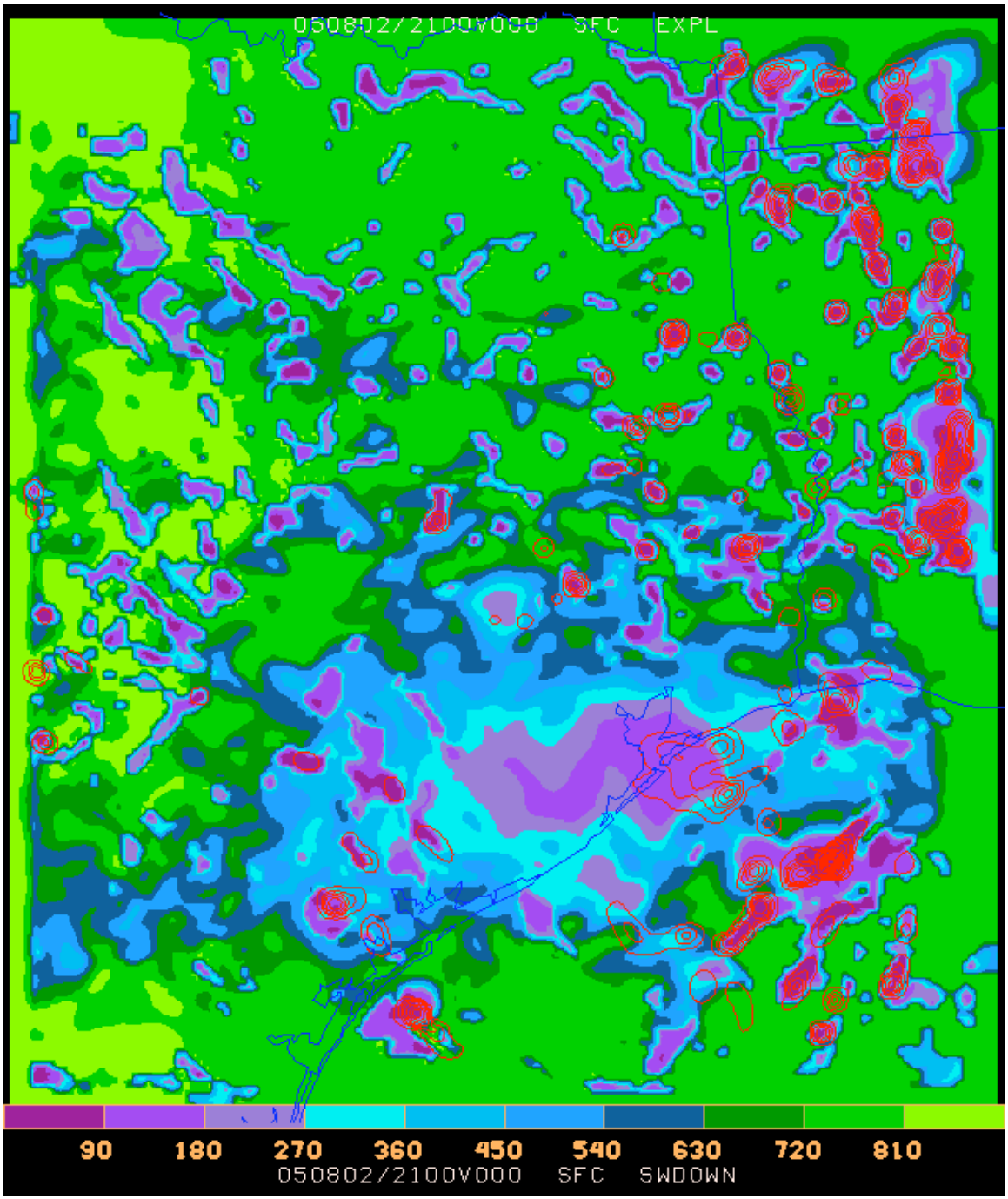

Figure 32: Shortwave solar radiation reaching the ground (shading) and 1-h precipitation (red contours), 21Z August 2, 2005, orignudg4day3 model run.

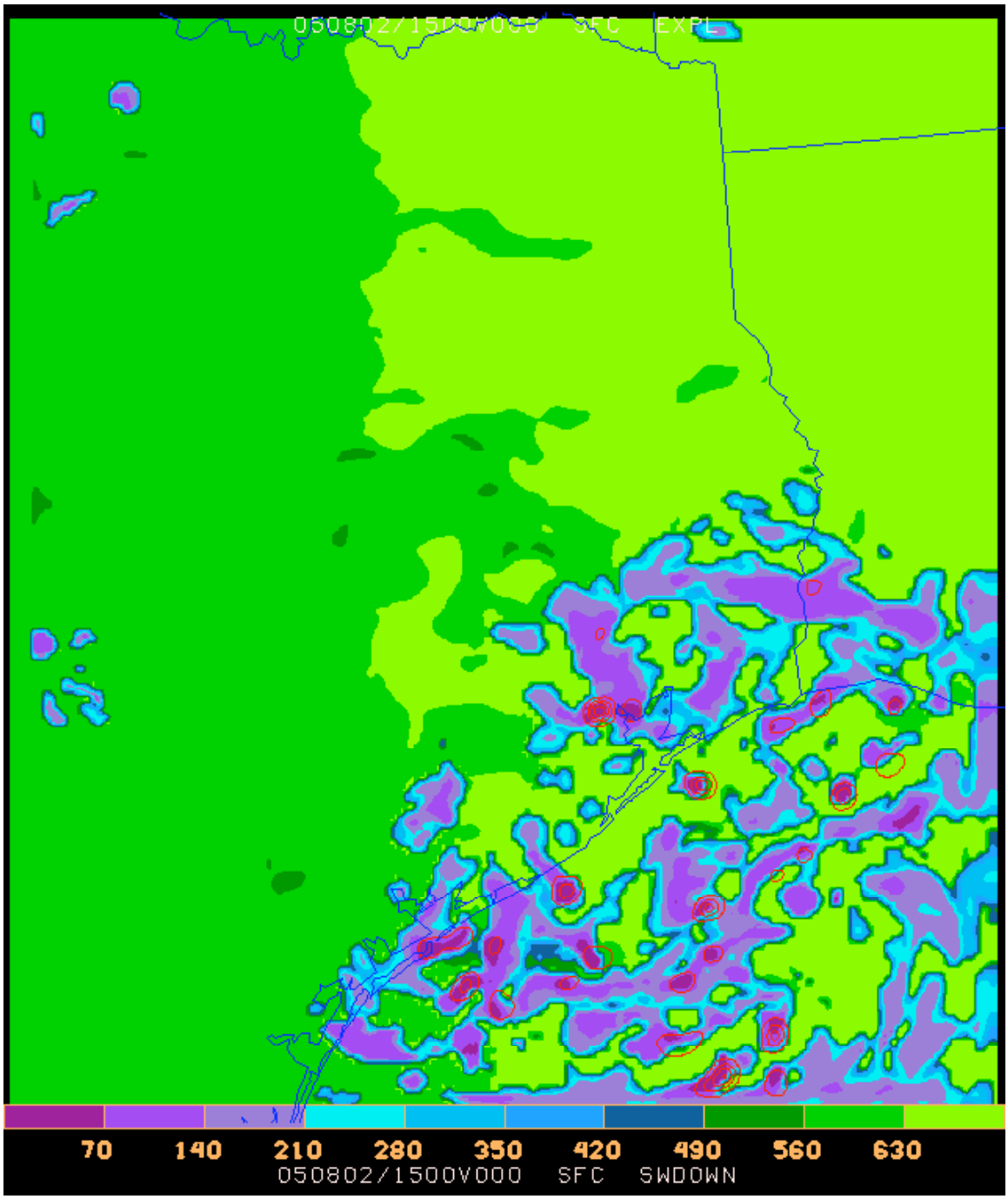

Figure 33: Shortwave solar radiation reaching the ground (shading) and 1-h precipitation (red contours), 15Z August 2, 2005, grell4day3 model run.

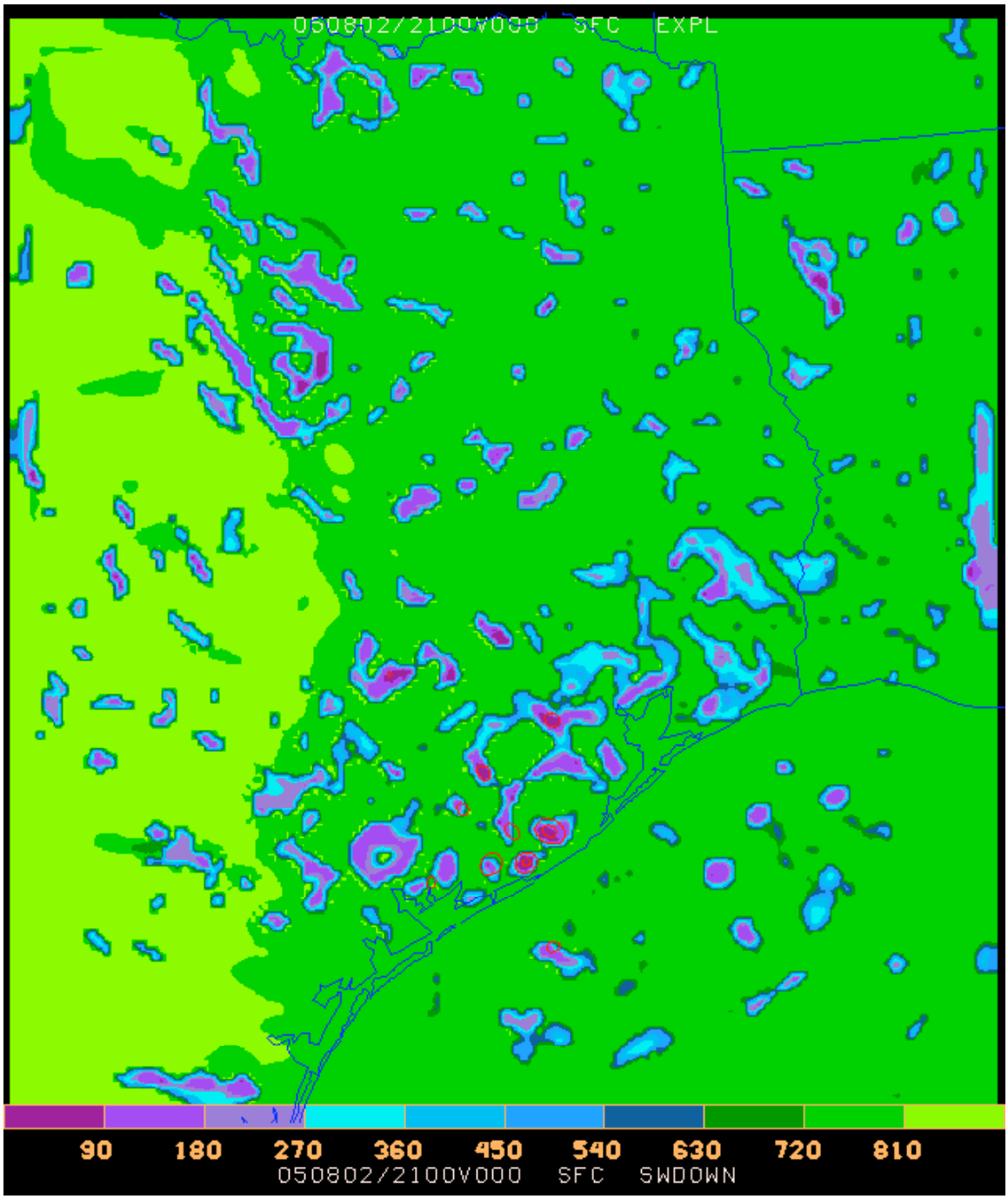

Figure 34: Shortwave solar radiation reaching the ground (shading) and 1-h precipitation (red contours), 21Z August 2, 2005, grell4day3 model run.

e) Implications

Clouds and precipitation were considered first in this model evaluation because they affect all other aspects of model accuracy. When there is extensive coastal cloud cover or precipitation, the sea breeze will be significantly modified. The development of the

nighttime sea-breeze low-level jet should depend on the robustness of the sea breeze during the day. Statistical comparisons of models and observations for understanding the characteristics and performance of the obs nudging will not be useful in areas of widespread convection where temperatures and winds are strongly affected by random variations in convection. Mixing heights will likewise reflect convective activity in areas where such convection occurs.

With regard to the sea breeze, a sea breeze relatively undisturbed by convection only seems possible on July 30 in all model runs. In the grell4day3 run, convection is sufficiently scattered that a well-developed sea breeze is possible on the other three days. Since the nonudg4day3 model run will only possibly have a sea breeze on July 30, an assessment of the effect of nudging on the sea breeze is only possible on that date.

In view of the widespread convection, the nighttime sea-breeze low-level jet will constitute a stringent test of the obs nudging. With the sea breeze expected to be underdeveloped, the numerical model dynamics should be unable to reproduce the sea-breeze low-level jet, leaving a substantial difference between observations and model. It will be useful to examine how well the model handles large disagreements between simulation and observations.

All days and model simulations had substantial areas over land with clear skies, so it should be possible to do an extensive comparison of mixing heights on all days. Over water, the widespread nature of the convection probably masked the natural planetary boundary layer, but with no offshore observations for nudging during this period, nudging is not expected to have an effect on offshore mixing heights anyway.

Statistical comparisons of model output with observations should be viable throughout the period in the Dallas-Fort Worth area, because convection was relatively sparse there. In the Houston area, because of the strong and random influence of convection on observations, an analysis of all model runs is only viable for July 30, with the grell4day3 run worth examining on August 1 and 2 as well.

Finally, one important issue with respect to clouds and precipitation is the role of nudging in triggering convection. Of concern with nudging is the possibility that, with widely-spaced observations, nudging will produce artificial convergence and divergence patterns that will erroneously cause widespread triggering of convection. That was not a problem in the four days examined here. In all four days, the convection was more widespread without nudging than with it, and there was no apparent tendency for simulated convection to develop around profiler observing sites.

4. Mixing Heights and Land/Sea Breezes

a) Mixing Heights

The mixing heights, as noted at the end of the previous section, may generally be reliably compared only in the absence of widespread convection. Keeping this in mind, mixing heights are examined in this section at 16Z (1000 CST), while the planetary boundary layer is growing rapidly, and 21Z (1500 CST), when the planetary boundary layer is close to its maximum depth.

In general, the nudging runs (orignudg4day3, testnudg4day3, and nohve4day3) have rather similar mixing heights away from convection. An example of this is shown in Figs. 35-37, the mixing heights for orignudg4day3, testnudg4day3, and nohve4day3, respectively at 16Z August 1. At this point, differences in precipitation over the preceding few days are probably having an impact on the surface heat fluxes through modulation of the soil moisture. Nevertheless, the mixing heights across the domain are rather similar, both in pattern and magnitude. All three model runs produce mixing heights over 1000 m in north-central Texas and south-central Texas, and mixing heights are simulated to be around 600 m in the Houston area.

On July 30, the grell4day3 mixing heights are very similar to the orignudg4day3 mixing heights and are not shown here. In Figs. 38 and 39 are the orignudg4day3 and nonudg4day3 mixing heights for 16Z July 30 2005. It may be seen that the mixing heights with nudging (Fig. 38) are more spatially variable than the mixing heights without nudging (Fig. 39). For example, without nudging the mixing height almost nowhere exceeds 1500 m or is smaller than 400 m away from convection. With nudging, such areas are considerably more widespread. It is possible that the nudging is introducing false patterns of convergence and divergence, leading to areas with deeper and shallower boundary layers.

There are small mixing height differences at 21Z, too (Figs. 40-41), but most of these differences are directly influenced by convection and it does not seem possible to identify a systematic bias between the two model runs. The large difference in the southwestern part of the model domain is due to the presence of convection in one model run but not the other.

On July 31, mixing height growth in the morning is suppressed by cloudiness near the center of the model domain. Elsewhere, while there are differences between orignudg4day3 and nonudg4day3 mixing heights, there does not appear to be any systematic pattern or bias to the differences. The same is largely true at 21Z (Figs. 42-43) except for a broad area of central Texas in which the orignudg4day3 model run (and other nudging model runs produces mixing heights in excess of 2100 m while the nonudg4day3 simulation generally has mixing heights around 1800 m. At Cleburne, mixing heights were generally between 2100 m and 2700 m during the mid-afternoon, so the simulations with nudging were more accurate in this case.

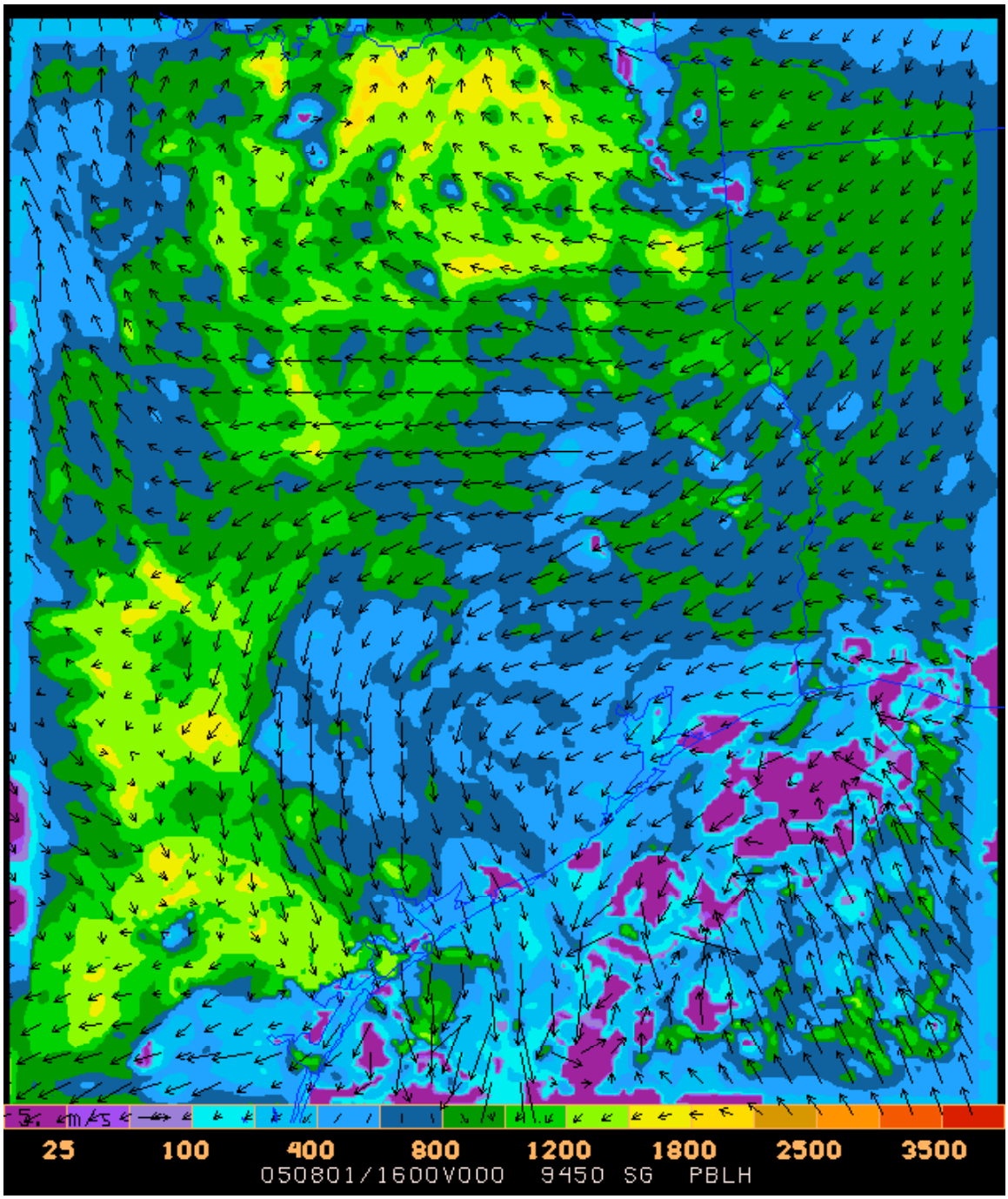

Fig. 35: Mixing heights (m) and .9450 sigma level winds, orignudg4day3 model run, 16Z August 1, 2005.

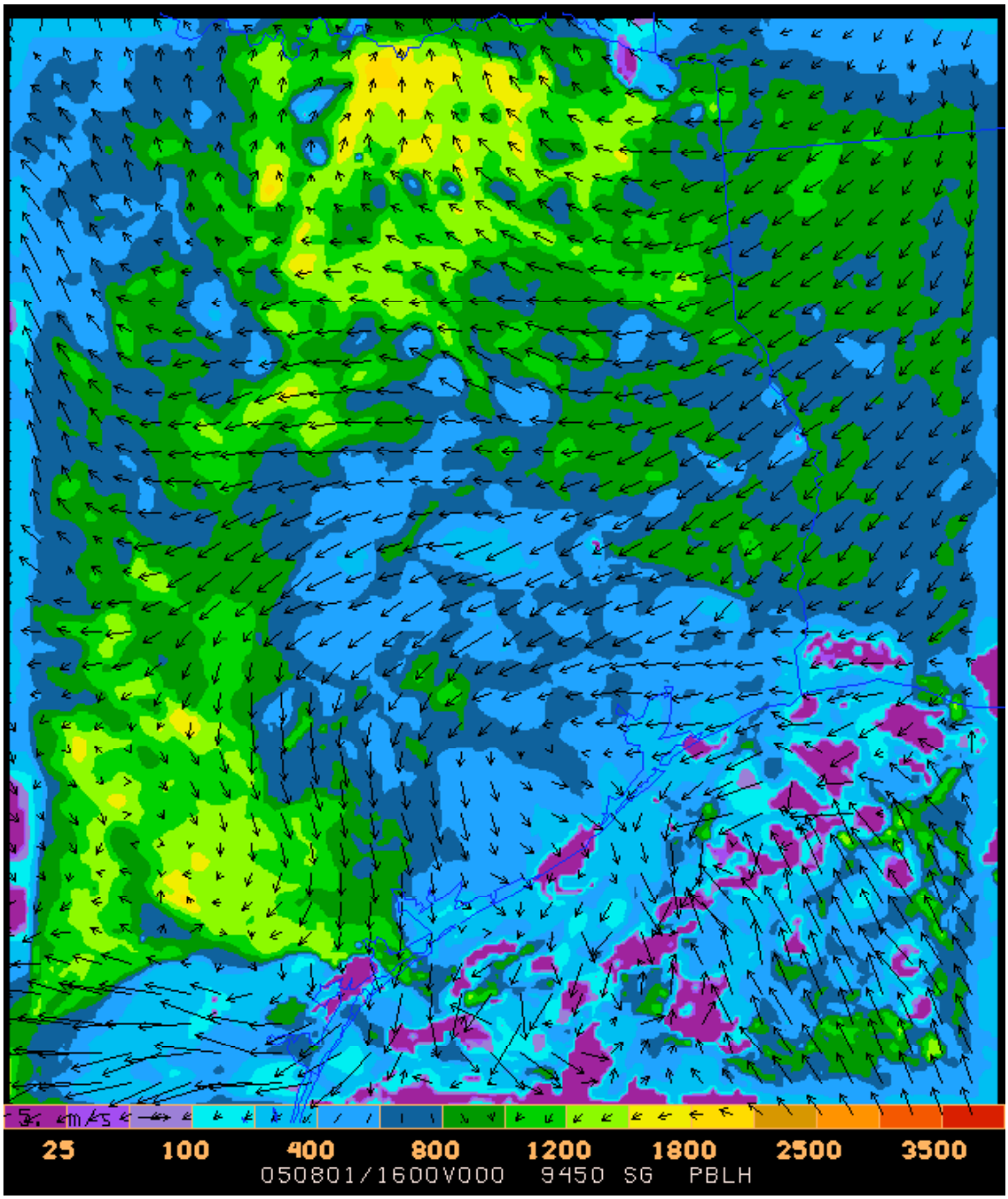

Fig. 36: Mixing heights (m) and .9450 sigma level winds, testnudg4day3 model run, 16Z August 1, 2005.

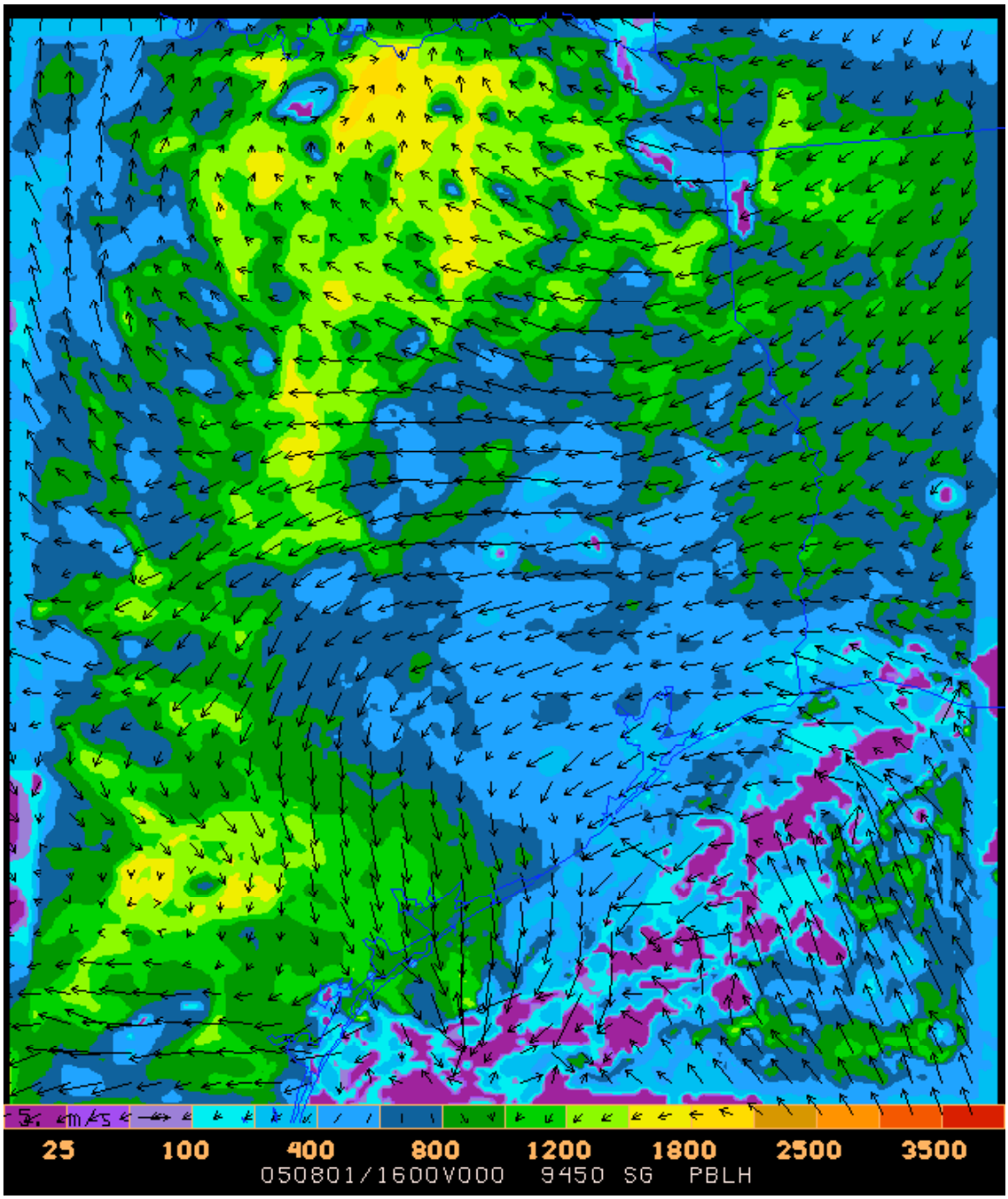

Fig. 37: Mixing heights (m) and .9450 sigma level winds, nohve4day3 model run, 16Z August 1, 2005.

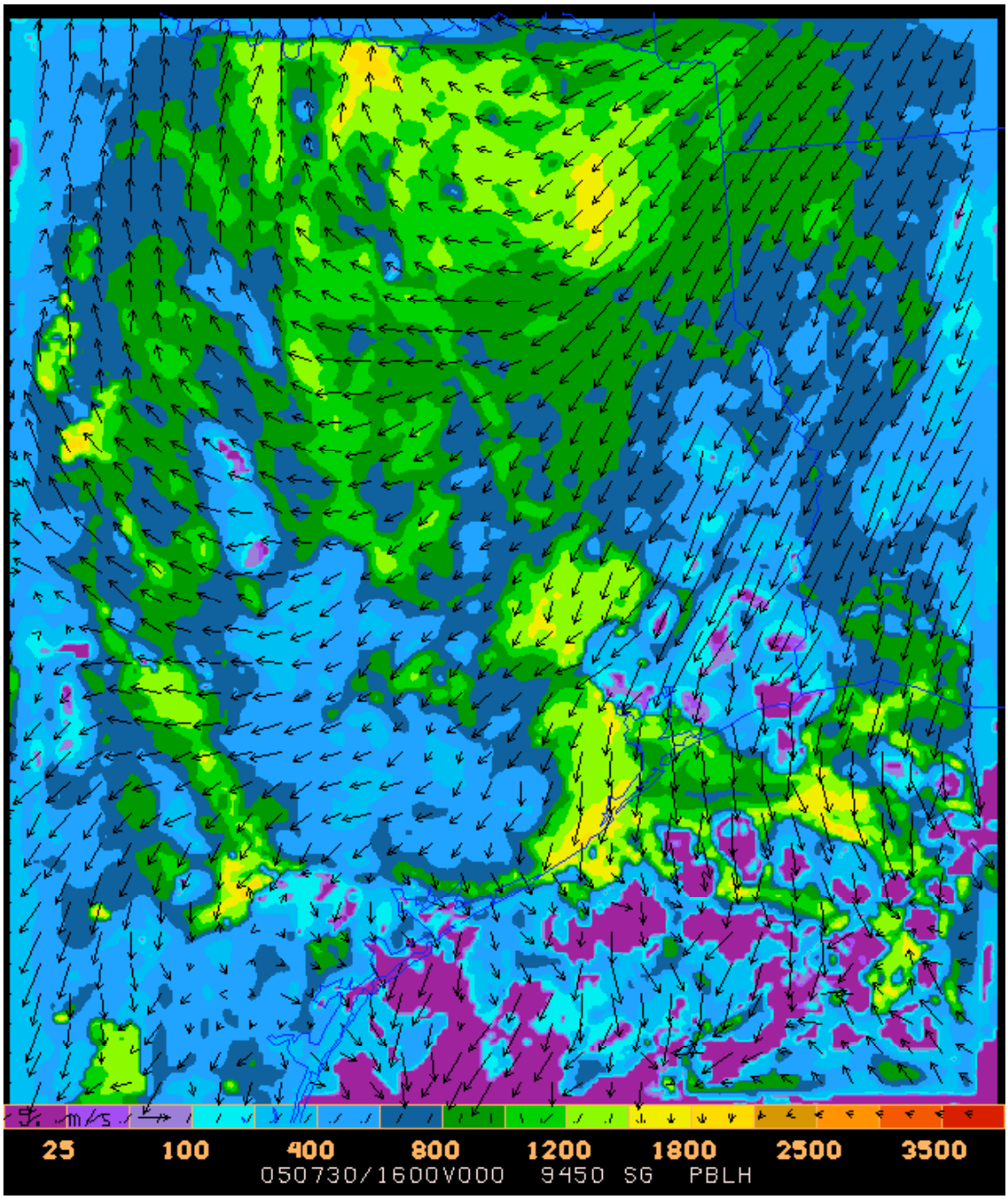

Fig. 38: Mixing heights (m) and .9450 sigma level winds, orignudg4day3 model run, 16Z July 30, 2005.

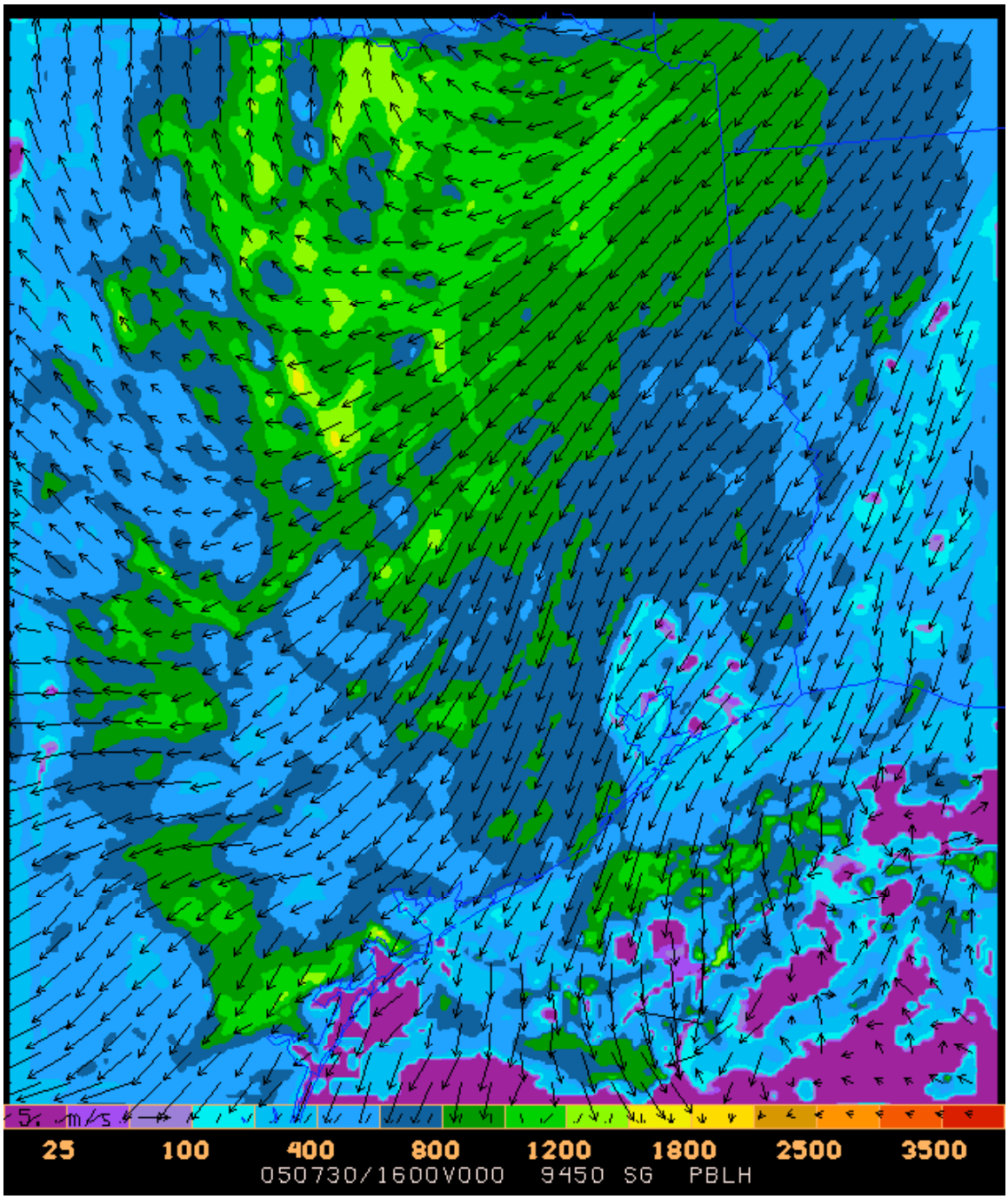

Fig. 39: Mixing heights (m) and .9450 sigma level winds, nonudg4day3 model run, 16Z July 30, 2005.

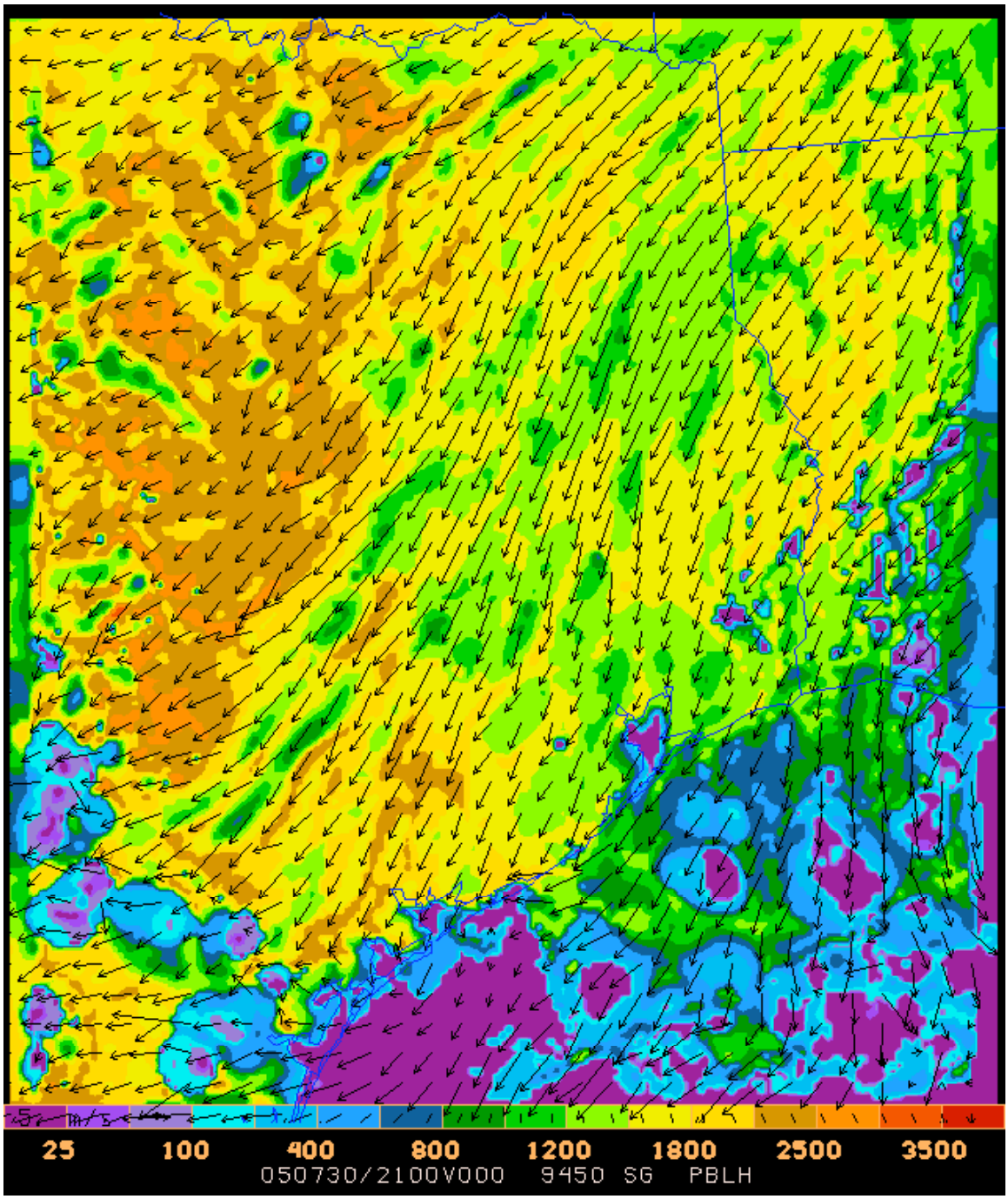

Fig. 40: Mixing heights (m) and .9450 sigma level winds, orignudg4day3 model run, 21Z July 30, 2005.

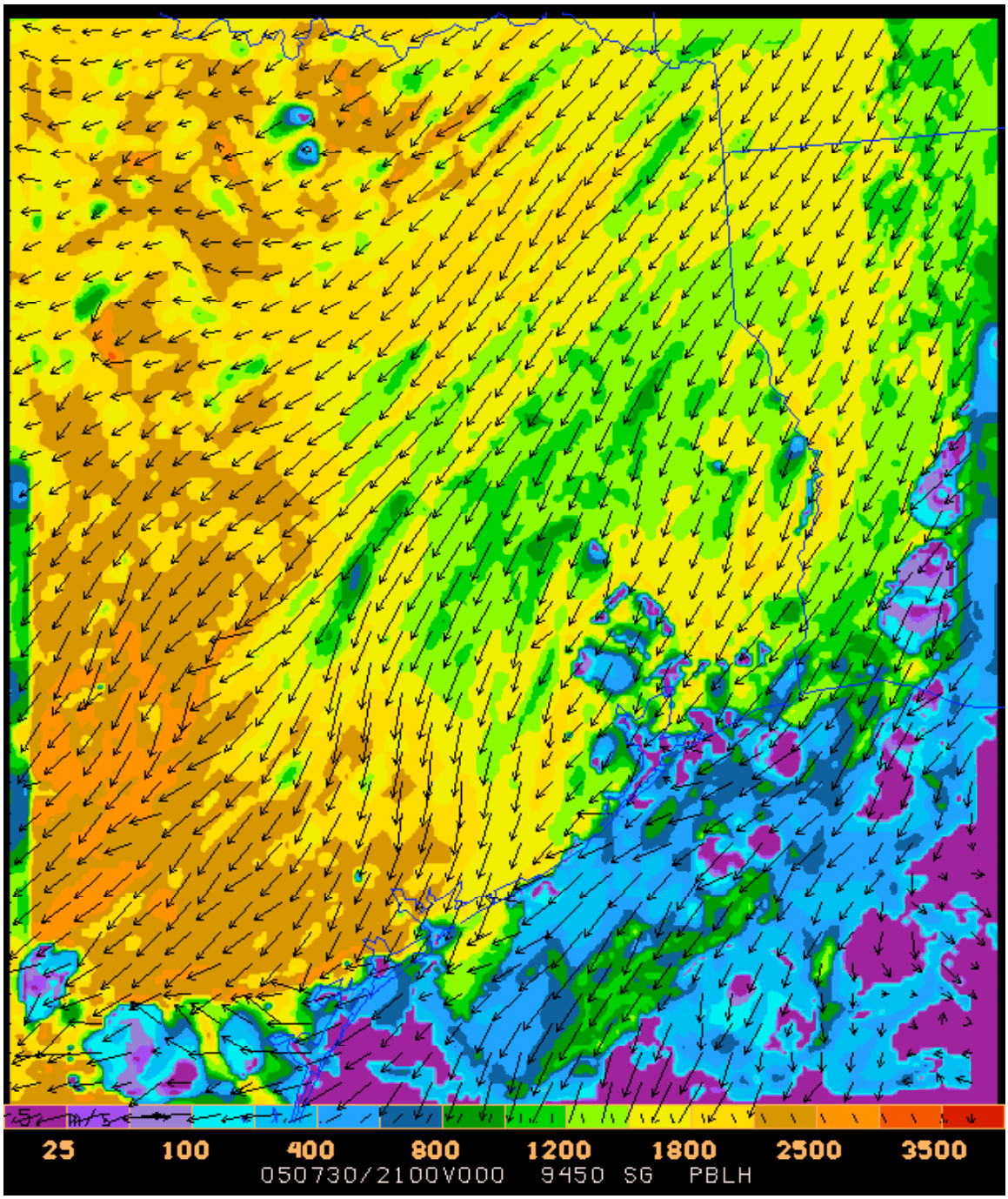

Fig. 41: Mixing heights (m) and .9450 sigma level winds, nonudg4day3 model run, 21Z July 30, 2005.

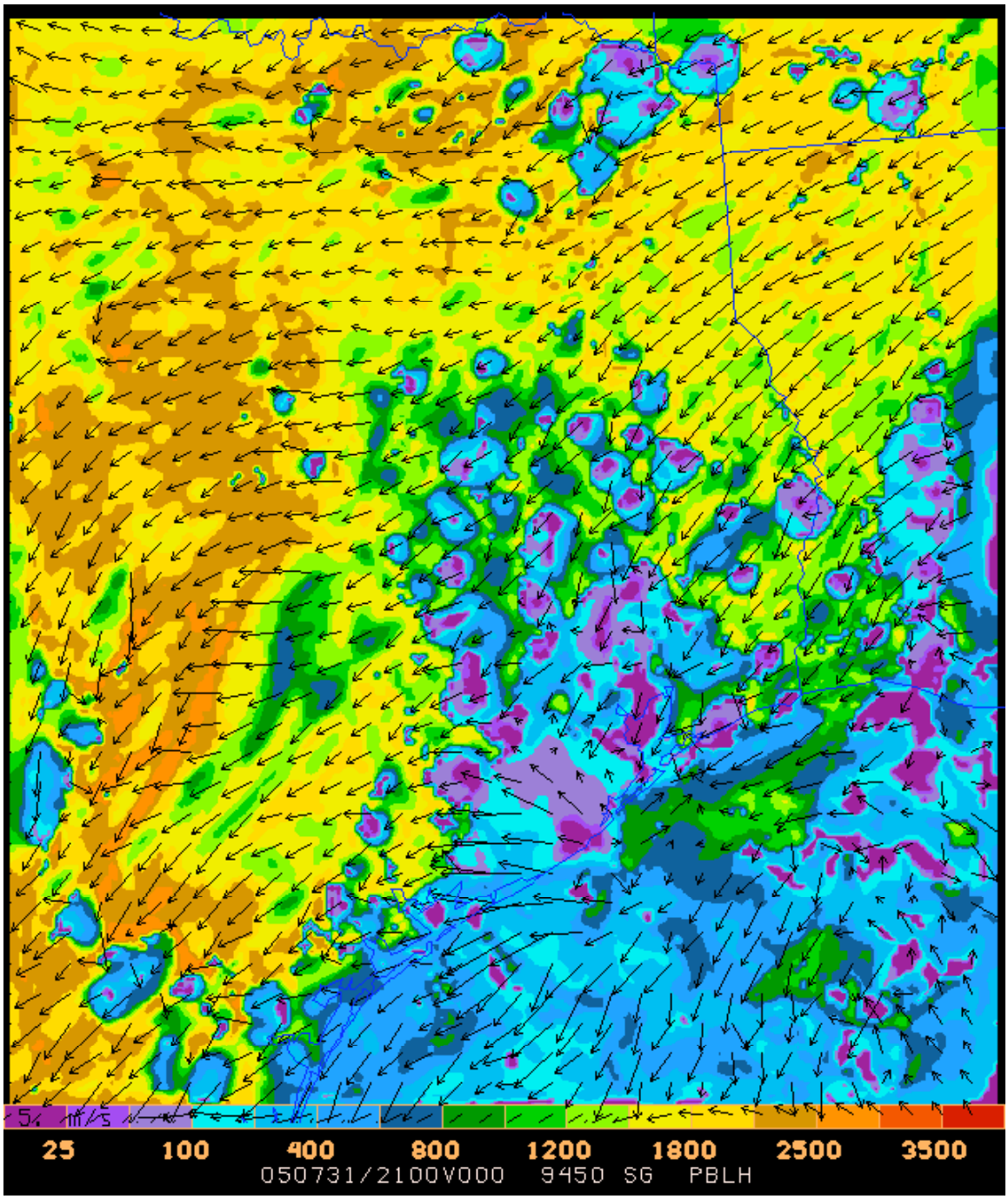

Fig. 42: Mixing heights (m) and .9450 sigma level winds, orignudg4day3 model run, 21Z July 31, 2005.

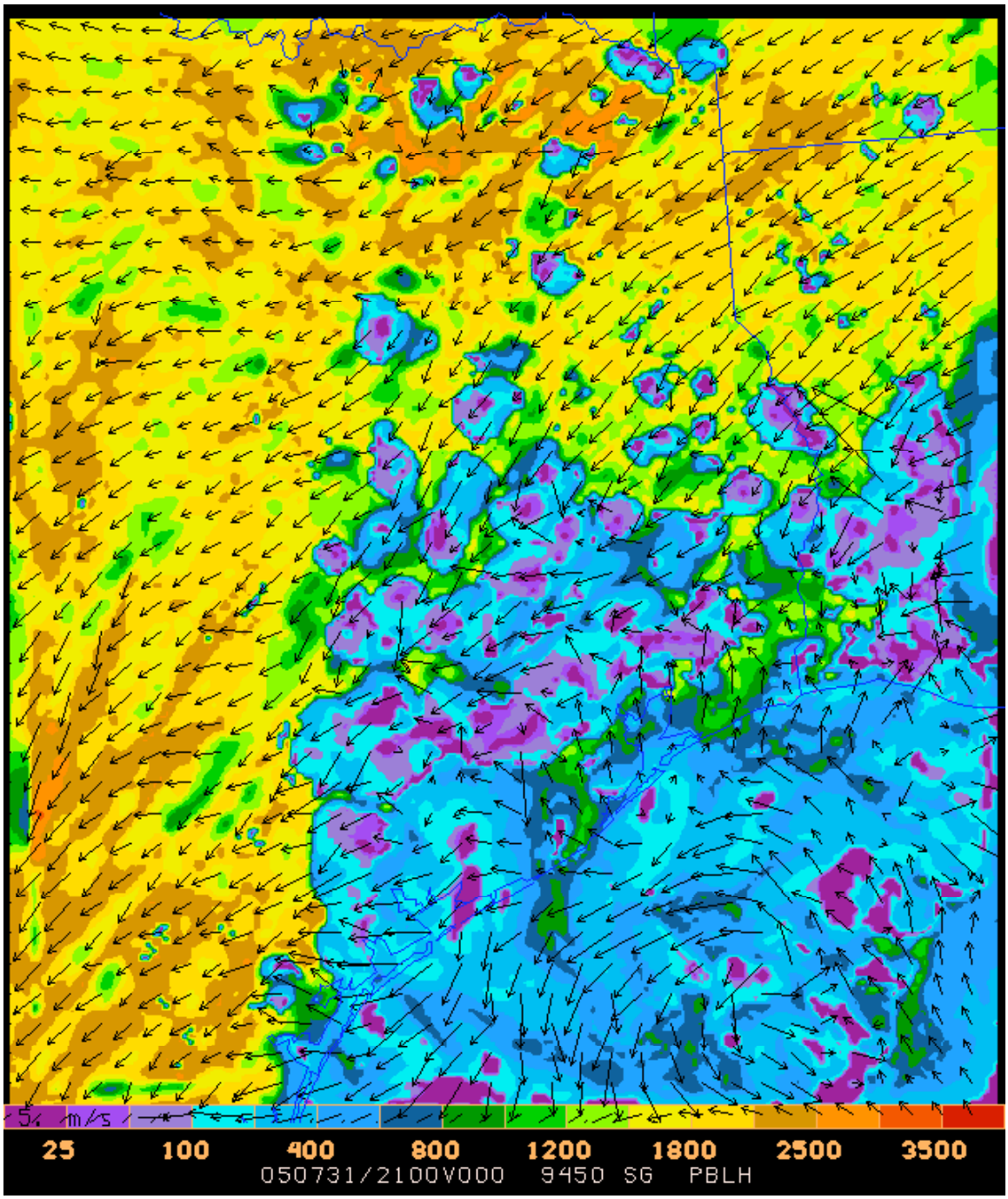

Fig. 43: Mixing heights (m) and .9450 sigma level winds, nonudg4day3 model run, 21Z July 31, 2005.

The mixing heights for 16Z August 1, 2005 from three model runs were shown in Figs. 35-37. Figs. 44 and 45 depict the mixing heights from the other two model runs. In this instance, both the grell4day3 simulation and the nonudg4day3 simulation predict shallower mixing heights over the central portion of the domain than the other three

simulations. Unfortunately, the differences are not large in locations where mixing height estimates are available.

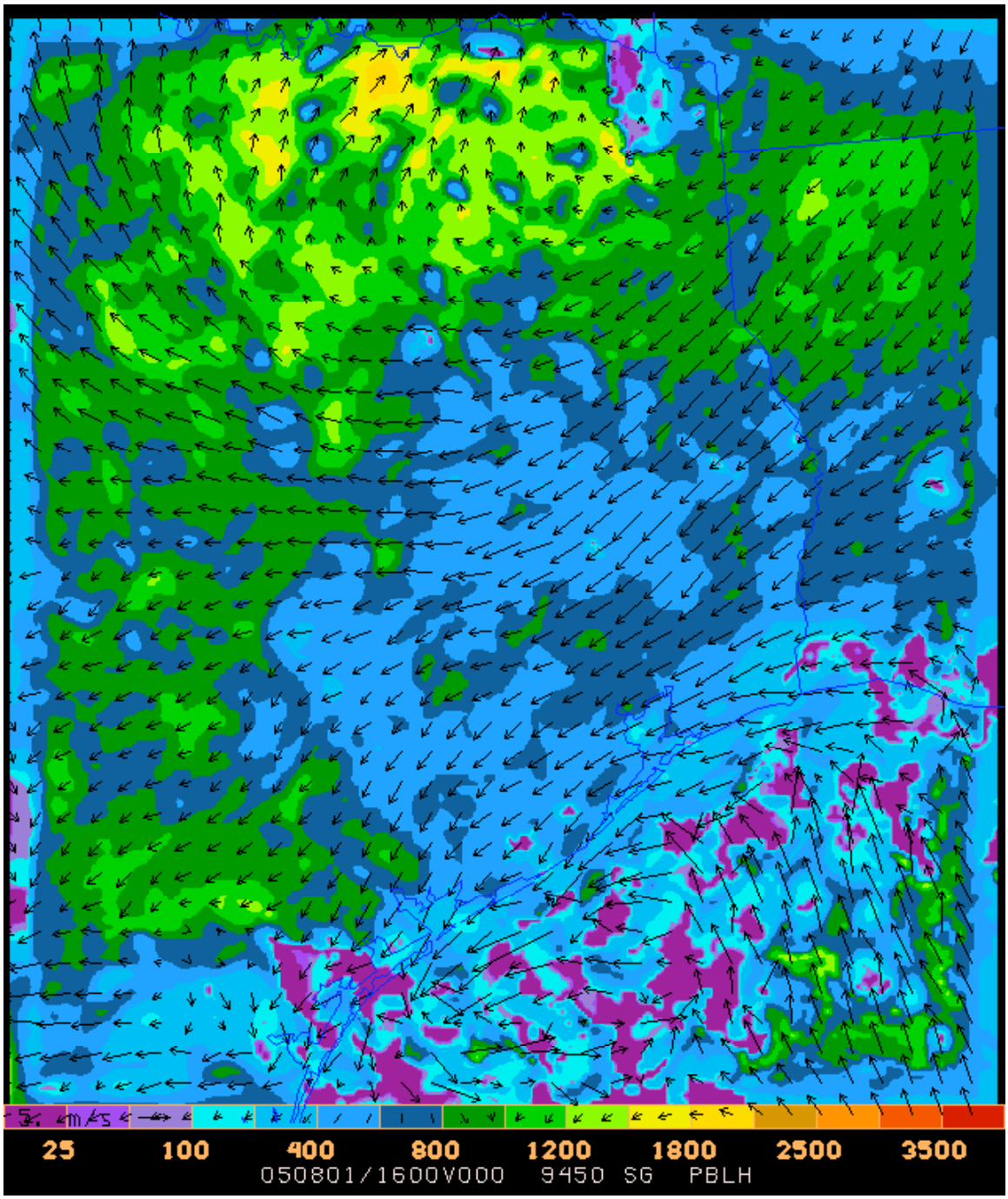

Fig. 44: Mixing heights (m) and .9450 sigma level winds, nonudg4day3 model run, 16Z August 1, 2005.

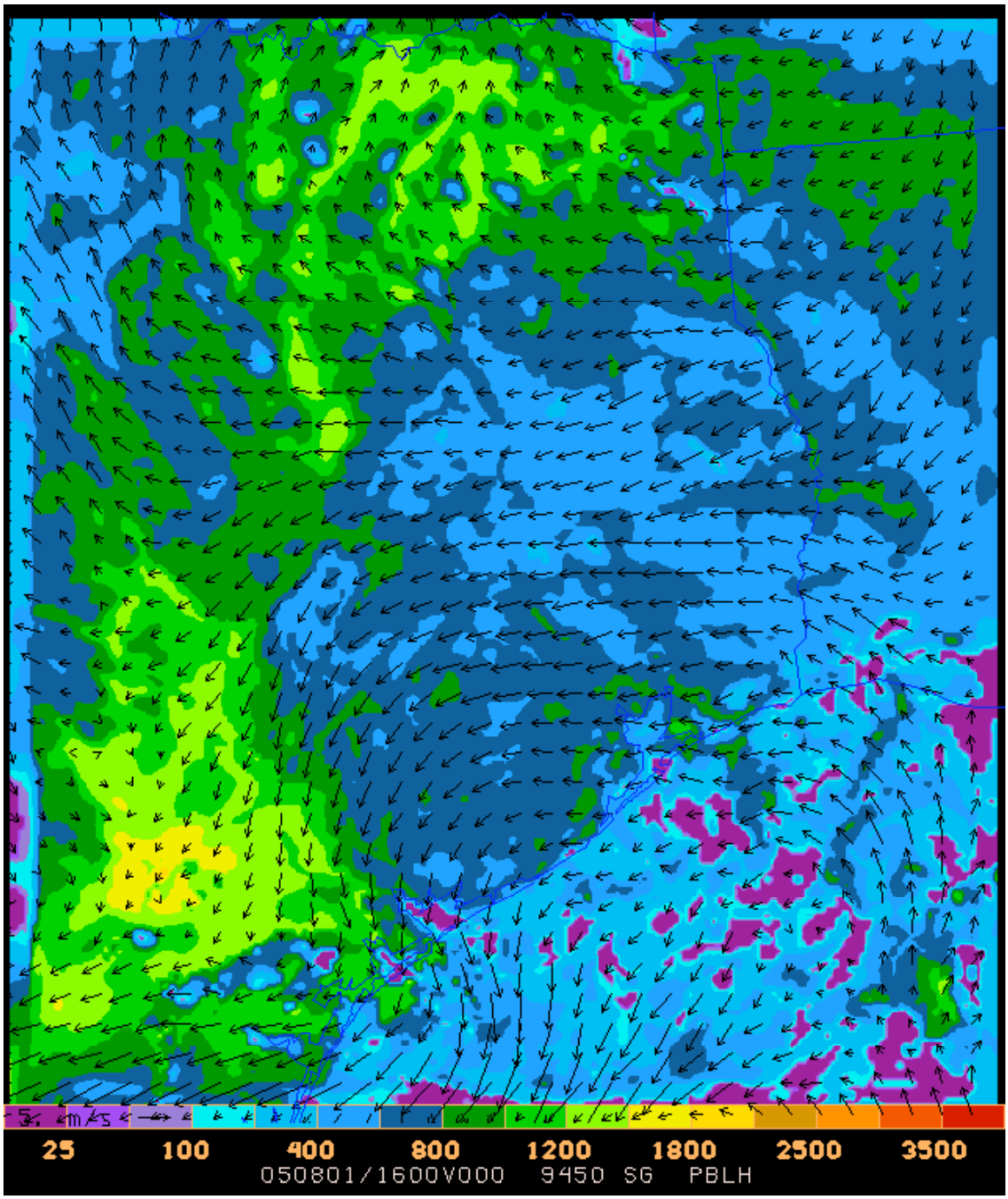

Fig. 45: Mixing heights (m) and .9450 sigma level winds, grell4day3 model run, 16Z August 1, 2005.

At 21Z on August 1, 2005, the mixing height patterns away from convection are nearly identical. Fig. 46 shows the mixing height estimate for the grell4day3 simulation. Mixing heights exceed 2100 m inland, but decline to 1000 m to 1500 m along the Gulf coastal plain.

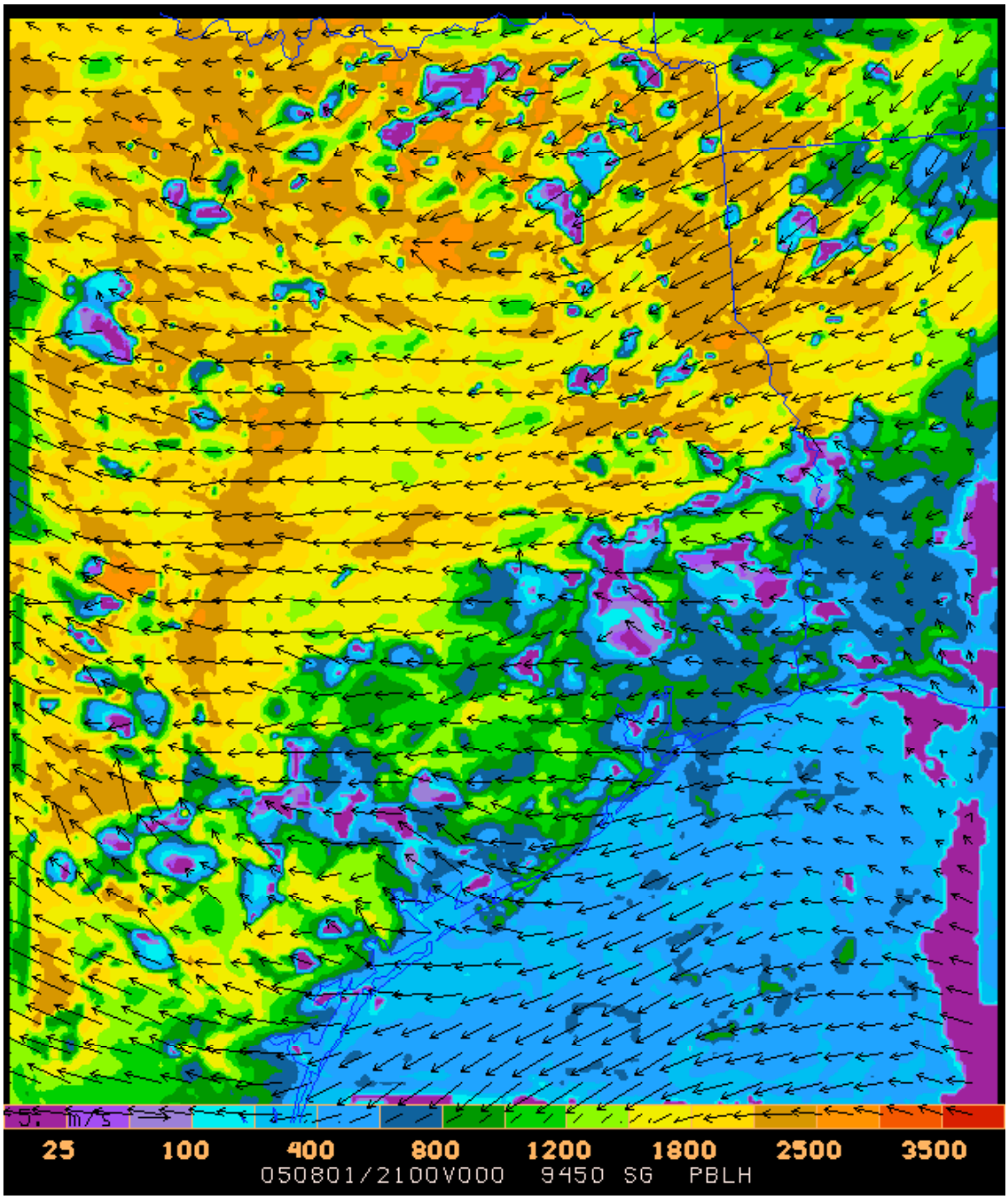

Fig. 46: Mixing heights (m) and .9450 sigma level winds, grell4day3 model run, 21Z August 1, 2005.

On the morning of August 2, 2005, there are considerable differences between orignudg4day3, nonudg4day3, and grell4day3 (Figs. 47-49). However, there is so much small-scale spatial variability that it would be difficult to determine which model run is most accurate.

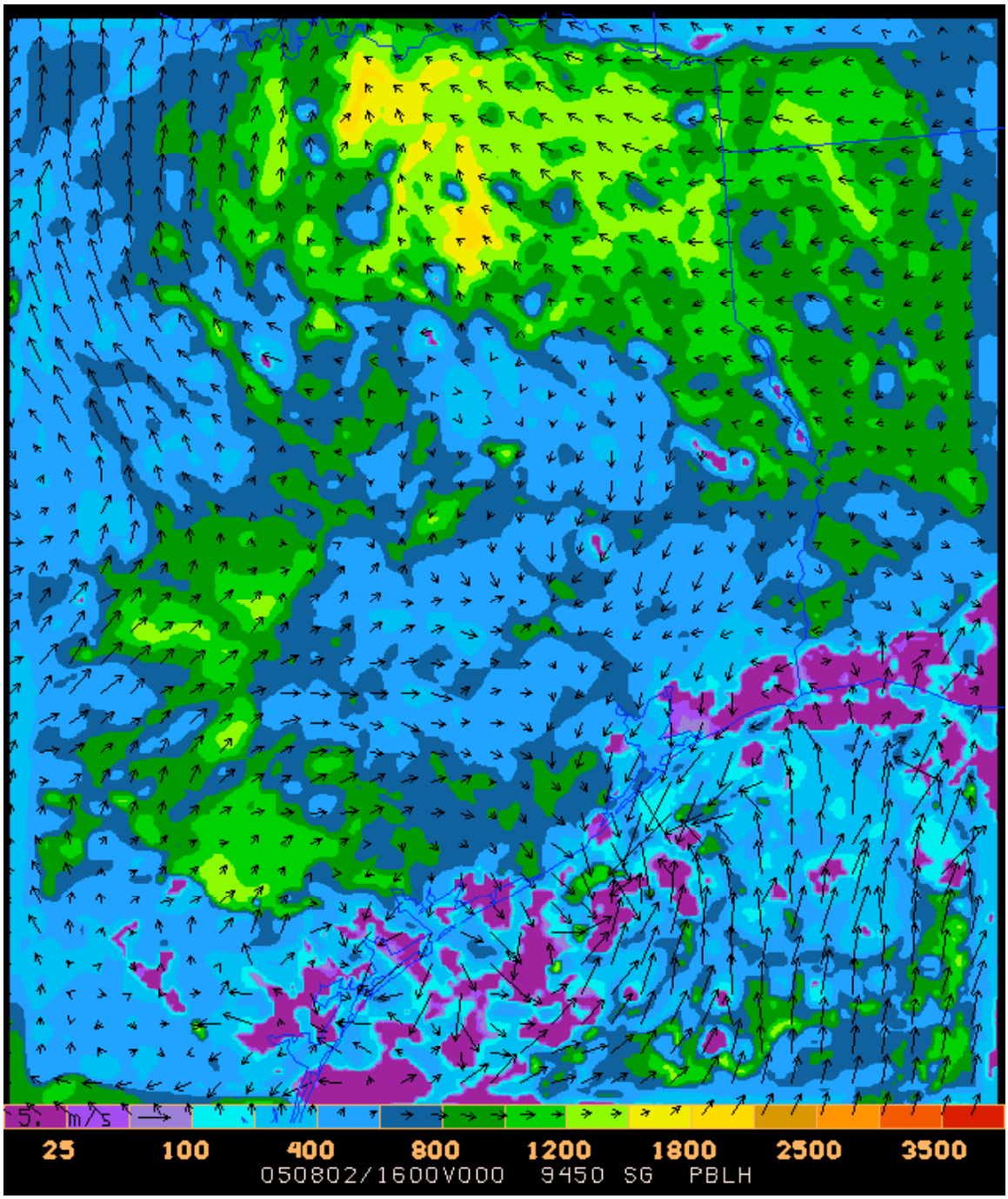

Fig. 47: Mixing heights (m) and .9450 sigma level winds, orignudg4day3 model run, 16Z August 2, 2005.

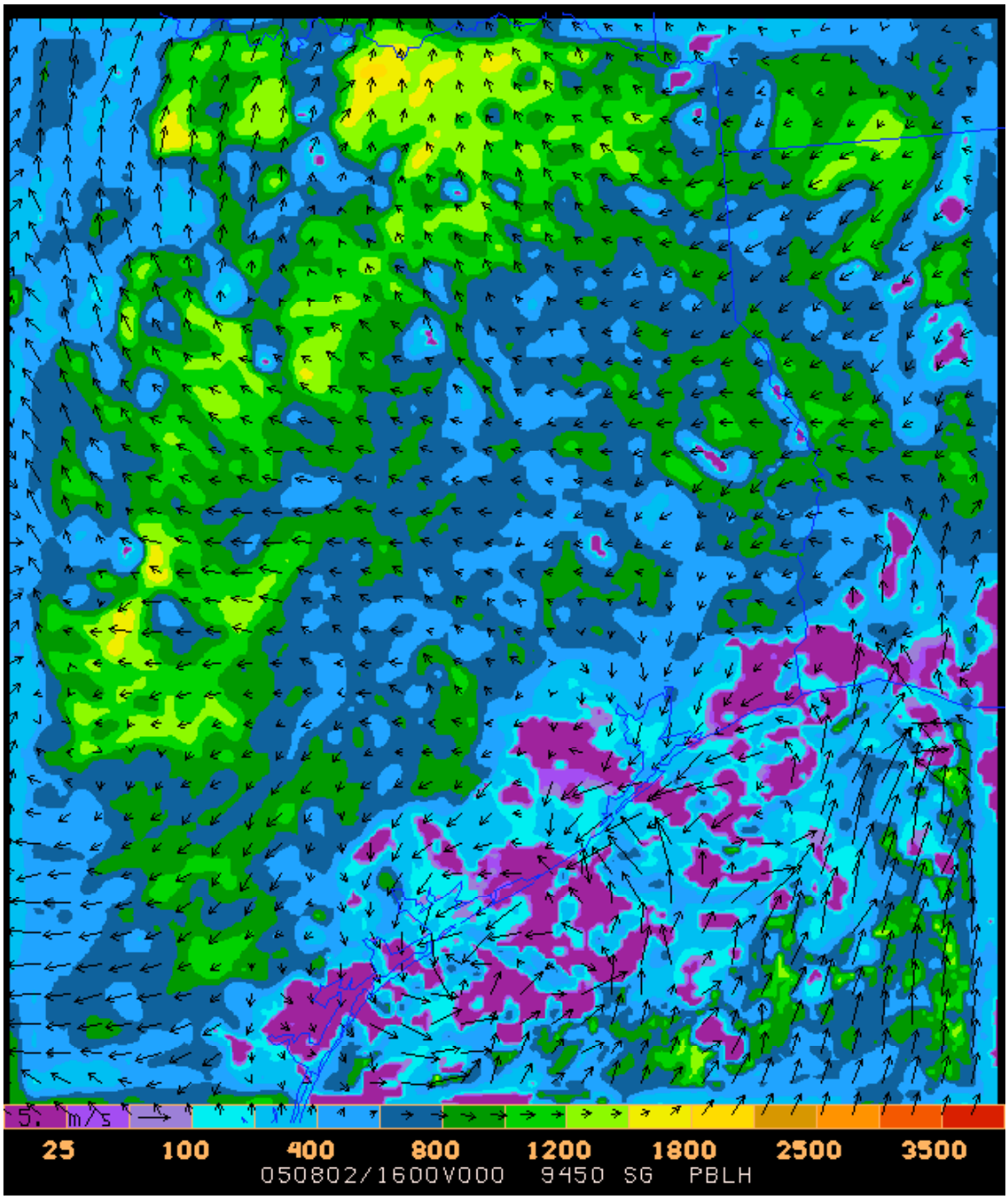

Fig. 48: Mixing heights (m) and .9450 sigma level winds, nonudg4day3 model run, 16Z August 2, 2005.

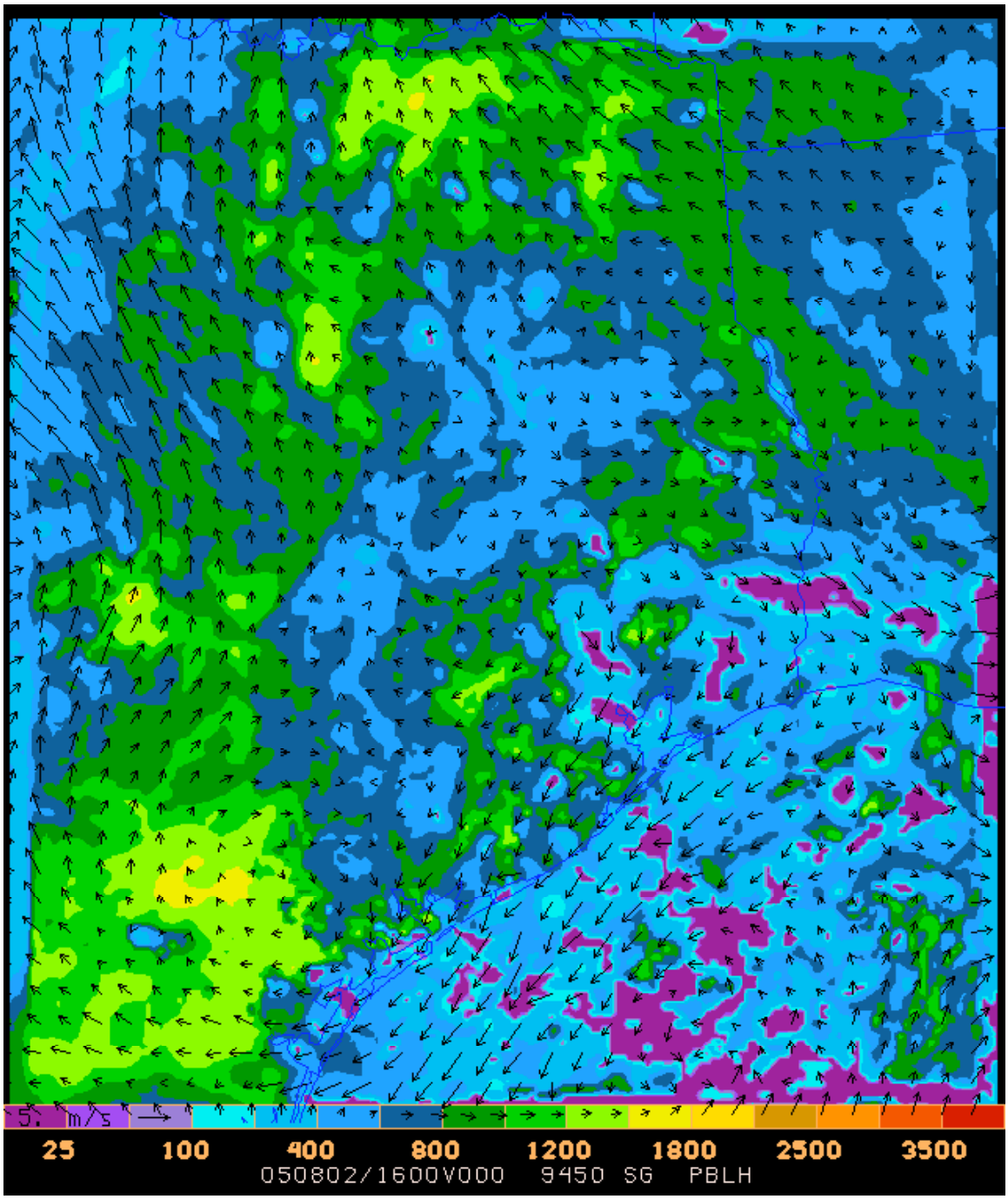

Fig. 49: Mixing heights (m) and .9450 sigma level winds, grell4day3 model run, 16Z August 2, 2005.

Except for the influence of convection and cloud cover, mixing heights are generally similar across all model simulations during the afternoon of August 2, 2005 (not shown).

In general, the mixing heights at times exhibit a few hundred meters of spread among model runs, indicating that the nudging affects the mixing heights either directly or

indirectly through the precipitation distribution. The mixing heights with nudging are not clearly better or worse than the mixing heights without nudging.

b) Sea Breeze

The daytime sea breeze can only be compared among model runs on July 30, 2005, because that was the only day in which most model runs did not have widespread convection along the coast. However, this day also featured moderate northeasterly winds, which normally suppresses sea breeze and coastal oscillation development.

The orignudg4day3 model simulation at 21Z July 30, 2005 (Fig. 50) has no sea breeze in Louisiana. Along the coast between Galveston and Port Arthur, nearshore winds have weakened and turned slightly onshore. Near Galveston Bay the winds along the Gulf Coast are shore-parallel. Along Galveston Bay, particularly near the Ship Channel area, a clear bay breeze has developed, with winds from the east-southeast impinging on winds from the north-northeast. From Lake Jackson southwestward, a more classical sea breeze has developed, and the sea breeze front penetrates progressively farther inland with distance along the coast until it reaches the area of convection in south-central Texas.

The sea breezes from the other nudging runs are similar and are not shown here.

The nonudg4day3 model simulation (Fig. 51) is similar to the others south of Lake Jackson, but exhibits considerable differences elsewhere. Along the Gulf Coast near Galveston, the winds over water are onshore, producing a gulf breeze front from Galveston southwestward. At the same time, over Galveston Bay itself, the winds are from the northeast everywhere, with no indication of a bay breeze.

The actual winds were unlike any model run in the Galveston area. Winds across Houston, Galveston, and Galveston Bay during the afternoon were from the northeast at about 10 miles per hour. There was no bay breeze in evidence on July 30. Similarly, there was no gulf breeze in the vicinity of Galveston. From Lake Jackson northeastward, all coastal winds were blowing from land to sea.

On this day, neither the nudged nor the unnudged model run can be said to perform better along the coast. Because temperatures are nearly identical between the two runs, the difference is attributable to the direct effect of nudging on the wind field and the indirect effect of variations in offshore convection.

To examine the nighttime aspects of the coastal oscillation, attention is given to the evenings of July 31 and August 1. Both of these days featured erroneous widespread coastal convection in most of the model simulations, so it is expected that the models will not have the proper coastal oscillation dynamics in place. As a result, there should be a substantial impact on the winds between the ground and 700 m or so due to obs nudging.

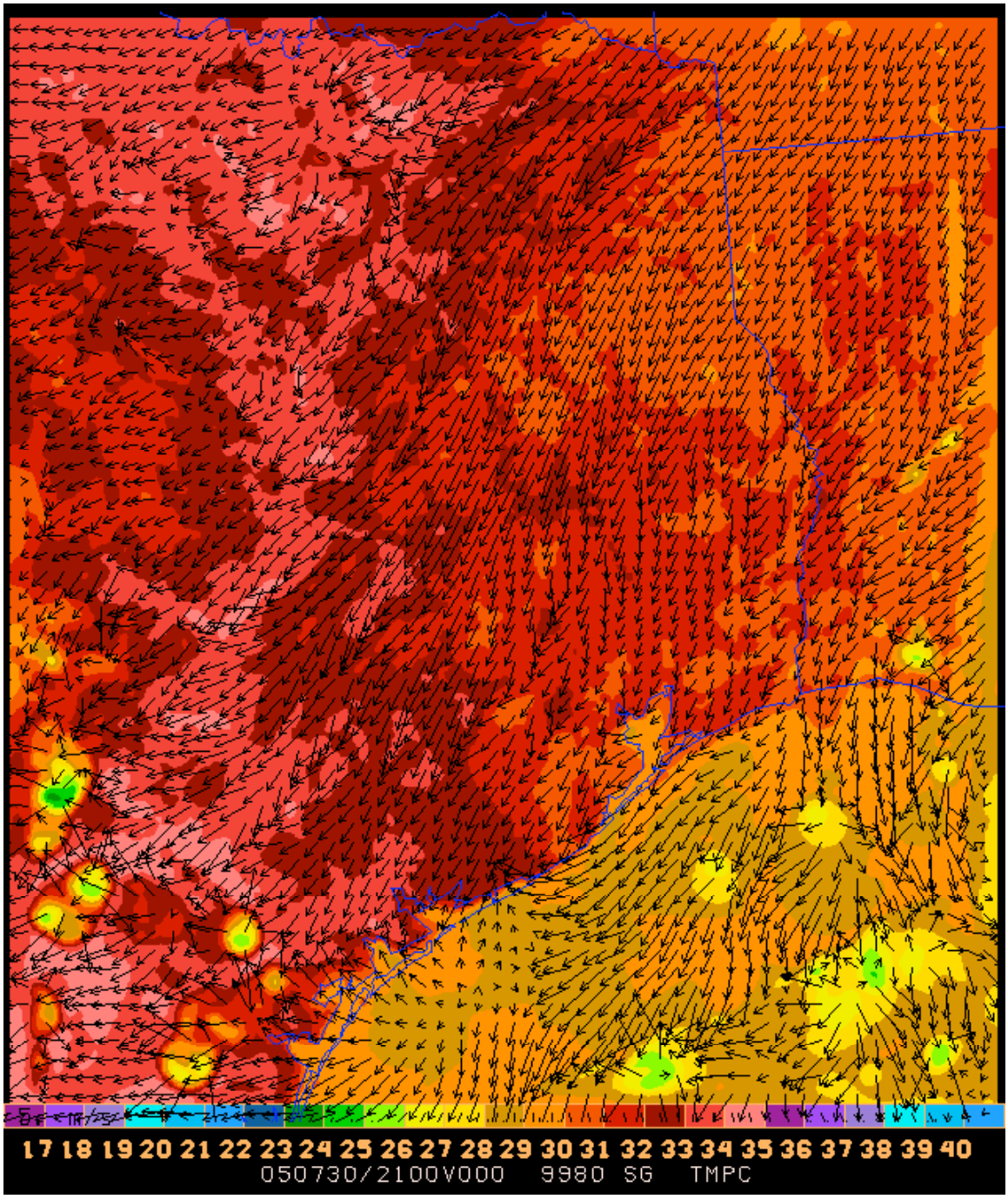

Fig. 50: Temperatures (°C) and winds, .9980 sigma level, orignudg4day3 model run, 12Z July 30, 2005.

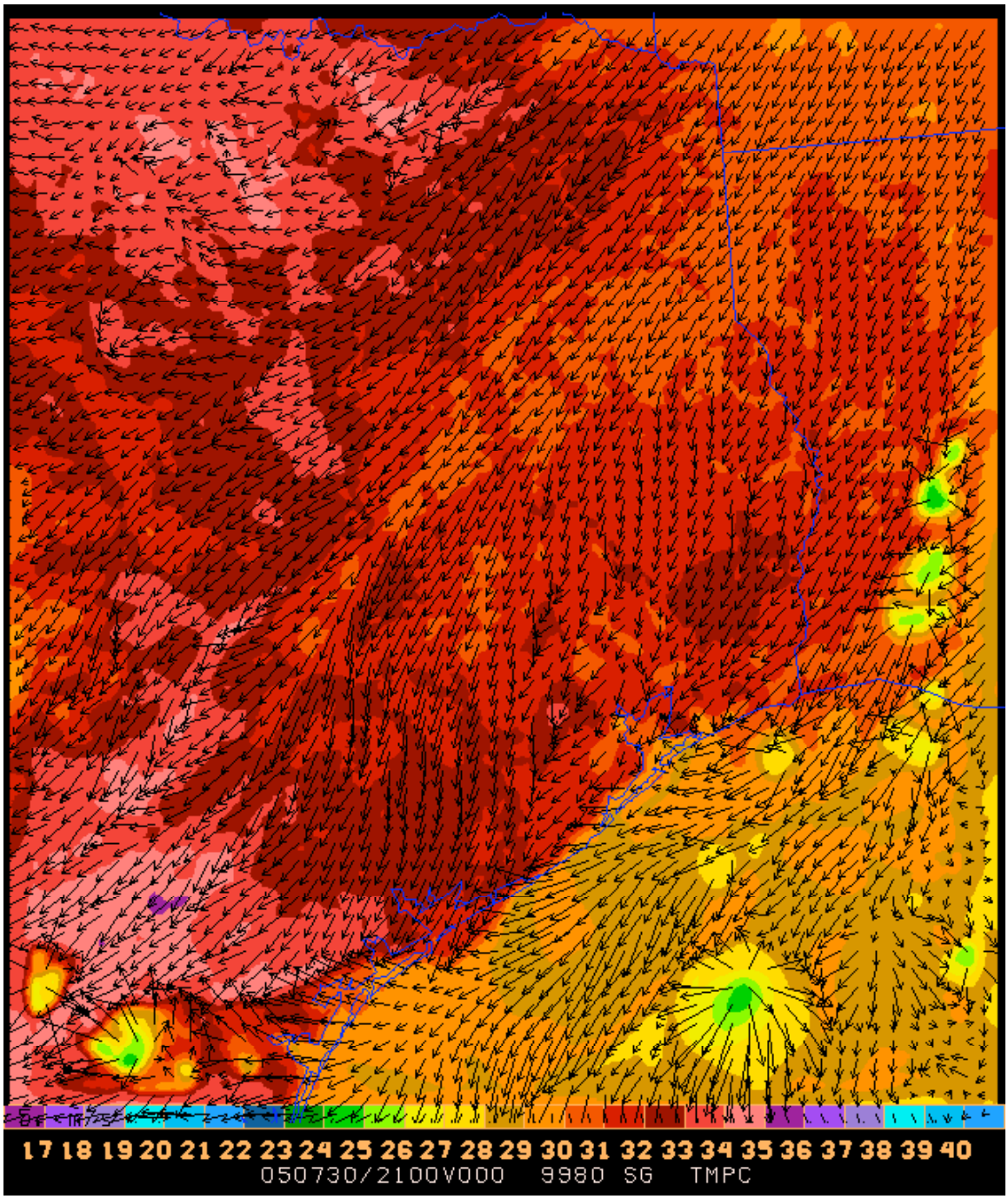

Fig. 51: Temperatures (°C) and winds, .9980 sigma level, nonudg4day3 model run, 12Z July 30, 2005.

Fig. 52 shows the nonudg4day3 winds at sigma=.9450 (about 500 m above ground level) at 06Z August 1, 2005. Moderate northeasterlies prevail along the coast, while moderate southeasterlies are present across North Texas.

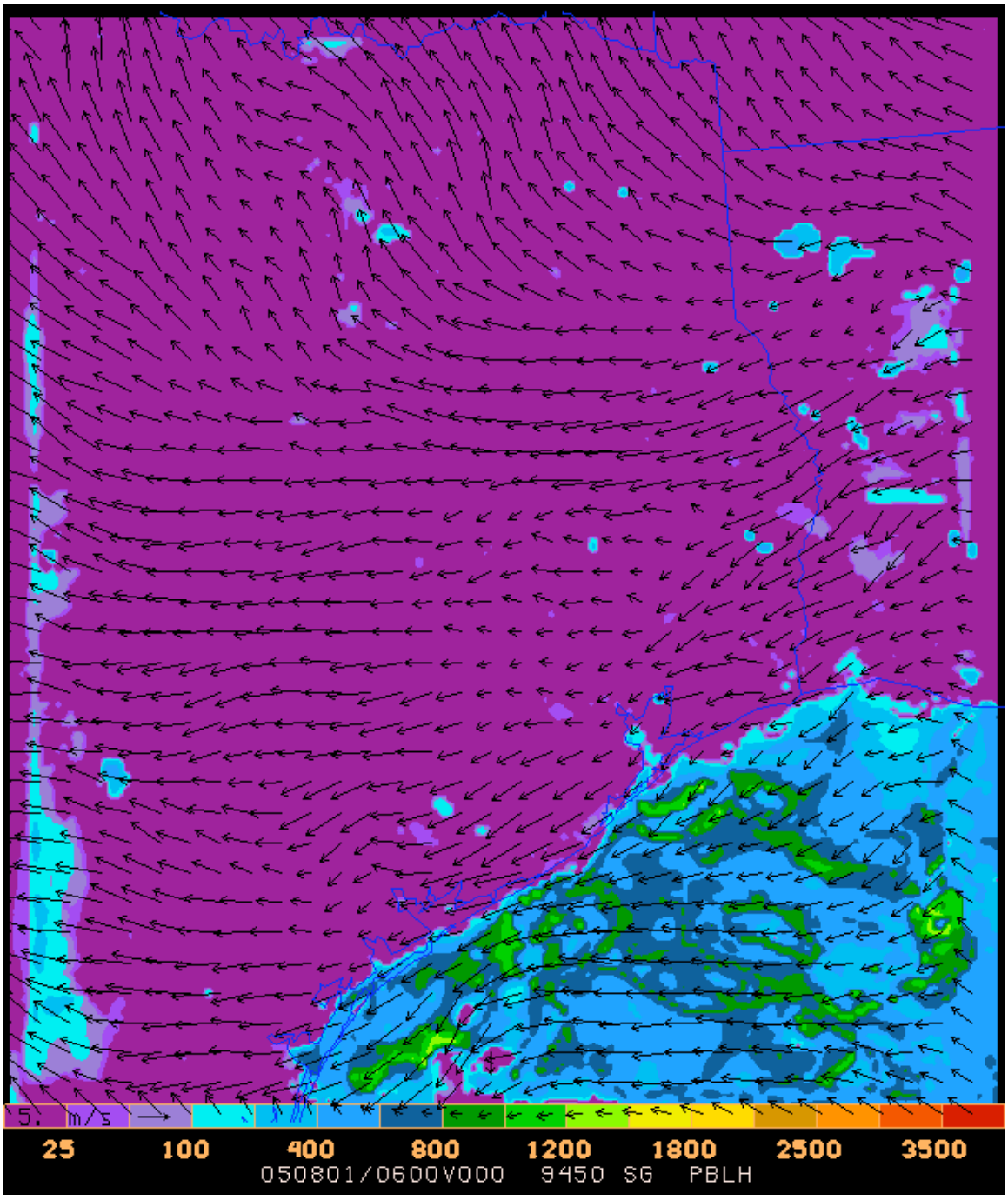

Fig. 52: Mixing heights (m) and .9450 sigma level winds, nonudg4day3 model run, 06Z August 1, 2005.

Compare the wind field in Fig. 52 with that from the orignudg4day3 model run (Fig. 53). With the obs nudging, the northeasterly wind along the coast is entirely eliminated and wind speeds offshore are weakened substantially. Since obs nudging drives the model winds closer to the observed winds, it is proper to conclude that the winds in Fig. 53 are a substantial improvement over the winds in Fig. 52.

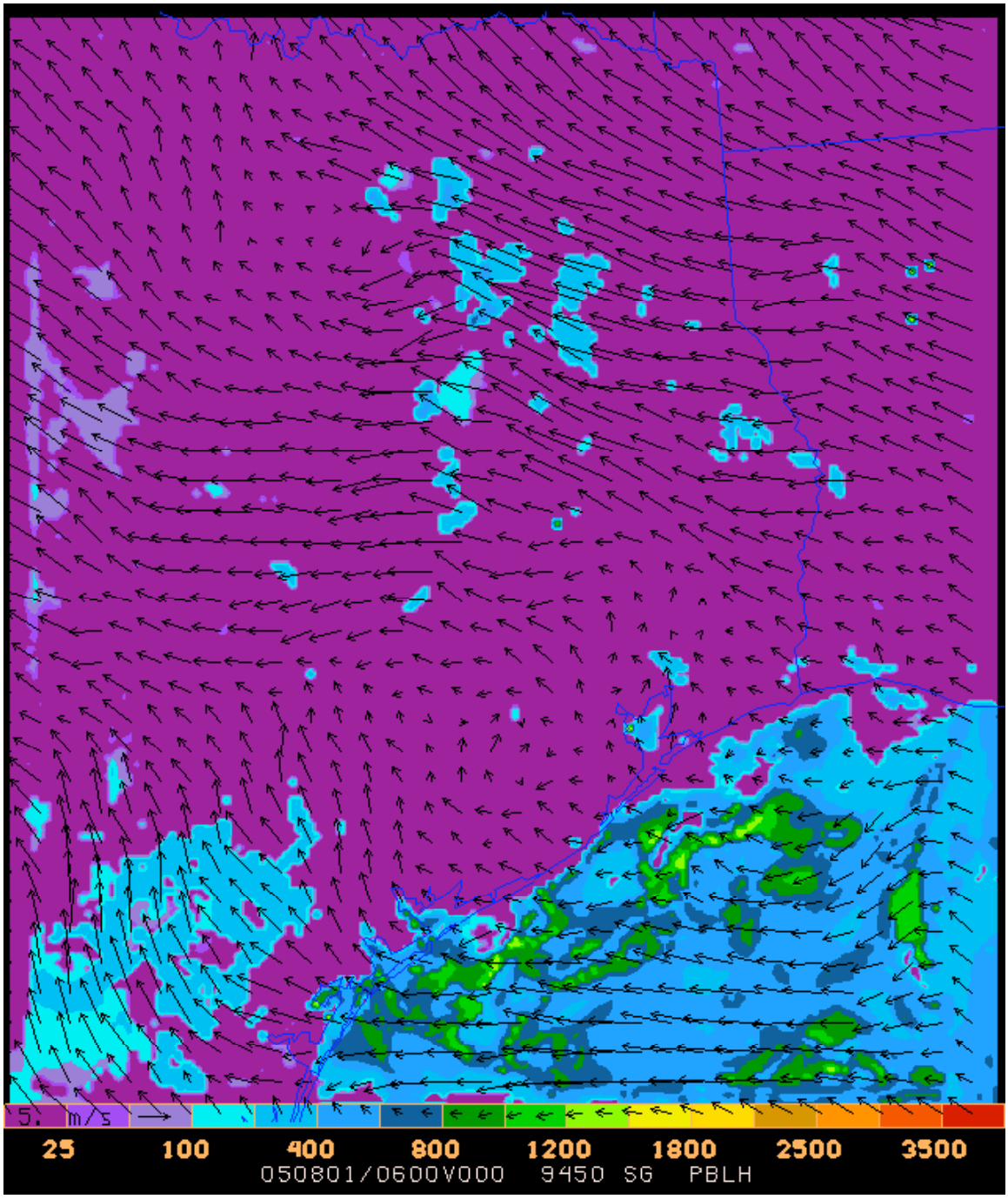

Fig. 53: Mixing heights (m) and .9450 sigma level winds, orignudg4day3 model run, 06Z August 1, 2005.

It is important to examine whether small-scale variations in the wind field have been introduced by the nudging. In this case, the magnitude of such variations is a bit stronger with nudging than without nudging. Thus, for this day at least, it may be appropriate to use a larger radius of influence.

The testnudg4day3 model run uses a smaller radius of influence but a larger time window, so it is not obvious whether the net effect would be more or less noise than orignudg4day3. The winds at 06Z August 1, 2005 (not shown) are similar to those in Fig. 53, except that some northeasterlies are present west of Houston.

Ordinarily it would be possible to compare the orignudg4day3 run, the nonudg4day3 run, and the nohve4day3 run to determine whether the winds at Huntsville (HVE) are improved by nudging even if the wind data at HVE itself is withheld from the assimilation procedure. In this instance, however, the nohve4day3 run had convection in the vicinity of HVE, so the winds in that model run were not representative of expected nudging performance at HVE.

Finally, the grell4day3 run (not shown) is similar to the orignudg4day3 run, except that stronger southeasterlies are present in the Victoria area.

At 12Z August 1, 2005, the nonudg4day3 winds have remained from the same directions or even strengthened (Fig. 54). In the orignudg4day3 run, winds in North Texas have become more southerly, and a zone of northwesterlies has developed between Houston and Victoria (Fig. 55). This latter zone is strongest between available observations, so it is difficult to verify, but the winds at LDB (Ledbetter) and LPT (LaPorte) are consistent with the wind pattern.

The grell4day3 run produces a similar wind pattern (not shown). The testnudg4day3 run is also similar in most of the domain, but in the area of interest between Houston and Victoria, the run produces two centers of anticyclonic circulation, with an offshore wind maximum that is much weaker (Fig. 56). Clearly the different nudging parameters in the testnudg4day3, particularly the smaller radius of influence, are producing smaller-scale wind features, but it is not known whether the smaller scale or the larger scale is more correct.

With the convection having dissipated, it is possible to compare the nohve4day3 model run with the runs with full nudging and no nudging to determine whether nudging without HVE (Huntsville) winds produces an improved simulation at HVE. Fig. 57 shows the nohve4day3 model output for 12Z August 1. The winds simulated in the vicinity of HVE are about 5 m/s from the east. This differs substantially from the nonudg4day3 simulation, which features winds of about 8 m/s from the northeast. The actual winds at HVE, similar to the winds in Fig. 55, are from the east at about 3 m/s. The use of obs nudging has made a substantial improvement in the wind field at this particular location even when no winds from this location are assimilated.

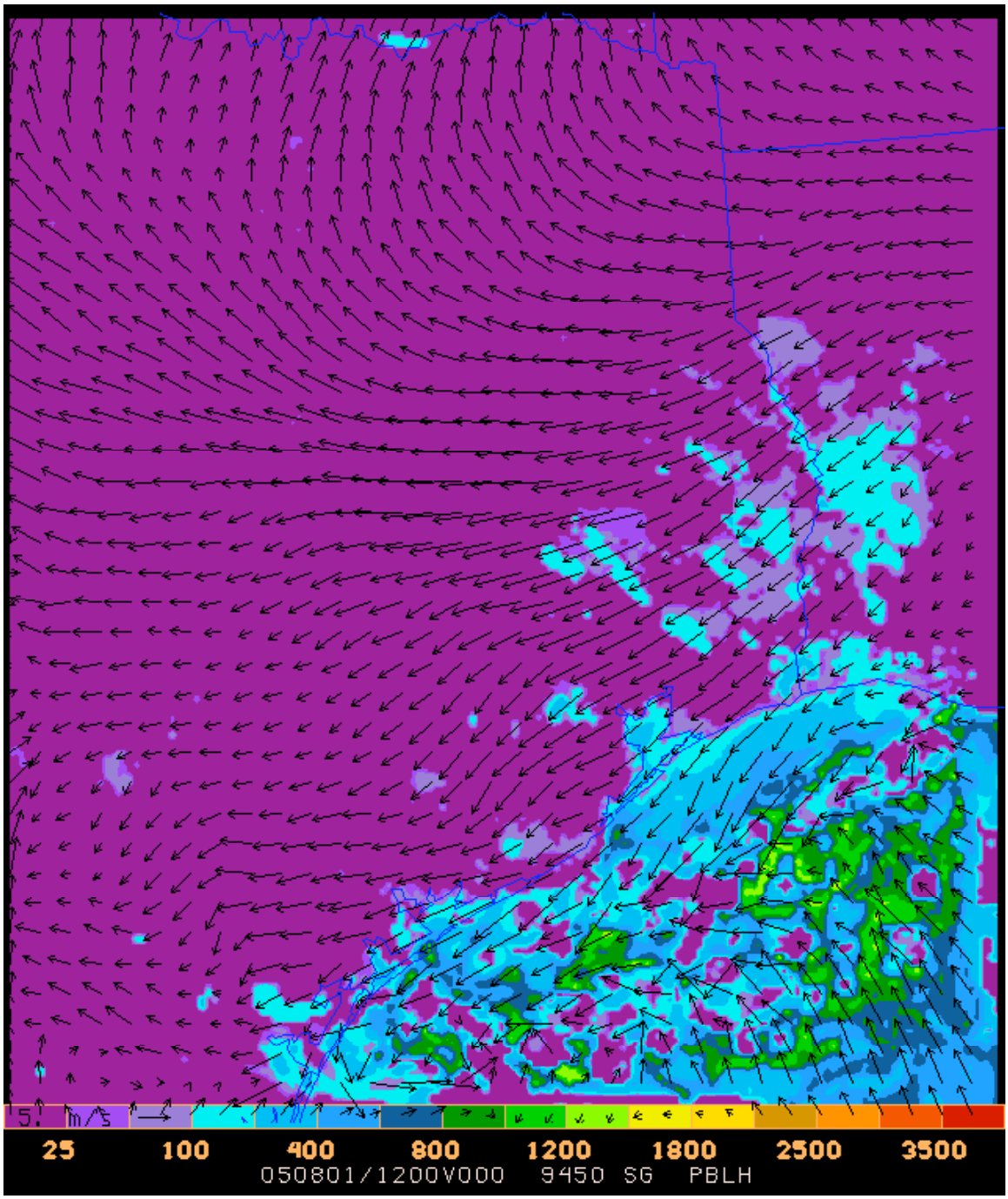

Fig. 54: Mixing heights (m) and .9450 sigma level winds, nonudg4day3 model run, 12Z August 1, 2005.

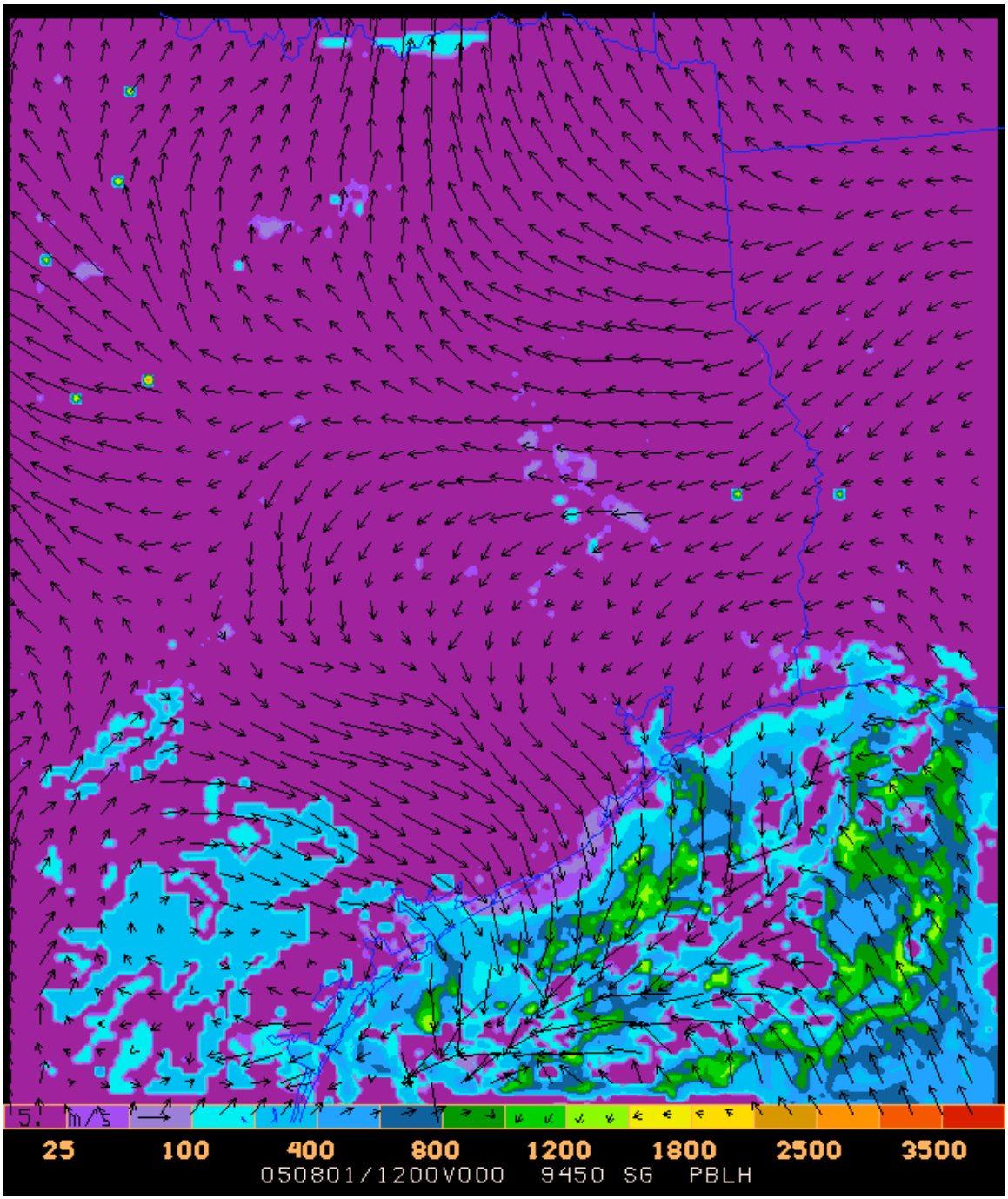

Fig. 55: Mixing heights (m) and .9450 sigma level winds, orignudg4day3 model run, 12Z August 1, 2005.

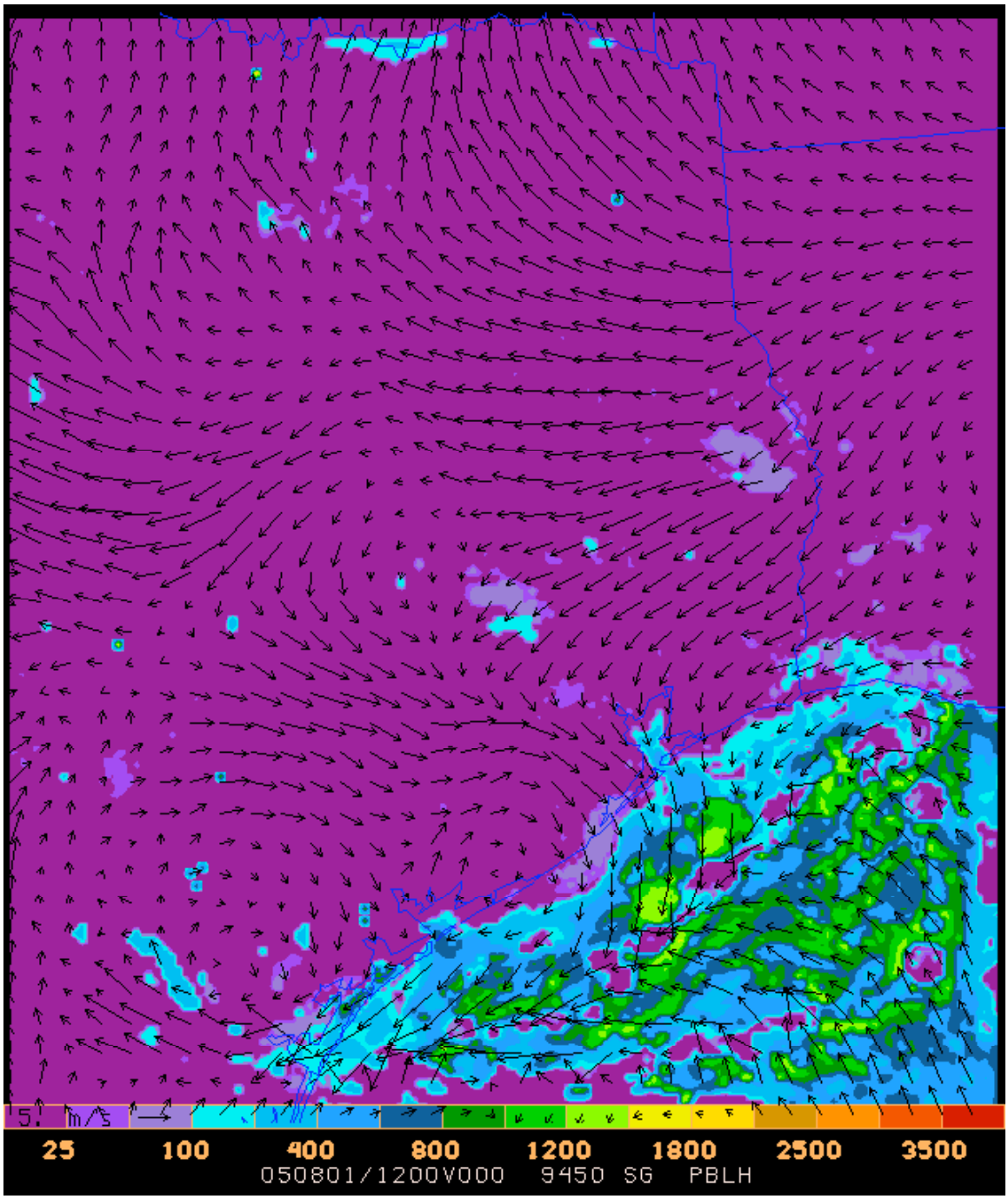

Fig. 56: Mixing heights (m) and .9450 sigma level winds, testnudg4day3 model run, 12Z August 1, 2005.

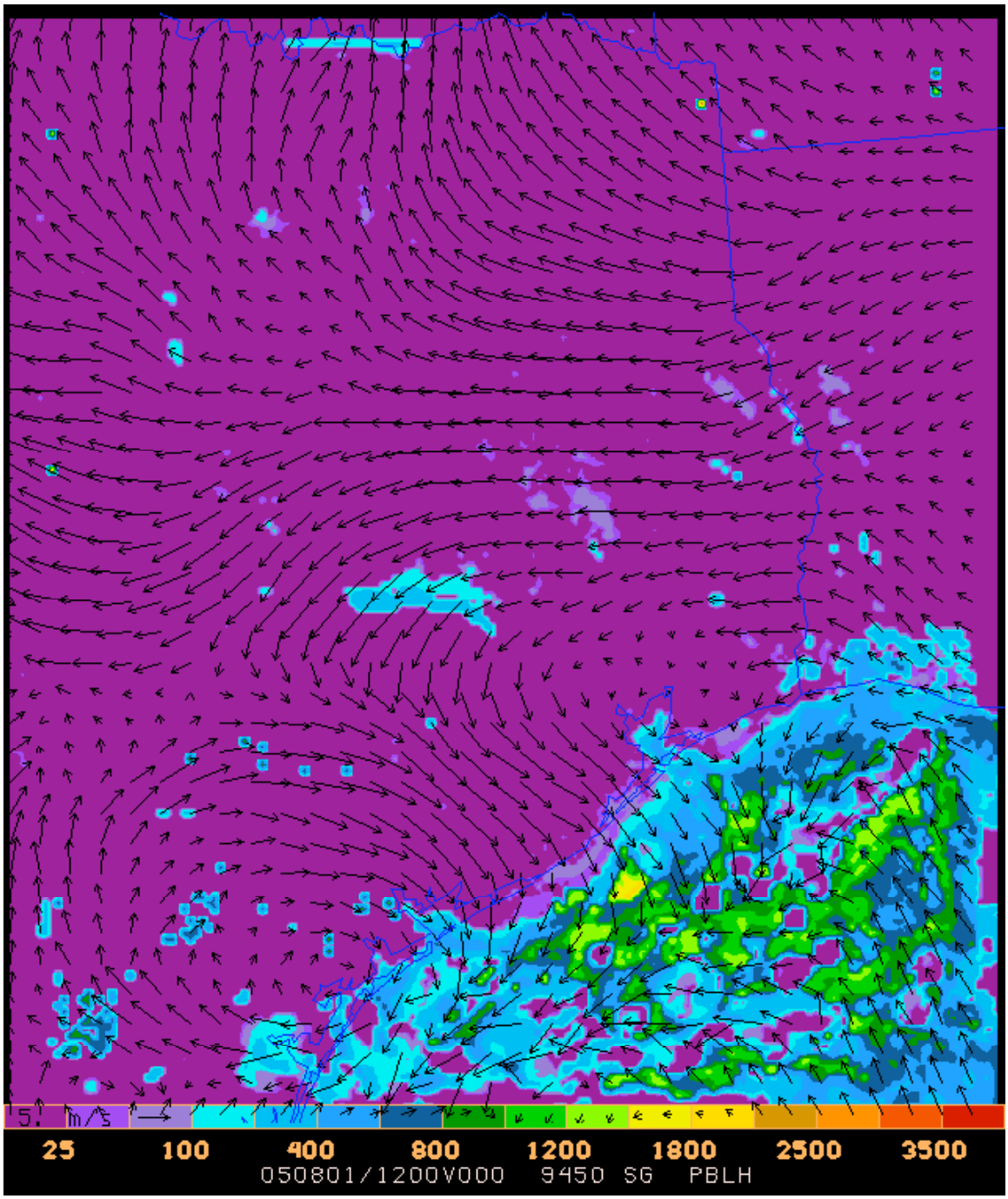

Fig. 57: Mixing heights (m) and .9450 sigma level winds, nohve4day3 model run, 12Z August 1, 2005.

The following evening, despite the widespread convection, a moderate sea-breeze low-level jet formed in most simulations. The jet may be seen in Fig. 58, from the orignudg4day3 model run, as a band of strong southerly winds approximately 200-250 km from the coastline. The jet is reasonably continuous, despite the substantial role probably played by obs nudging from a few profiler sites.

The other model runs with nudging have similar wind fields (Fig. 59). The outlier is the simulation without nudging, which has winds from the southeast rather than the south and has no sea-breeze coastal-oscillation. The strongest winds are near Houston, where the runs with data assimilation show weaker winds.

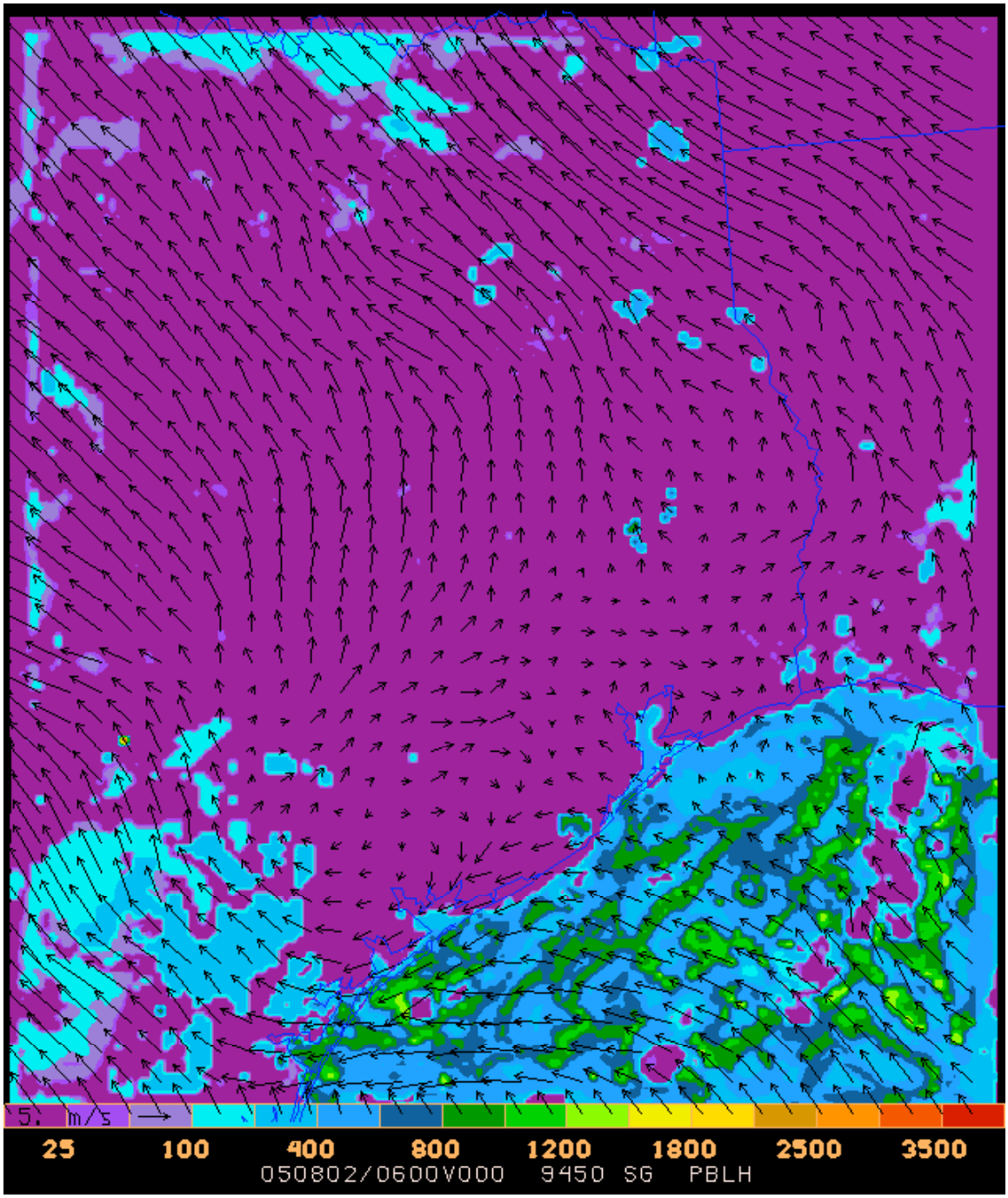

Fig. 58: Mixing heights (m) and .9450 sigma level winds, orignudg4day3 model run, 06Z August 2, 2005.

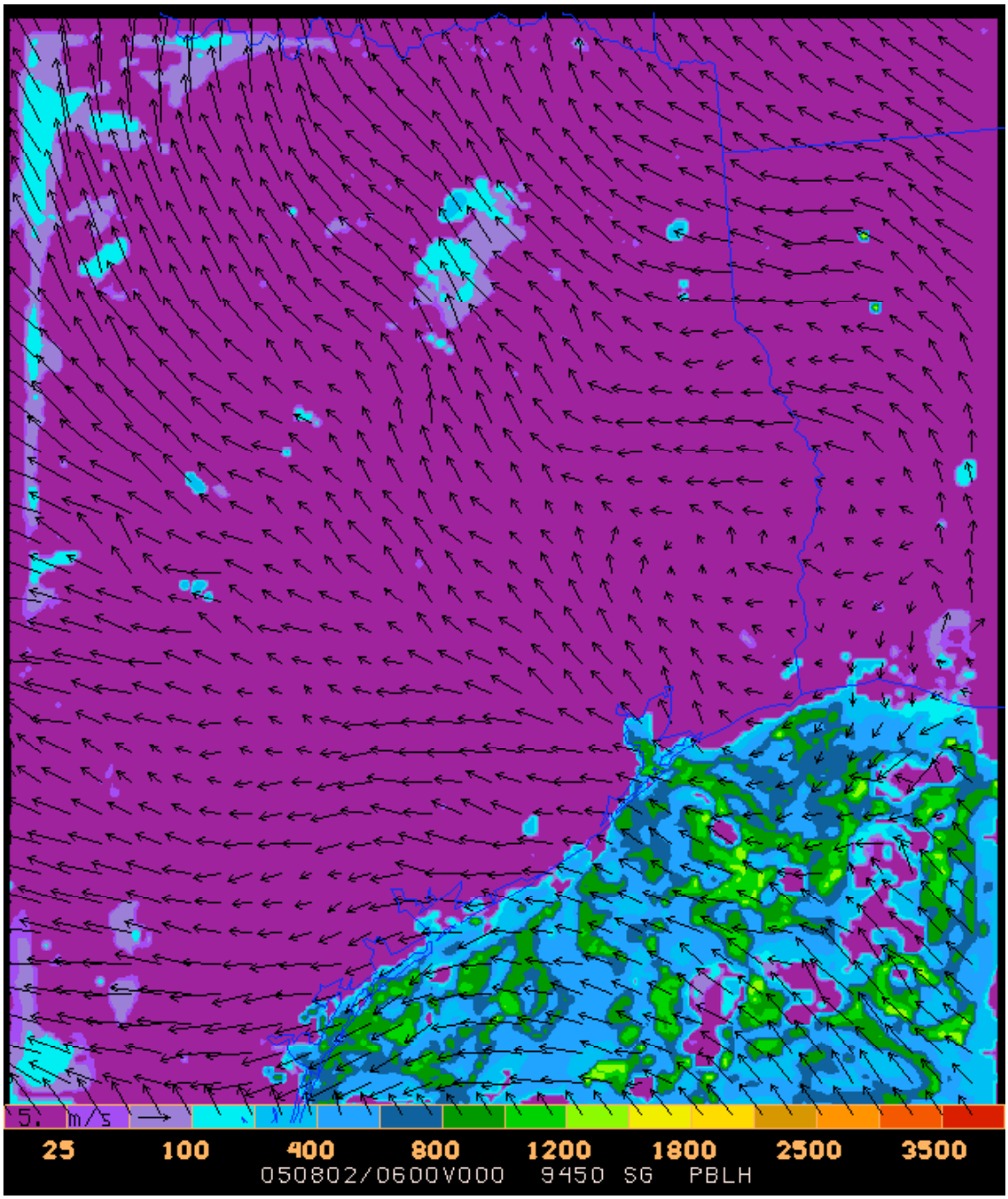

Fig. 59: Mixing heights (m) and .9450 sigma level winds, nonudg4day3 model run, 06Z August 2, 2005.

There is a significant difference at HVE between the nonudg4day3 run and the orignudg4day3 run. Is nudging able to capture the sea-breeze low-level jet, even without assimilating observations from HVE? Fig. 60 shows that, even without HVE data, the obs nudging is able to produce the correct light southwesterlies at HVE roughly continuous with the entire sea-breeze low-level jet.

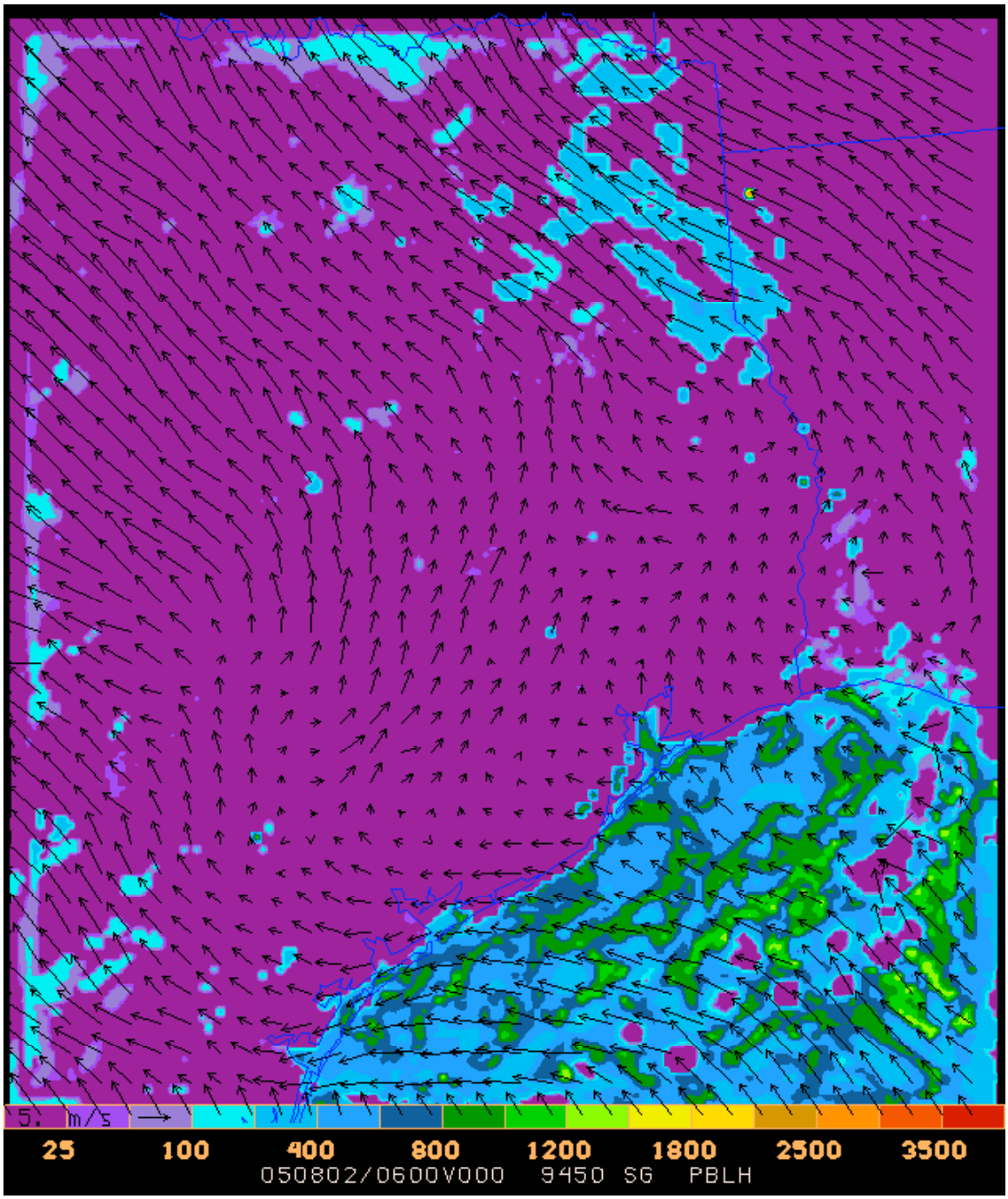

Fig. 60: Mixing heights (m) and .9450 sigma level winds, nohve4day3 model run, 06Z August 2, 2005.

Although nohve4day3 was able to improve the model simulation at HVE through nudging, the 12Z August 2 time had its best model performance from testnudg4day3 (not shown). The winds at HVE were correctly simulated to be from the southwest rather than from the northwest like most other simulations.

To summarize the sea-breeze low-level jet model performance, the obs nudging performed very well. The simulation without nudging completely missed the sea-breeze low-level jet on the nights of July 31 and August 1. The nudging was able to produce a coherent sea-breeze low-level jet that migrated inland and rotated clockwise with time. An experiment withholding data from HVE demonstrated that the data assimilation was able to greatly improve the wind field at HVE even without HVE observations being assimilated.

5. Wind and Temperature Statistics

a) Methods

The Metstat (version 2) software package is used here for computing performance statistics with wind and temperature observations. For surface data input to the Metstat program, three data sources were available: National Climatic Data Center (NCDC) hourly observations, TCEQ hourly observations, and TCEQ 5-minute observations.

The NCDC hourly observations include land-based reports (METARs) and buoy, C-MAN, and PORTS coastal observations. All observations represent instantaneous or very short term (3-5 min) averages. Because the coastal observations are located near topographic discontinuities which may or may not be faithfully represented by the local model topography, the marine and coastal observations were excluded from this assessment. Such observations should be included in the future after careful examination of the comparative topography. This report henceforth refers to this verification data set as METAR data. The METAR observations are typically taken a few minutes before the top of the hour; no correction is applied here for this time offset. The error introduced by this offset should be much smaller than other sources of error.

Given the choice between hourly and 5-minute TCEQ observations, the 5-minute observations are preferred because the MM5 model output represents instantaneous values rather than hourly averages. (A different choice would be made if the model output consisted of hourly averages.) The observations at the top of the hour, corresponding to a 5-minute average beginning at that time, are used; no correction is applied here for the small effective time offset.

Rather than merge the two validation data sets, validation statistics are computed separately for the two. The observations have different geographical distributions; the TCEQ is more heavily weighted toward urban areas, for example. Also, meteorological siting characteristics for the METAR observations tend to be superior to the TCEQ observations. Separating the validation statistics permits comparison of the characteristics of the two data sets for performance evaluation.

Metstat input files for the two data sets were generated from the data files posted on the TAMU TexAQS-II web site (http://www.met.tamu.edu/texaqs2) using software written for this purpose. Individual station data files were merged and sorted by time, and station

location information was added to each line of data during the merger process. This was accomplished using a brief shell script. Two FORTRAN 77 programs (one for each data set) reformatted the merged files into Metstat input format. The scripts, programs, and Metstat input files are available upon request.

During the course of evaluation, it was discovered that the 5-minute reports from stations C641 (Beeville), C647 (Palestine), and C651 (Temple) included invalid data. These threestations were therefore excluded from the performance evaluation.

In Section 3 it was noted that "statistical comparisons of model output with observations should be viable throughout the period in the Dallas-Fort Worth area, because convection was relatively sparse there. In the Houston area, because of the strong and random influence of convection on observations, an analysis of all model runs is only viable for July 30, with the grell4day3 run worth examining on August 1 and 2 as well." Because separate validation approaches are appropriate for North Texas and Southeast Texas, statistics are computed on these two regions separately. Fig. 61 shows the boundaries of these regions.

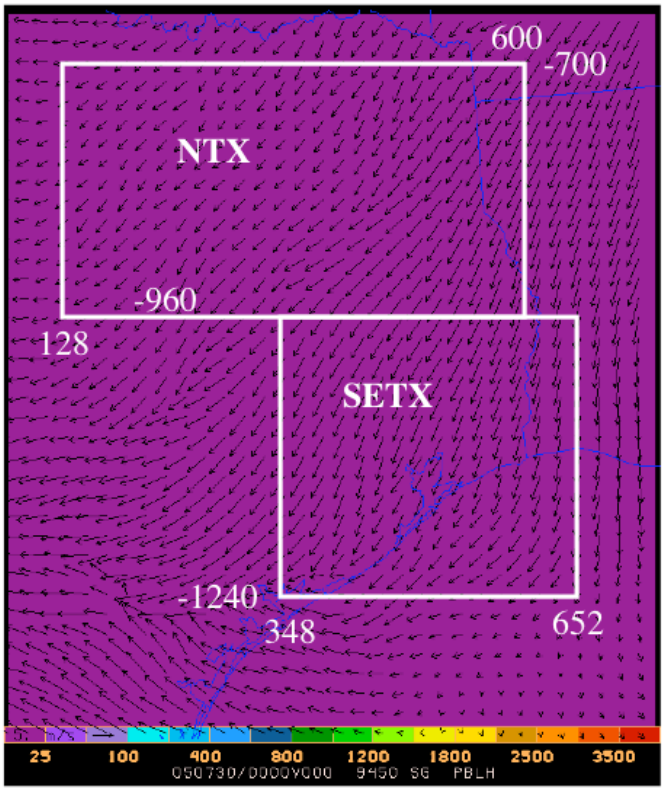

Figure 61: Boundaries of North Texas (NTX) and Southeast Texas (SETX) model validation regions. The numbers correspond to the grid point indices relative to the center of the outermost grid.

b) Performance Evaluation, North Texas

Fig. 62 shows the wind direction bias for the North Texas region. In this and other images, errors are grouped by model run and validation data set. So, for example, the first group of bars is labeled "grell4day3 North_Texas TCEQ_Data", meaning that the model run is grell4day3, the region verified is North Texas, and the verification data set was the 5-minute TCEQ data.

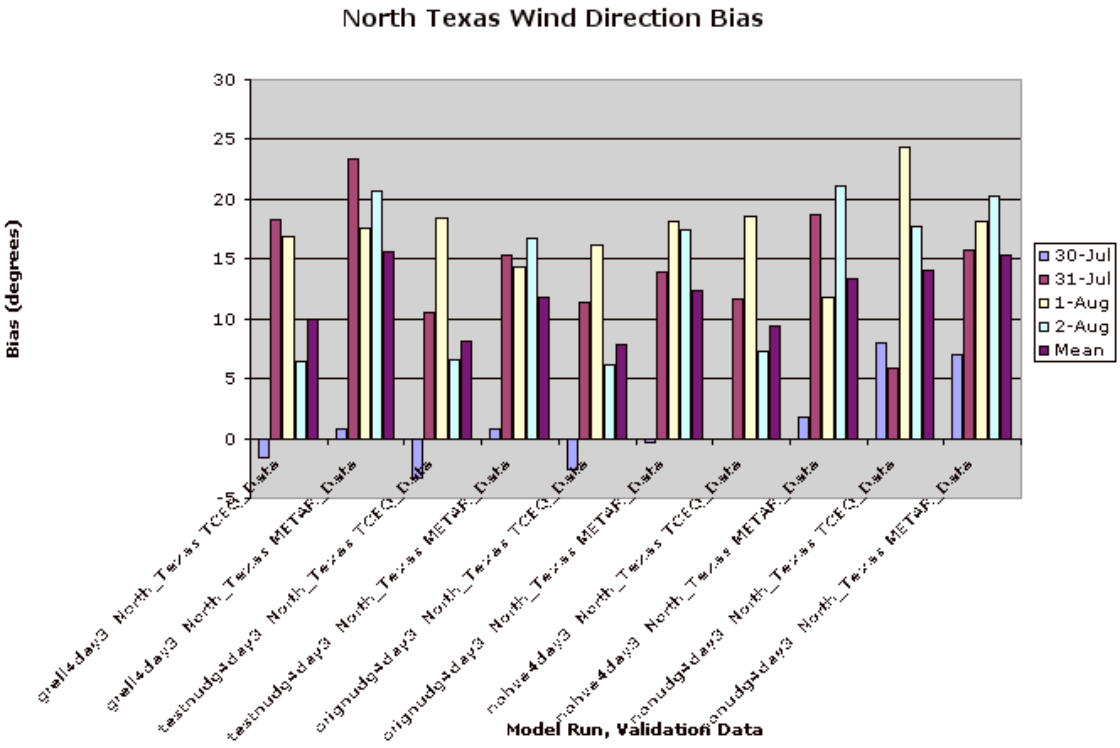

Figure 62: Wind direction bias in North Texas region for five model runs, using two verification data sets (METAR and TCEQ). The five bars for each model run correspond to July 30, July 31, August 1, August 2, and the mean of all four days.

The model bias is generally smaller for the METAR data than the TCEQ data. Biases are relatively small on July 30 but larger on the other three days. The orignudg4day3 run consistently has one of the smallest biases. The nonudg4day3 run has the largest biases on average, except when compared to grell4day3 using METAR data.

The wind speed bias for North Texas occurs mainly on July 30 (Fig. 63). With respect to speed, the bias is generally smaller for the TCEQ data than for the METAR data. There is little difference in performance among the model runs with nudging. The nonudg4day3 run had slightly smaller wind speeds than the other runs.

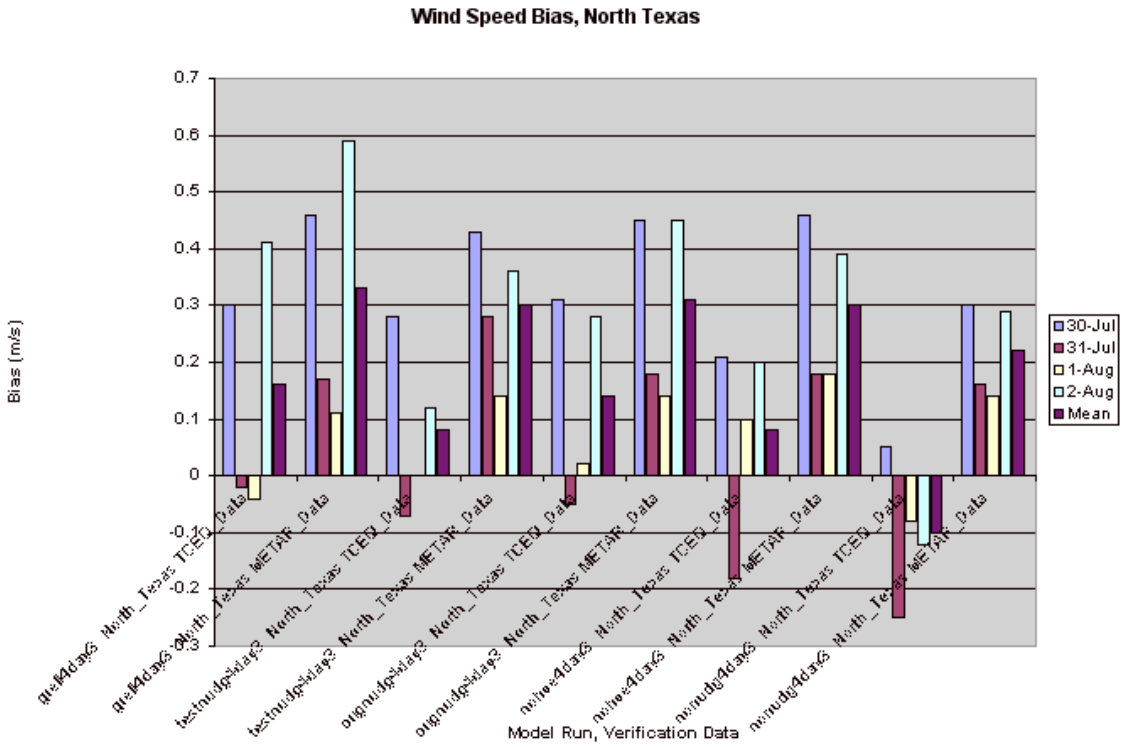

Figure 63: Wind speed bias in North Texas region for five model runs, using two verification data sets.

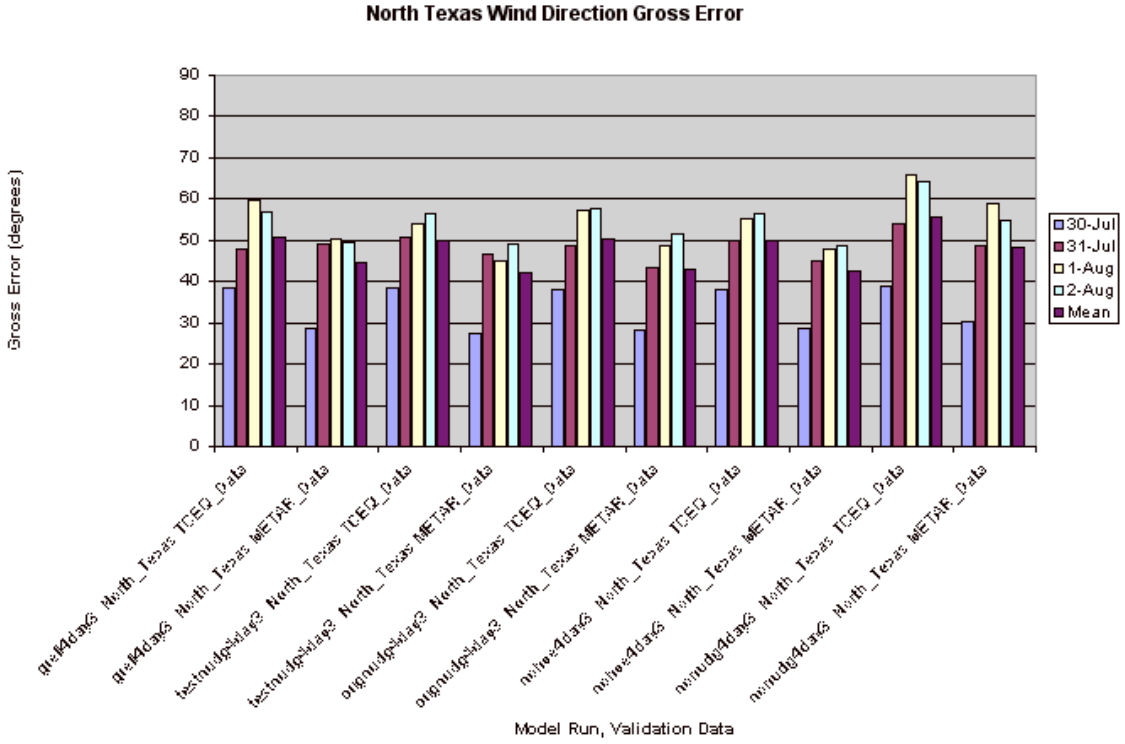

Figure 64: Wind direction gross error in North Texas region for five model runs, using two verification data sets.

The wind direction gross error for North Texas (Fig. 64) is similar to the wind direction bias, in that the largest gross error is found in the nonudg4day3 model run. The METAR gross error is smaller than the TCEQ data gross error.

A detailed look at model wind performance in North Texas is provided by hourly Metstat time series for the orignudg4day3 and nonudg4day3 model runs. Fig. 65 shows the observed and simulated wind direction, and Fig. 66 shows the observed and simulated wind speed.

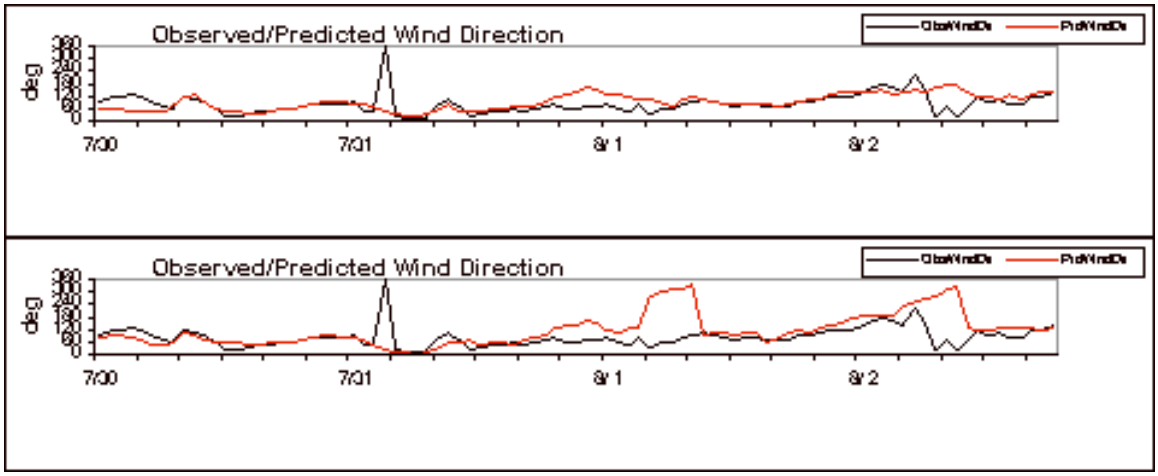

Figure 65: Observed (black) and predicted (red) wind direction, orignudg4day3 (top) and nonudg4day3 (bottom) model runs, averaged over all North Texas METAR observations.

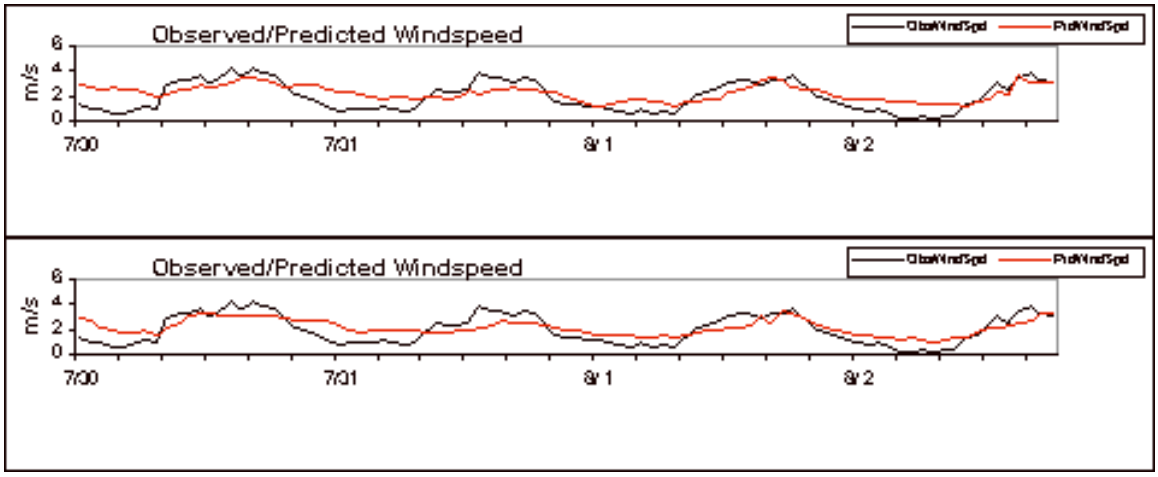

Figure 66: Observed (black) and predicted (red) wind speed, orignudg4day3 (top) and nonudg4day3 (bottom) model runs, averaged over all North Texas METAR observations.

After a few hours of differences, the predicted wind directions track the actual wind directions closely until the evening of July 31 (Fig. 65). The spike in the observed wind

direction early on July 31 is an artifact of the mean wind direction temporarily becoming slightly west of north. Significant directional errors are present during the evening of July 31, while wind speeds are about 2 m/s. Larger errors appear in the nonudg4day3 around sunrise on August 1 and August 2, but the actual wind speeds are near zero at that time, so the errors do not represent large transport issues.

The wind speeds with and without nudging are very similar (Fig. 66). Both models underestimate the wind speed during the day and overestimate it at night. The orignudg4day3 run has a slight tendency for erroneously higher wind speeds in the pre-dawn hours. The consistent weakness of the diurnal cycle in the wind speed, with and without nudging, suggests a problem with the vertical mixing parameterization.

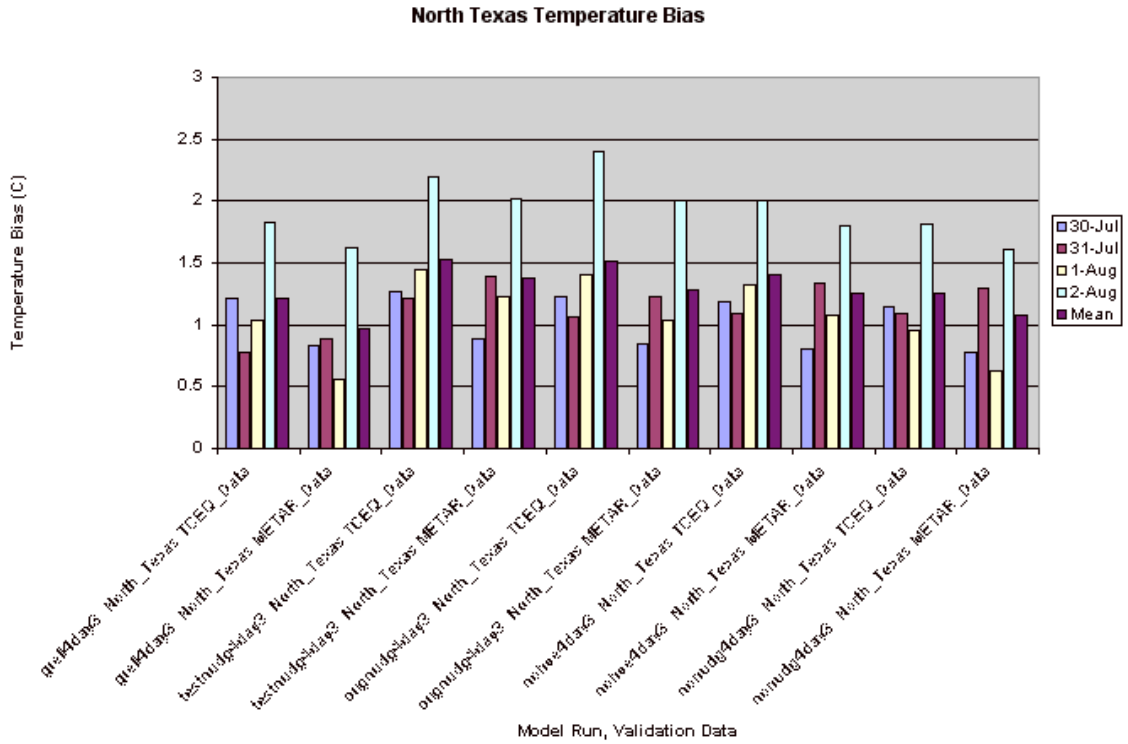

Figure 67: Temperature bias (C) in North Texas region for five model runs, using two verification data sets.

The temperature performance in North Texas shows less consistent improvement from nudging (Fig. 67). This is to be expected, since the topography in North Texas is relatively featureless and the distribution of convection changed little. Indeed, the nonudg4day3 run has the second-smallest bias, after grell4day3. The unsystematic component of the RMS error (Fig. 68) also has very little overall difference among the model runs. The METAR validation data set is associated with smaller biases and smaller unsystematic errors than the TCEQ data set.

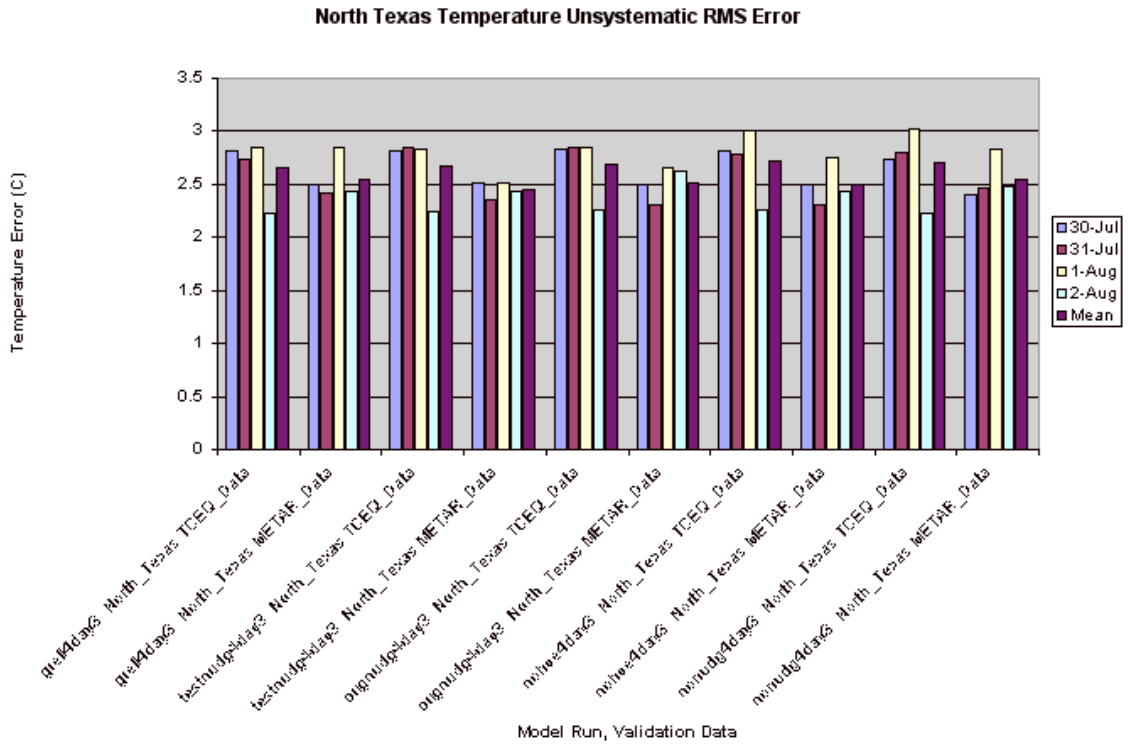

Figure 68: Temperature unsystematic root-mean-square error (C) in North Texas region for five model runs, using two verification data sets.

Figure 69 shows the Index of Agreement among the models and validation data sets. Consistent with Figs. 67-68, there is little difference among the models, but the Index of Agreement is considerably higher for the METAR data set than for the TCEQ data set.

To further investigate the temperature performance, the observed (by METAR) and predicted temperatures are shown in Fig. 70 and the RMS temperature error time series are shown in Fig. 71. There is a consistent diurnal signal, with the model repeatedly warming temperatures too rapidly and too much in the morning, then cooling to realistic values around sunset. Model temperature performance seems unaffected by nudging.

Temperature RMS errors have the largest value at the time when the biases are largest: during the daytime, particularly around noon. RMS errors average close to 4 K during this period. Errors are much smaller (around 2 K) at night. The index of agreement (Fig. 72) is similar, with a large index of agreement at night and a comparatively small index of agreeement during daytime.

Overall, nudging has produced a modest improvement in wind over the North Texas region, and negligible impact on temperature.

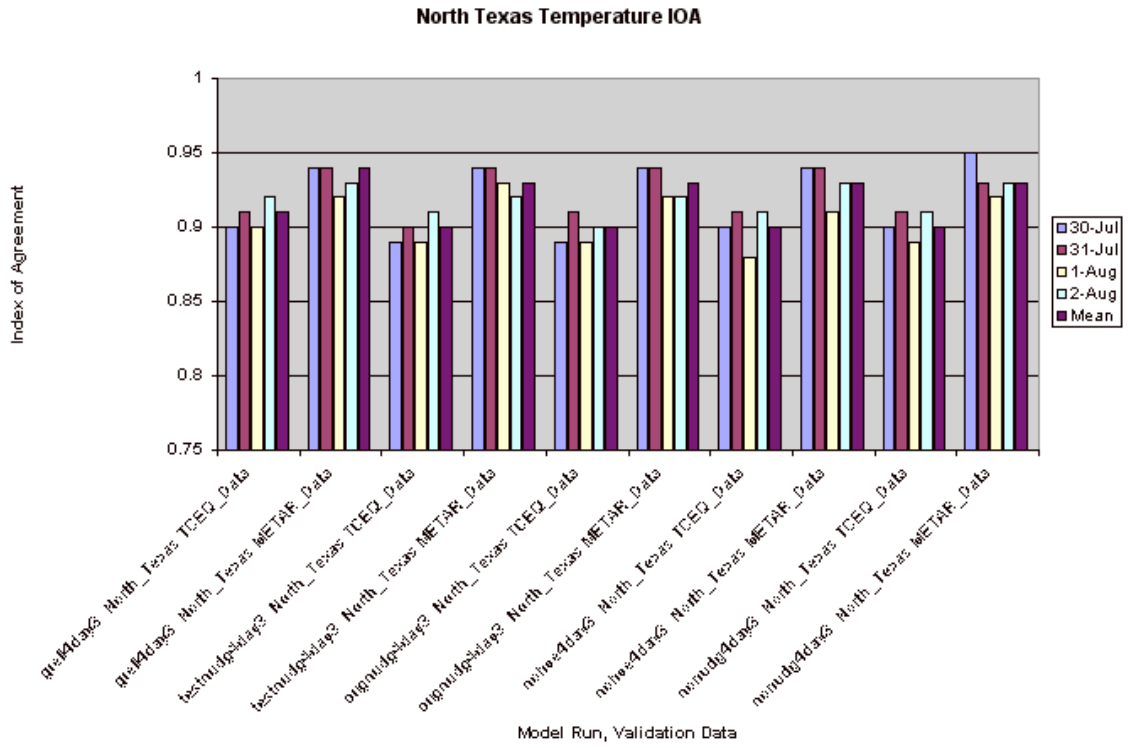

Figure 69: Temperature Index of Agreement (unitless) in North Texas region for five model runs, using two verification data sets.

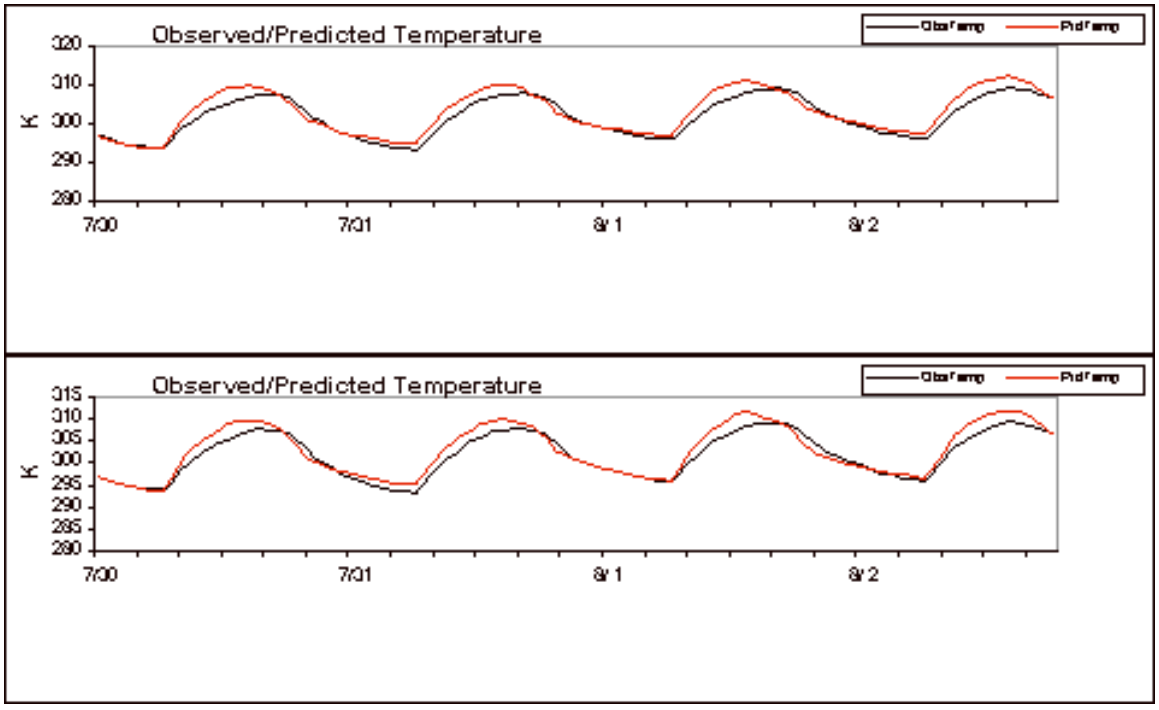

Figure 70: Observed (black) and predicted (red) temperature, orignudg4day3 (top) and nonudg4day3 (bottom) model runs, averaged over all North Texas METAR observations.

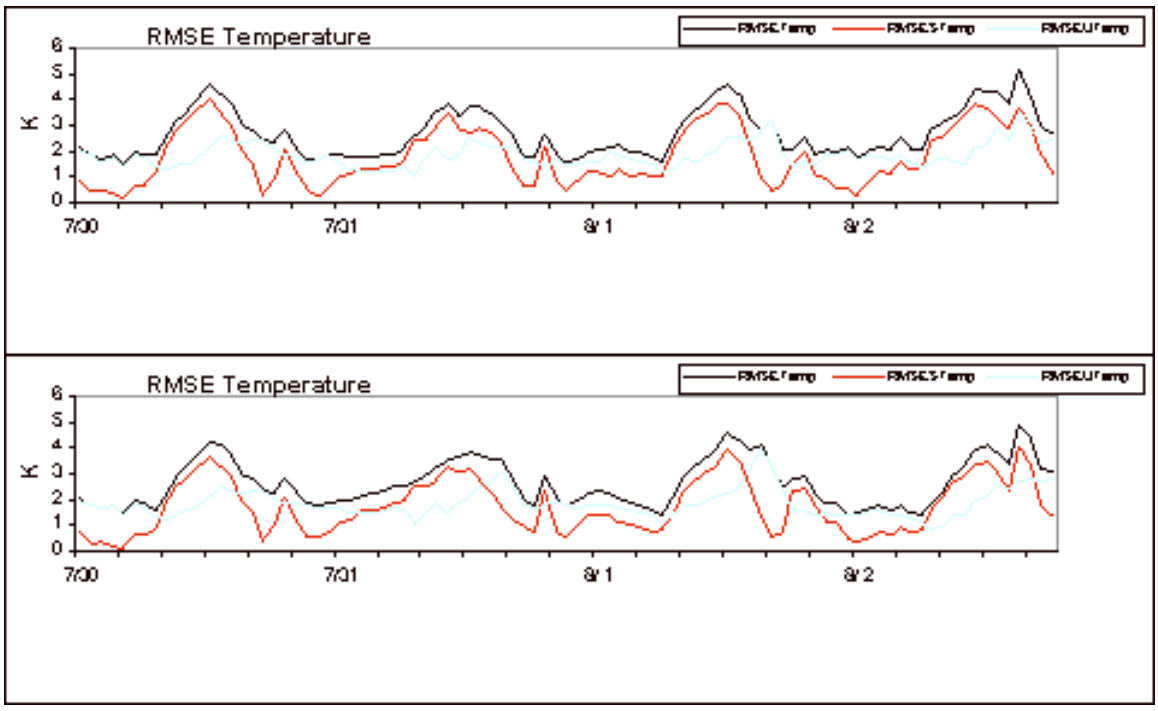

Figure 71: Total (black), systematic (red), and unsystematic (cyan) RMS temperature error (K), orignudg4day3 (top) and nonudg4day3 (bottom) model runs, averaged over all North Texas METAR observations.

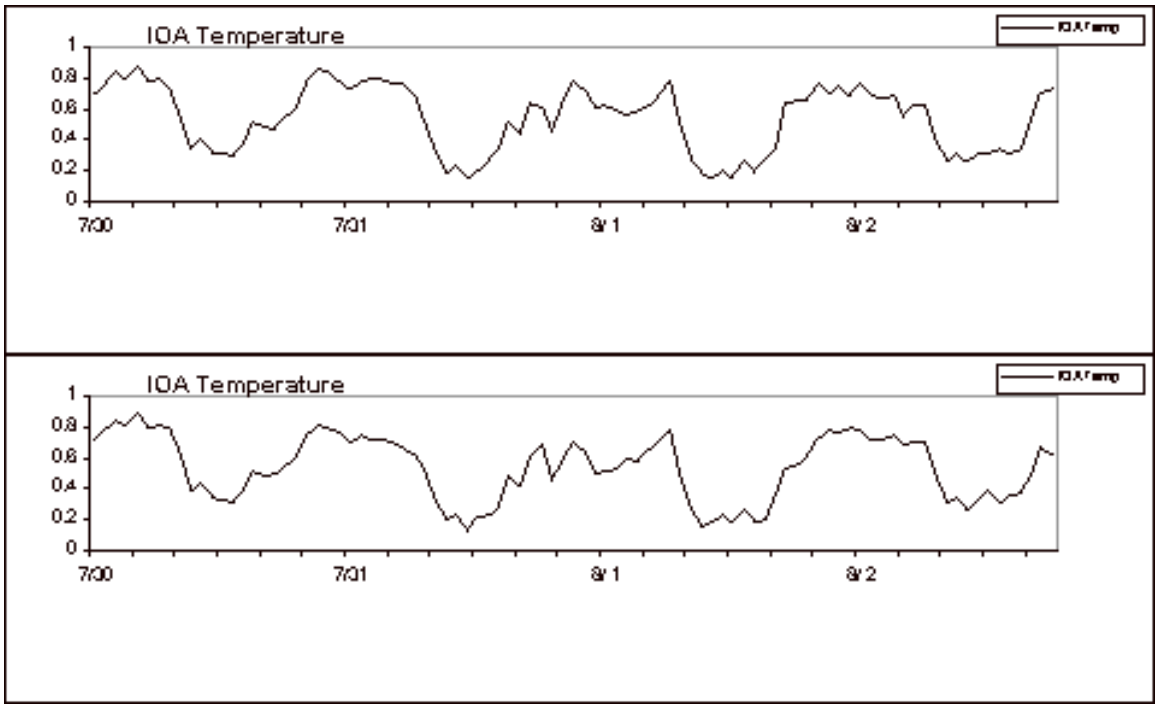

Figure 72: Index of Agreement for temperature, orignudg4day3 (top) and nonudg4day3 (bottom) model runs, computed over all North Texas METAR observations.

c) Performance Evaluation, Southeast Texas

The wind direction bias for Southeast Texas is shown in Fig. 73. Recall that winds are likely to be poor after July 30 in all but the grell4day3 model run. As in North Texas, most biases are positive, indicating that the model wind is rotated slightly clockwise from the actual wind. Most daily biases associated with the grell4day3 model run are considerably smaller than the biases associated with the nonudg4day3 run.

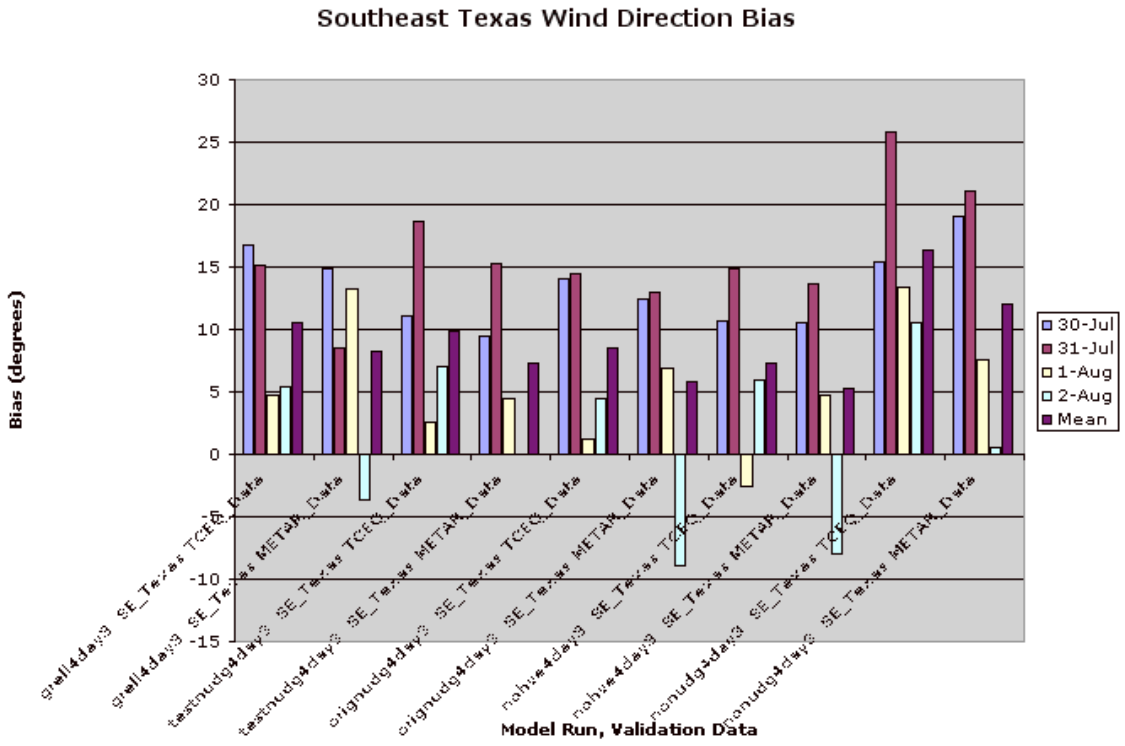

Figure 73: Wind direction bias in Southeast Texas region for five model runs, using two verification data sets (METAR and TCEQ).

Unlike North Texas, the wind speed bias (Fig. 74) is smaller with nudging than without. The bias is smallest for the grell4day3 run, which has relatively less error due to convection. The reduction of the convection error has as large an impact as the assimilation of wind profiler data. The bias is larger for the METAR observations than for the TCEQ observations.

The wind direction gross error (Fig. 75) indicates a dramatic improvement due to nudging. The improvement is across the board, with grell4day3 not better than the other nudging simulations.

Fig. 76 compares the observed and predicted wind speeds. The wind speeds are similar at most times, but the nonudg4day3 run systematically has wind speeds too strong between midnight and 6:00 AM CST.

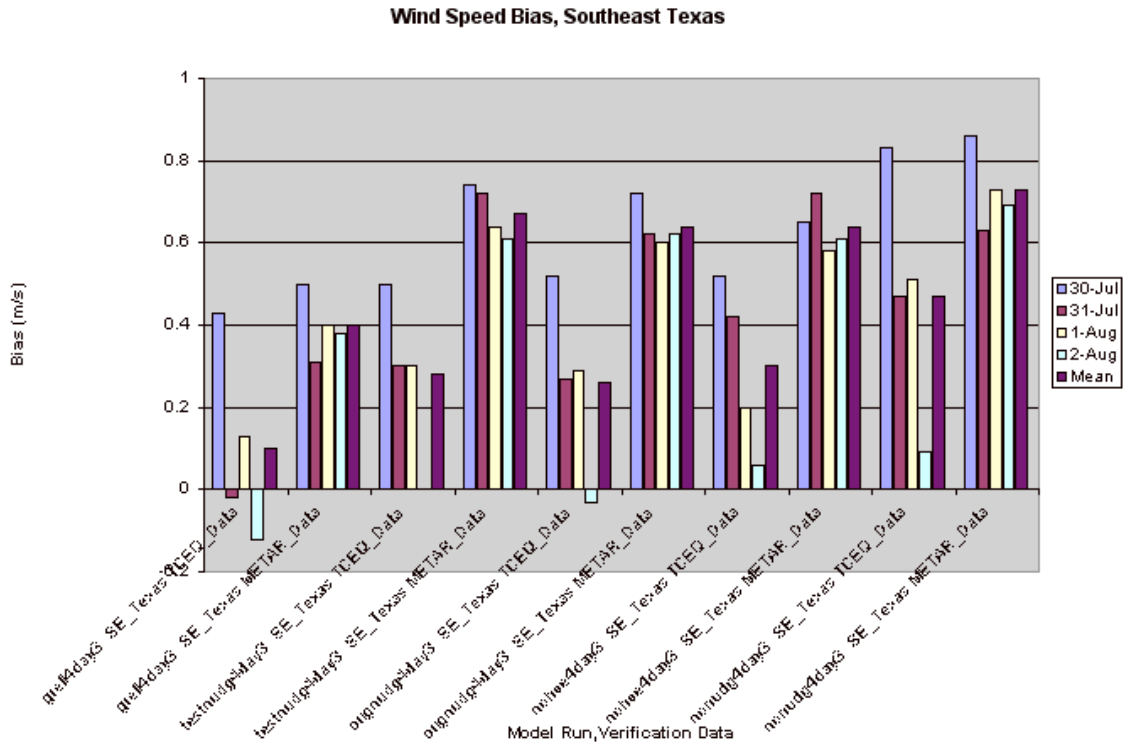

Figure 74: Wind speed bias in Southeast Texas region for five model runs, using two verification data sets (METAR and TCEQ).

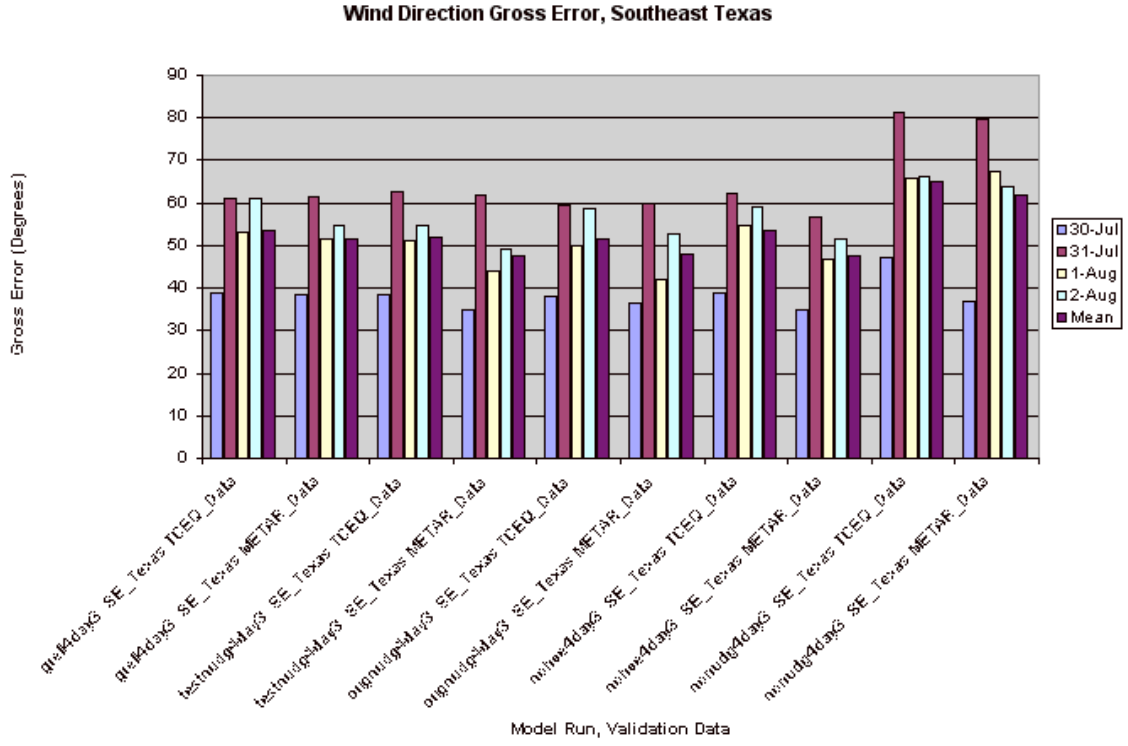

Figure 75: Wind direction gross error in Southeast Texas region for five model runs, using two verification data sets (METAR and TCEQ).

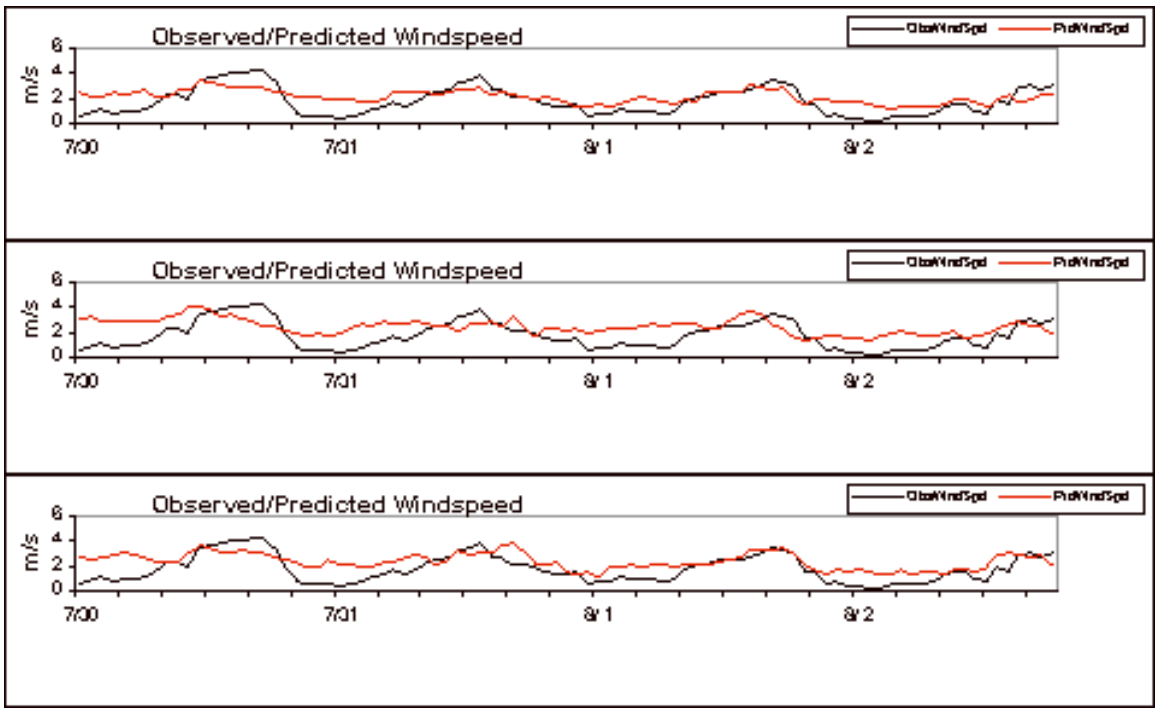

Figure 76: Observed (black) and predicted (red) wind speed, grellnudg4day3 (top), nonudg4day3 (middle), and orignudg4day3 (bottom) model runs, averaged over all Southeast Texas METAR observations.

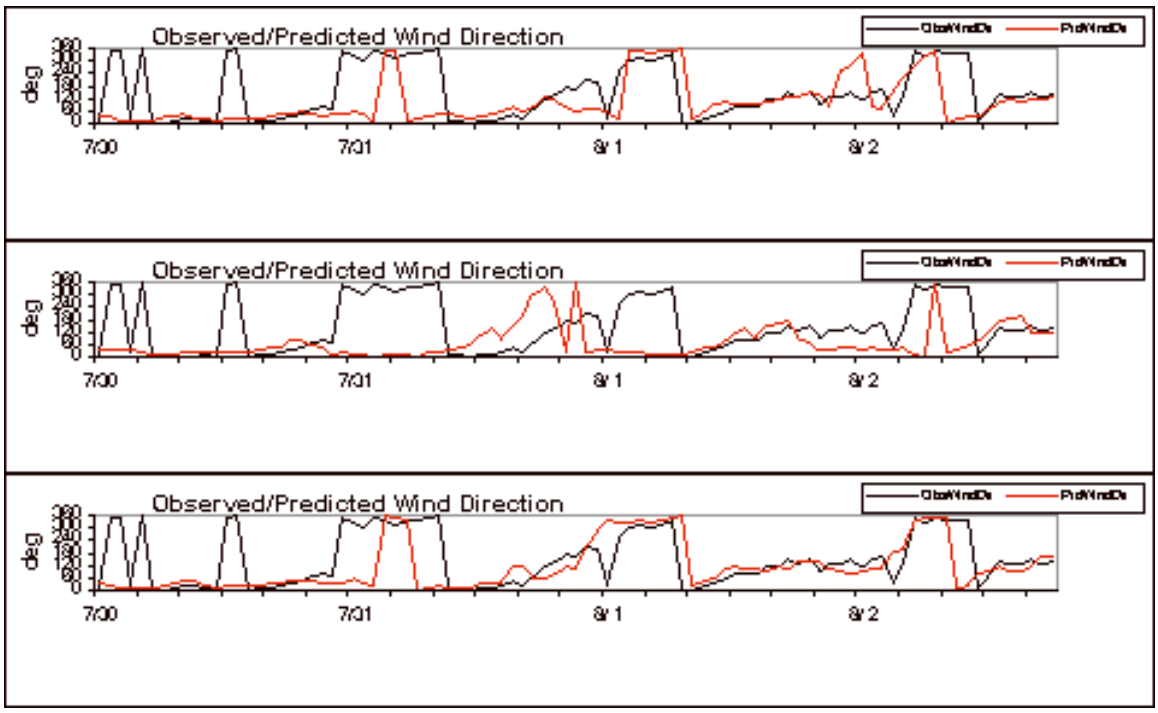

Figure 77: Observed (black) and predicted (red) wind direction, grellnudg4day3 (top), nonudg4day3 (middle), and orignudg4day3 (bottom) model runs, averaged over all Southeast Texas METAR observations.

The wind direction (Fig. 77) in the nonudg4day3 run includes substantial direction error late on July 31 and around midnight the following night as well. Nudging sucessfully eliminates most of these errors, except for a short-lived error around midnight in grell4day4.

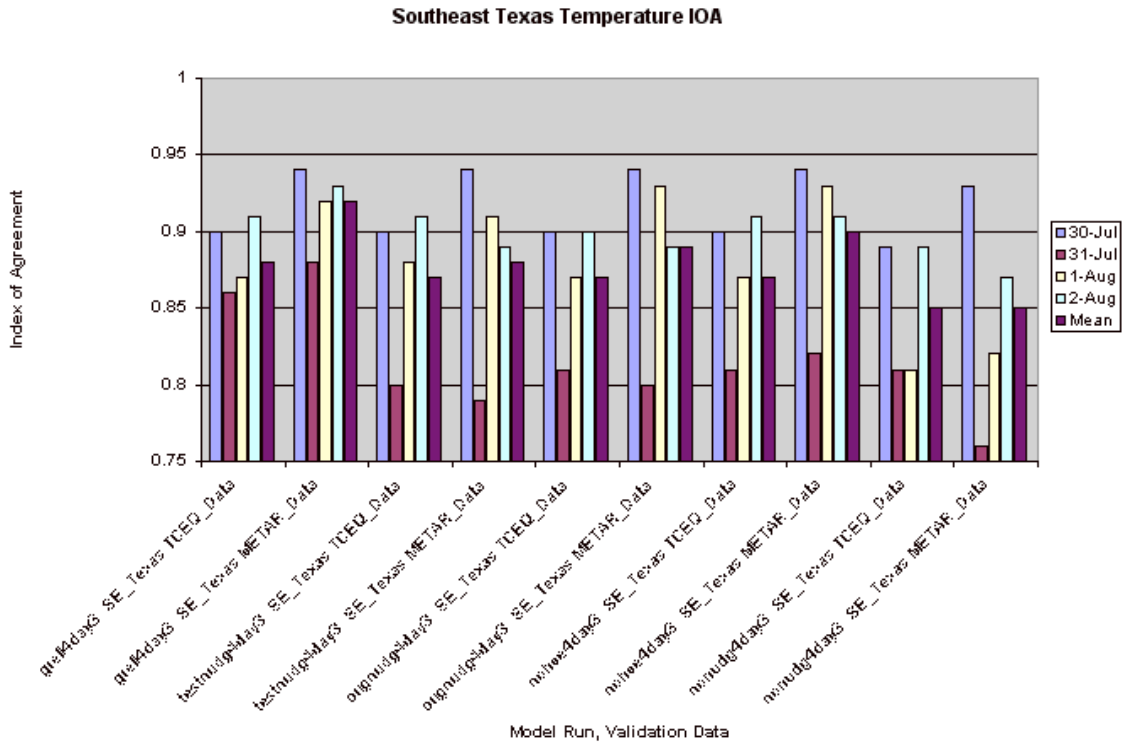

Figure 78: Temperature Index of Agreement in Southeast Texas region for five model runs, using two verification data sets (METAR and TCEQ).

The models had a difficult time with simulating temperature in southeast Texas, at least partly because of the extensive convection. Fig. 78 shows that the Index of Agreement was relatively high on July 30 (especially when computed with METAR data) and lower on other days. The Index of Agreement was lowest for the nonudg4day3 run, which had the most difficulty with convection; on July 30 the nonudg4day3 run is only slightly worse than the other simulations.

The temperature traces are shown in Fig. 79. In North Texas, there was a substantial warm bias (Fig. 70). In Southeast Texas, the temperature rise is at approximately the right time and magnitude, particularly on July 30 when convective activity was limited. The effect of convection is readily discerned on the other days, because both the nonudg4day3 and orignudg4day3 runs have premature cooling in the afternoons of July 31 and August 1. Even the grell4day3 run had too much convection on July 31, leading to a cold bias in afternoon temperaturees.

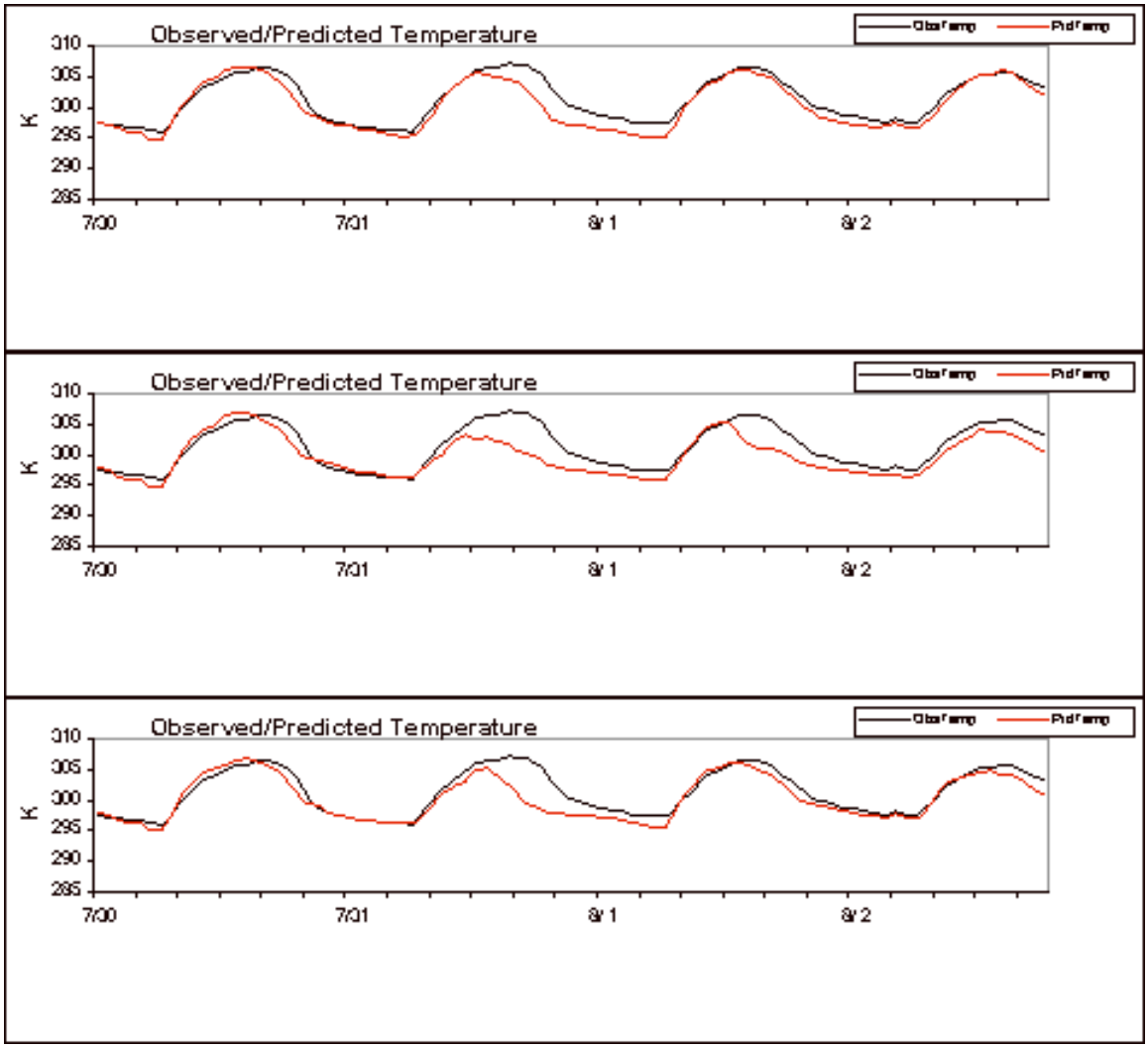

Figure 79: Observed (black) and predicted (red) temperature, grellnudg4day3 (top), nonudg4day3 (middle), and orignudg4day3 (bottom) model runs, averaged over all Southeast Texas METAR observations.

d) Summary

Nudging had a minor impact on winds in North Texas, where wind errors were initially relatively small, and a major impact on winds in Southeast Texas, where errors were larger. The winds are more accurate in grell4day3 in Southeast Texas, apparently due to the absence of spurious convection. For similar reasons, the temperature forecast in grell4day3 is more accurate, with convection leading to negative temperature biases during the afternoon.

The METAR observations were generally in better agreement with the model simulations than were the TCEQ observations. Both observational data sets consistently demonstrated the benefits produced by nudging. The better agreement with METAR

observations is consistent with the hypothesis that the METAR observations are more accurate or spatially representative than the TCEQ observations.

The sensitivity forecasts, nohve4day3 and testnudg4day3, were indistinguishable from orignudg4day3, except for occasional apparently random differences.

Model temperatures exhibited a warm bias during the day in North Texas.

6. Vertical Profilers of Wind and Temperature

Because the wind nudging occurs throughout the depth of the troposphere (in the case of the NOAA tropospheric profilers), wind fields are affected at all levels, not just at the surface. The time available for this project does not permit a comprehensive performance evaluation of the vertical distribution of winds and temperatures. Instead, examples will be shown of the impact of the nudging and the differences among the various simulations.

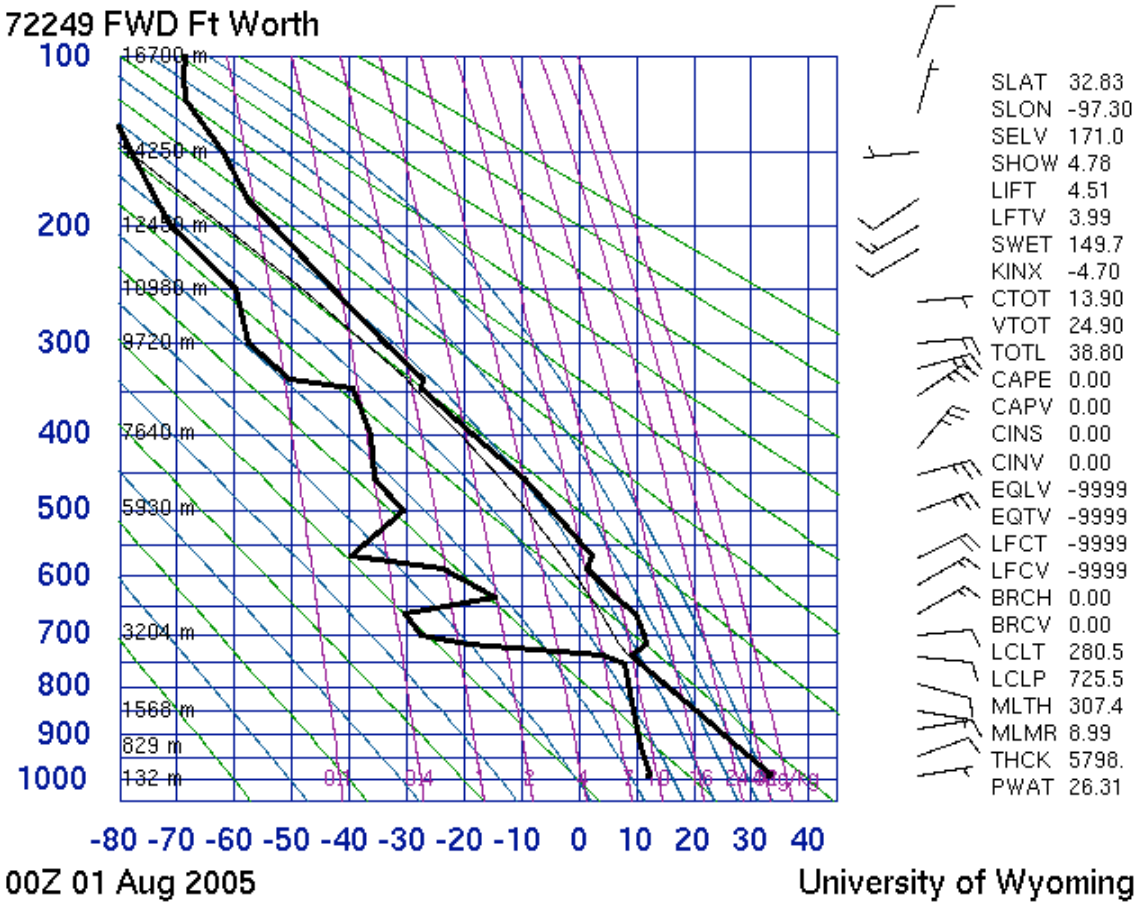

Figure 80: Observed sounding, Fort Worth, Texas, 00 UTC August 1, 2005.

Figure 80 shows the observed sounding from Fort Worth at 00 UTC August 1, 2005 (6:00 PM CST July 31, 2005), and Figure 81 shows the corresponding soundings from three model runs.

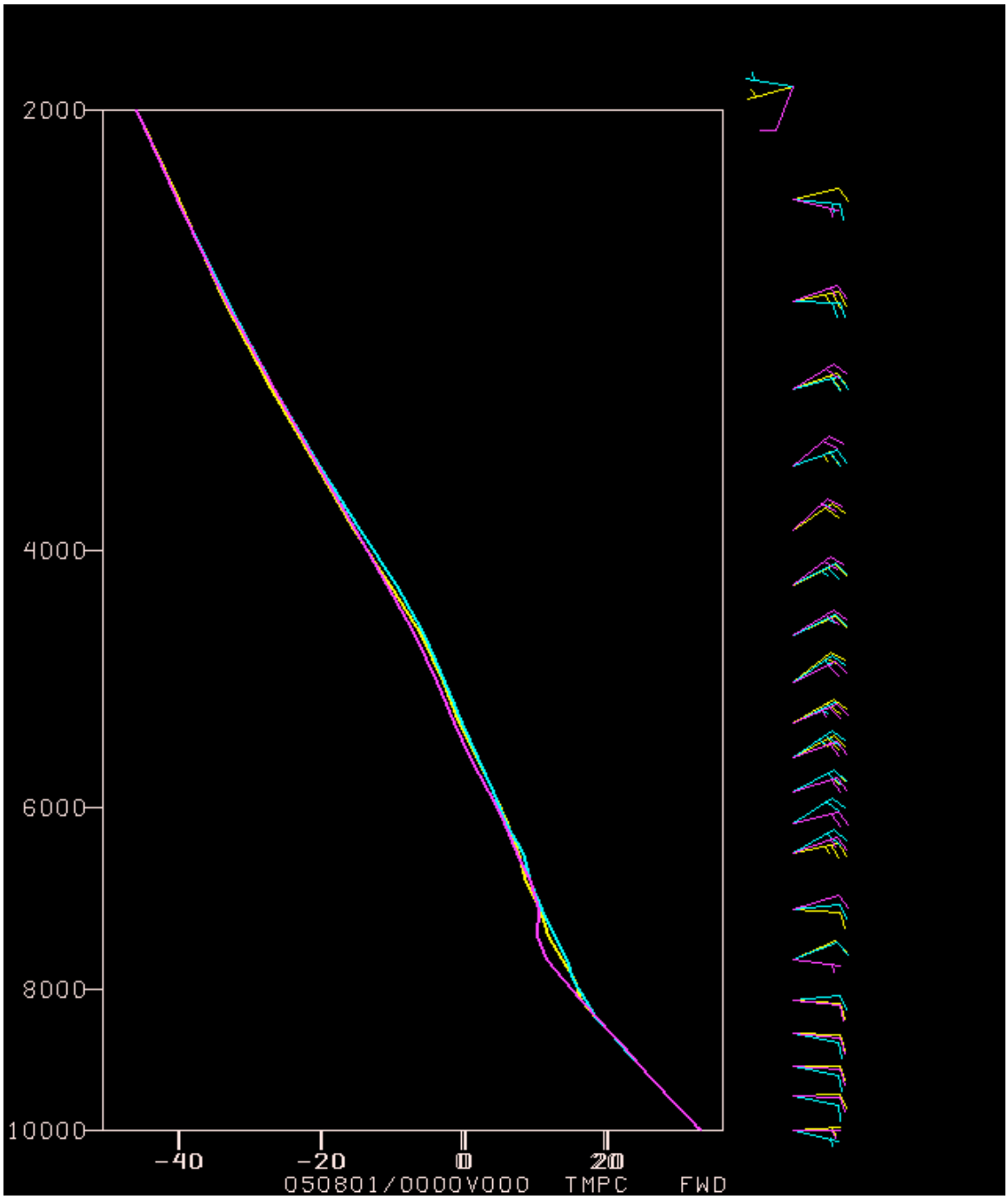

Figure 81: Simulated vertical profiles of temperature and wind, 00 UTC August 1, 2005. Vertical coordinate is sigma. Violet: nonudg4grid3. Yellow: orignudg4grid3. Cyan: grell4grid3.

All soundings show a well-mixed layer in the lower troposphere, with some variation in the height of the top of the mixed layer. The observed mixed layer extends up to about 740 mb, or about sigma=7600. The nonudg4grid3 sounding has a similar mixed-layer height, while the other two model simulations have a significantly shallower mixed layer. However, Figs. 42 and 43 show that there is considerable spatial variation of the mixing height during this day, with nonudg4grid3 being deeper in some places and orignudg4grid3 being deeper in others. Thus it seems that the superior performance of nonudg4grid3 in this instance is essentially a random occurrence.

There are slight variations of temperature in the free troposphere, but these do not appear to be systematic and the magnitude of variation is within the range of observation error. Such temperature changes may be caused by variations in convection or by convergence and divergence patterns produced by adjustment to the observational nudging.

Winds are also similar in all three simulations. The largest differences occur near sigma=8000, which is within the mixed layer for nonudg4day3 and above the mixed layer for the other simulations. Here, the nonudg4day3 wind is from the east-southeast, reflecting the winds in the rest of the mixed layer, while the winds in the other two models are from the northeast, reflecting the winds in the free troposphere.

The spatial pattern of wind fields produced by data assimilation is investigated in Figs. 82 and 84. These images are for 09 UTC August 1, 2005. This particular date and time are chosen because the simulations had the greatest difficulty with overprediction of convection in southeast Texas during the preceding day, and consequently would be expected to have significant errors overnight due to erroneous development (or lack thereof) of the sea breeze coastal oscillation and low-level jet. Because the coastal oscillation is triggered by pressure differences during the day and the winds essentially drift on their own during the night, an accurate nighttime pressure distribution is insufficient to produce an accurate nighttime wind pattern. A level near the expected core of the sea-breeze low-level jet is chosen for analysis.

Figure 82 shows the wind simulations with and without nudging. The change in the wind field due to nudging is dramatic in the southern portion of the domain. The no-nudging simulation (upper left panel) has northeasterly winds across the Texas coastal plain, with wind speeds approaching 15 kt between Houston and Victoria. In stark contrast, the orignudg4day3 run (upper right panel) preserves the northeasterlies over the water but features southwesterlies over land. Southwesterly flow at this time of night is consistent with the expected rotation of the sea-breeze low-level jet.

The testnudg4day3 run (lower left panel) does not have the same broad area of southwesterlies as the orignudg4day3 run. Both runs are consistent with the near-coastal profilers at Beeville and LaPorte, as would be expected since both runs nudge to the profiler observations. However, the testnudg4day3 run produces two patches of southwesterly flow, in contrast to the more spatially coherent pattern of orignudg4day3. The difference between the two simulations is caused by the radius of influence of the nudging, which is set to 150 km in the testnudg4day3 simulation and 240 km in the

orignudg4day3 simulation. With a smaller radius of influence, the testnudg4day3 simulation is producing smaller-scale adjustments to the wind field.

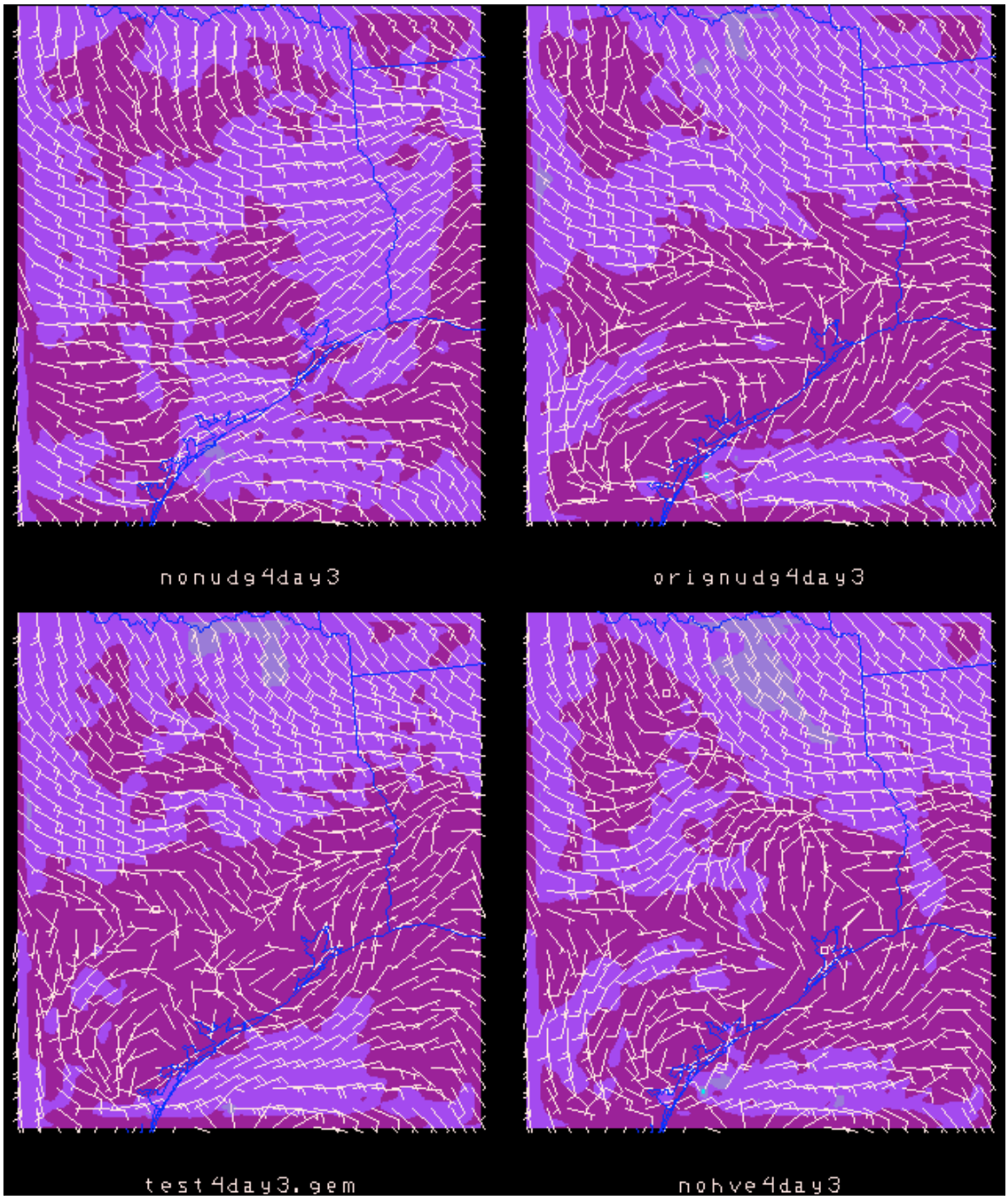

Figure 82: Sigma 9550 (approximately 400 m above ground level) wind simulations, 09 Z (3:00 AM CST) August 1, 2005, from four different simulations (labeled). Wind speeds are shaded in 5 m/s increments, and wind barbs have their conventional meaning (one long barb is 10 kt, etc.).

Which model run is more correct? Without additional profilers, it is not possible to verify the wind field directly, but indirect verification may be obtained from the surface wind pattern. Fig. 83 shows the Texas surface observations for one hour before the time shown in Fig. 82, and Fig. 84 shows the Texas observations one hour after the time shown in Fig. 82.

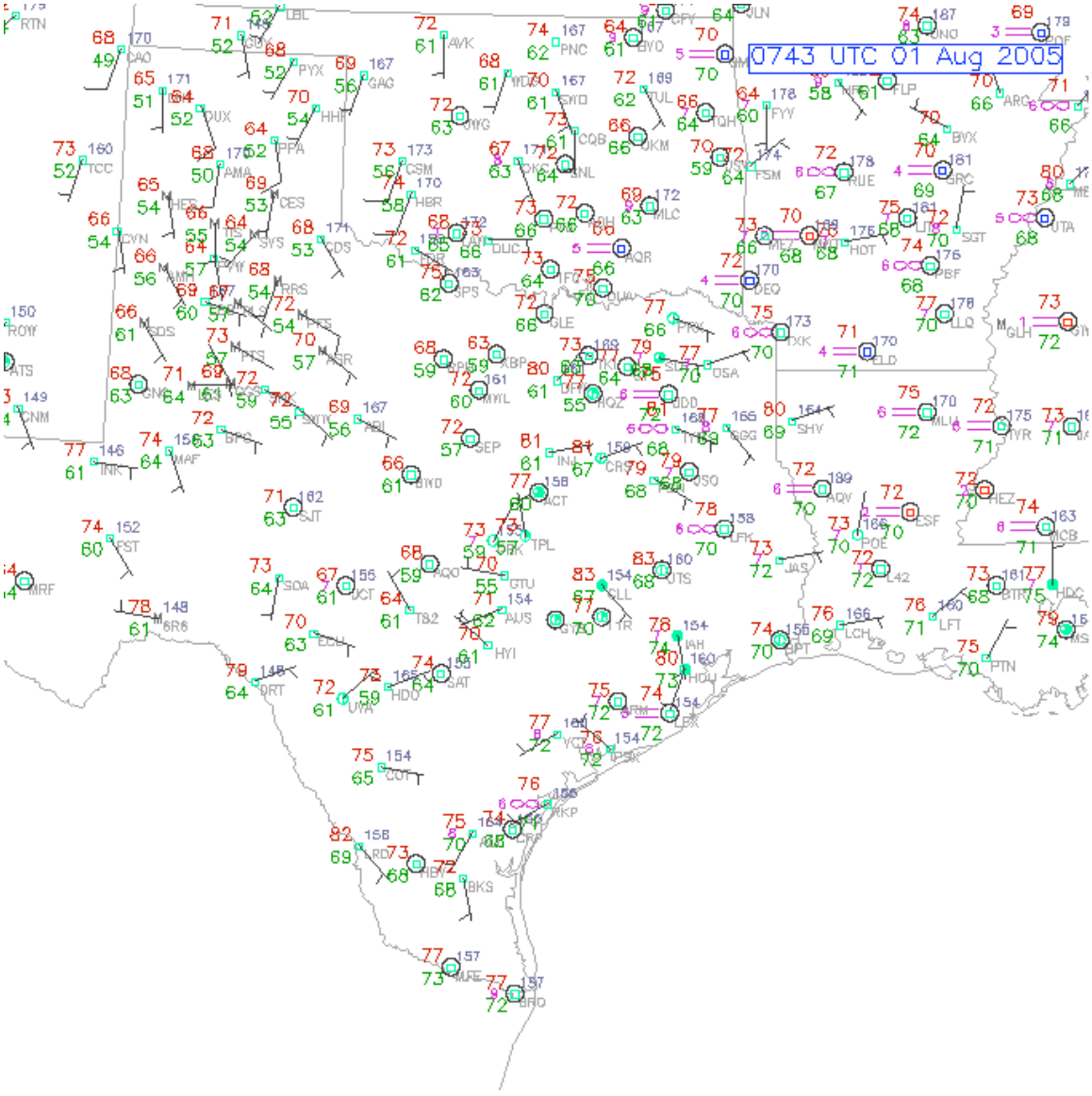

Figure 83: Surface map, south-central United States, 0743 UTC August 1 2005. Figure courtesy of NCAR.

At 0743 UTC (Fig. 83), winds at many locations along the Texas coastal plain are shore-parallel, such as the southwest winds at Alice, Victoria, and Rockport. The extended area of southwest winds are consistent with the orignudg4day3 model run, not the testnudg4day3 model run.

At 0943 UTC (Fig. 84), the winds at these and other locations have continued to veer and have become westerly or northwesterly. This evolution is consistent with the sea-breeze coastal oscillation, and a similar evolution is present in the profiler winds at Beeville and LaPorte (not shown). The broad area of surface winds experiencing this coastal oscillation also independentently confirms the orignudg4day3 model run.

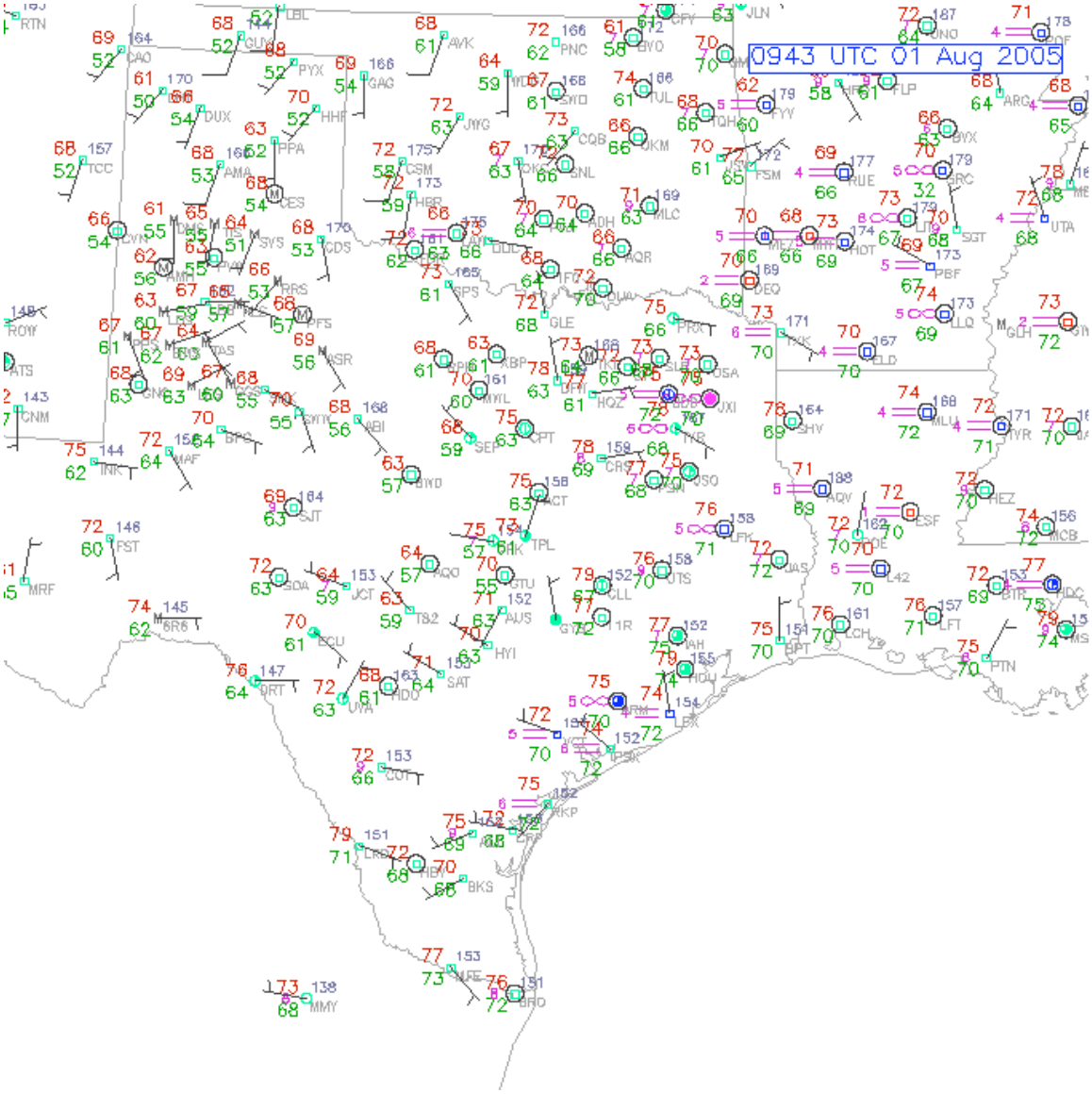

Figure 84: Surface map, south-central United States, 0943 UTC August 1 2005. Figure courtesy of NCAR.

The lower right panel in Fig. 82 shows the wind field from the nohve4day3 model run. This run differs from orignudg4day3 in that the wind data from the Huntsville wind profiler were withheld from the data assimilation system. In the nohve4day3 simulation, the winds in the Huntsville area are strong from the north, while in orignudg4day3, they are weak from the southeast. The nonudg4day3 simulation had the winds strong from the northeast, so nohve4day3 is actually worse than nonudg4day3 in this area.

It appears that the westerly and northwesterly winds assimilated at LaPorte are causing the model to draw in air from all directions, including from the north, while the surface maps indicate the true source of air was from the southwest. This is an indication of the unreliable nature of assimilated wind patterns between observing stations when the wind patterns are not being caused by a large-scale weather feature.

Figure 85 repeats the nonudg4day3 winds in the upper left panel. In the upper right panel is the difference between the orignudg4day3 winds and the nonudg4day3 winds. The difference map shows that while there are some modifications to the wind field in North Texas, most of the differences arise along the coastal plain.

Despite the agreement between the orignudg4day3 winds and the surface winds, there are some artifacts apparent in the difference field. For example, because model simulations of the sea-breeze low-level jet produce a jet of fairly uniform width, the modified wind fields also would be expected over a fairly regular geographical area. Instead, the modification is broad in south-central Texas and narrower in southeast Texas. These variations are probably related to differences in spatial profiler coverage and the location of profiler observing sites relative to the location of the sea-breeze low-level jet.

Another possibly important difference occurs in the southwestern corner of the model domain. The surface winds (Figs. 83 and 84) show that the coastal oscillation covers this area too, yet the modification to the wind field is weak (Fig. 85) and the simulated winds with nudging remain easterly there (Fig. 82). This is apparently caused by the close proximity of the 4 km grid boundary and the lack of a sea-breeze low-level jet in the 12 km simulation. A more realistic simulation, especially near the grid boundaries, may result if observation nudging (with profilers) is employed on the 12 km domain as well as the 4 km domain.

The lower left panel in Fig. 85 shows the difference between the grell4day3 run and the nonudg4day3 run. A comparison of this panel with the upper right panel gives an indication of the importance of the extend of the previous day's convection on the nighttime wind fields with data assimilation. In this instance, the effect is minimal and mainly occurs offshore where no profiler observations were available and winds will thus depend more on previous details of the simulation.

Finally, the lower right panel in Fig. 85 shows the difference between the nohve4day3 run and the orignudg4day3 run. These differences are due entirely to the presence or absence of data from Huntsville during the assimilation. Differences for the most part only exceed 5 m/s in central Texas, in the vicinity of Huntsville, where the presence or absence of observations will have a direct influence. The spatial scale of the difference is governed partly by the radius of influence of the data assimilation. In this case, the significant differences extend close to the locations of other nearby profilers. This is appropriate, and indicates that assimilation of Huntsville (and other profiler) winds is affecting the wind patterns on a regional basis, not just at the profiler location itself.

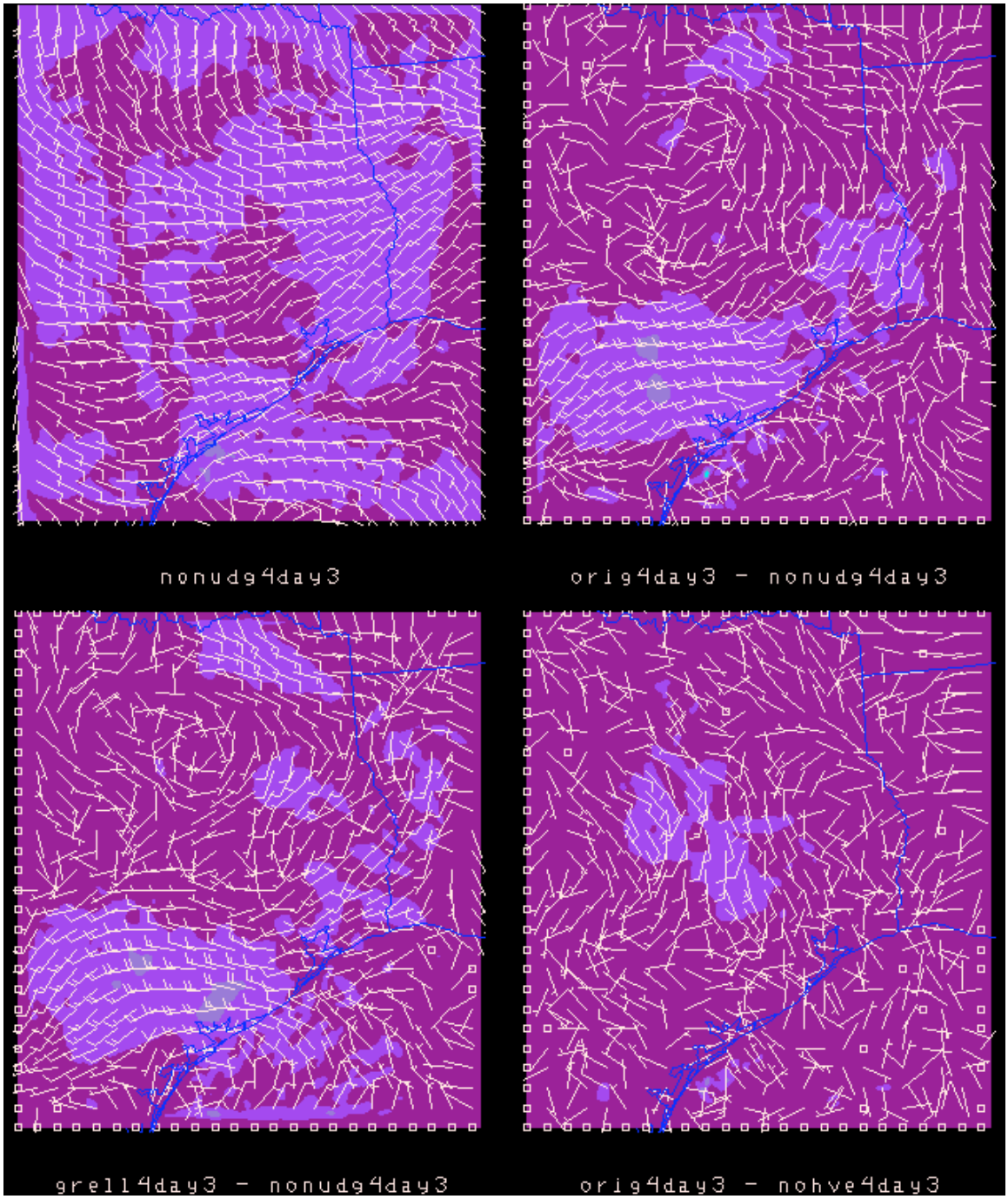

Figure 85: Sigma 9550 (approximately 400 m above ground level) wind simulations and difference fields, 09 Z (3:00 AM CST) August 1, 2005. Upper left: nonudg4day3 winds. Upper right: orignudg4day3 winds minus nonudg4day3 winds. Lower left: testnudg4day3 winds minus nonudg4day3 winds. Lower right: grell4day3 winds minus orignudg4day3 winds. Wind speeds are shaded in 5 m/s increments, and wind barbs have their conventional meaning (one long barb is 10 kt, etc.).

Examination of vertical profiles of temperature are also relevant for verifying appropriate selection of base state constants. Here the following constants are considered, all specified in the namelist.input of INTERPF: ptop (the top pressure level in Pa), p0 (the base state sea-level pressure in Pa), tlp (the base state lapse rate expressed as d(T)/d(ln P), ts0 (the base state sea level temperature in K), and tiso (the base state isothermal stratospheric temperature in K).

Of these, only ptop has the capacity to produce substantial degradation of the model forecast. If ptop is set to be within or close to the upper troposphere, the model run may be unable to dynamically adjust the temperature profile in response to deep convection, leading to a "runaway convection" situation. The tropical tropopause can occasionally occur above 10000 Pa, but always below 7500 Pa. Thus, the choice of 5000 Pa for ptop used in these simulations was appropriate and safe.

The other parameters come into play because many of the model variables (most importantly, pressure) are cast as departures from a basic state value, and the other parameters specify this basic state. Changes in these parameters will introduce random differences in the simulations, but simulation accuracy will not be systematically degraded unless atmospheric conditions depart a great deal from the base state values.

The p0 value of 101300 used in these simulations is appropriate. This value is within a few tenths of a percent of the average summertime mean sea level pressure in Texas.

The ts0 value of 304 K used in these simulations is appropriate. Because the temperature profile will vary linearly (with respect to the log of pressure) from this value at the ground throughout the troposphere, the ts0 value should not be an average of typical high and low temperatures but instead should be close to a typical high temperature value for the seasons of interest. Here, 304 K corresponds to 88 F, just a few degrees below the region-wide typical high temperatures in the low to mid 90s.

The tlp value of 45 used in these simulations is appropriate. The simplest way to check the tlp value is to confirm that the combination of p0, ts0, and tlp gives an appropriate value for base-state temperature at the altitude where the logarithm of pressure has decreased by 1 from its surface value. Here, that pressure would be about 37500 pa. and 304 K – 45 K = 259 K or –14 C. Fig. 80 shows a sample value for the actual temperature at that level, -20 C. Thus, the base state profile in the troposphere is similar to the actual temperature profile during the days of this simulation, and it should also work well for any warm-season simulations, from May through October.

The final base state parameter, tiso, was set to 200 K. This value, too, is appropriate. In Fig. 80, it can be seen that the lower stratosphere has a temperature of –69 C, or 204 K. The value of tiso represents a typical value for lower stratospheric temperature over Texas in the summertime.

7. Summary and Recommendations

This report has examined model performance with profiler nudging for the period July 30 through August 2, 2005. The purpose of this examination was not to do a comprehensive model performance evaluation but rather to investigate specific aspects of performance to validate the nudging input dataset and determine whether the observational nudging improves the simulation.

Visual inspection of graphical displays of the nudging input data identified some observations that looked odd or suspicious, but none that were clearly erroneous. The most anomalous wind was probably real and took place during a thunderstorm. Particularly for wind profiler data in close proximity to geographical areas of particular interest, it may be beneficial to manually examine the wind profiles prior to data assimilation and to exclude any observations that are either clearly erroneous or unrepresentative. No such exclusion was necessary here.

The weather during this period included occasional convection, but model simulations using the TCEQ model configuration produced extensive convection. Because convection can have a dramatic effect on local winds and thereby mask wind modifications due directly to data assimilation, a model run including the Grell cumulus parameterization on the 4 km grid was performed in addition to the other runs with no cumulus parameterization activated on the inner grid. The run with Grell had the desired effect of reducing the convection and precipitation during the period, producing a model simulation that on the whole had nearly the correct amount of convective activity. The use of this model configuration should be considered for future air quality simulations when excessive convection is an issue.

Other model simulations included a run with the configuration provided by TCEQ, a run with no nudging, a run with altered nudging parameters, and a run with data from one profiler withheld. Nudging reduced the convective activity compared to the run with no nudging. This drove the model in the correct direction, probably due to some combination of improved air parcel trajectories and improved convergence-divergence patterns. The nudging radius was set sufficiently broadly that no spurious convection was found to be triggered by small-scale convergence-divergence couplets induced by the data assimilation.

There was an insufficient number of sea breeze days to determine whether the nudging improved the sea breeze onset or penetration. Mixing heights were variable, and there was no systematic difference observed between mixing heights with and without data assimilation.

The coastal oscillation was much better incorporated into the nudged simulations than the simulation without nudging. On the evening in which Huntsville was unaffected by

convection, the nudged simulation, even with Huntsville data withheld, was found to give a markedly superior simulation at Huntsville.

Statistical validation against surface data was conducted separately over two regions (North Texas and Southeast Texas) and two data sets (METAR and TCEQ). The simulated temperatures warmed up too quickly during the morning in North Texas but were well behaved in Southeast Texas. Differences in temperature among the various simulations were primarily caused by differences in convection. Simulated surface wind speeds were typically too low during the day and too high at night, yielding a diurnal wind speed variation several times weaker than observations. Wind improvements due to nudging were small in North Texas but large in Southeast Texas where the erroneous convection would be expected to have a detrimental effect on the wind field especially in the absence of data assimilation.

In general, the model agreed better with METAR data than with TCEQ data. This is consistent with the generally better meteorological station site characteristics of the METAR data. Three TCEQ stations had to be discarded because their 5-minute data were not consistent with the metadata.

A detailed examination of winds during a period of time during the night when model errors were expected to be large showed that data assimilation had a massive impact on the wind field. The nudging parameter settings chosen by TCEQ performed better than an alternative set of parameter settings tested for the purpose of this study.

The base state model parameters were examined and compared to typical summertime conditions for eastern Texas, and were found to be suitable and appropriate for air quality simulations during ozone seasons.

8. Reference

Nielsen-Gammon, J. W., R. T. McNider, W. M. Angevine, A. B. White, and K. Knupp, 2007: Mesoscale model performance with assimilation of wind profiler data: Sensitivity to assimilation parameters and network configuration. *J. Geophys. Res.*, 112, D09119, doi:10.1029/2006JD007633.